ERDC/ITL TR-02-3

Information Technology Laboratory

US Army Corps
of Engineers®
Engineer Research and
Development Center

Earthquake Engineering Research Program

Seismic Analysis of Cantilever Retaining Walls, Phase I

Russell A. Green and Robert M. Ebeling

September 2002

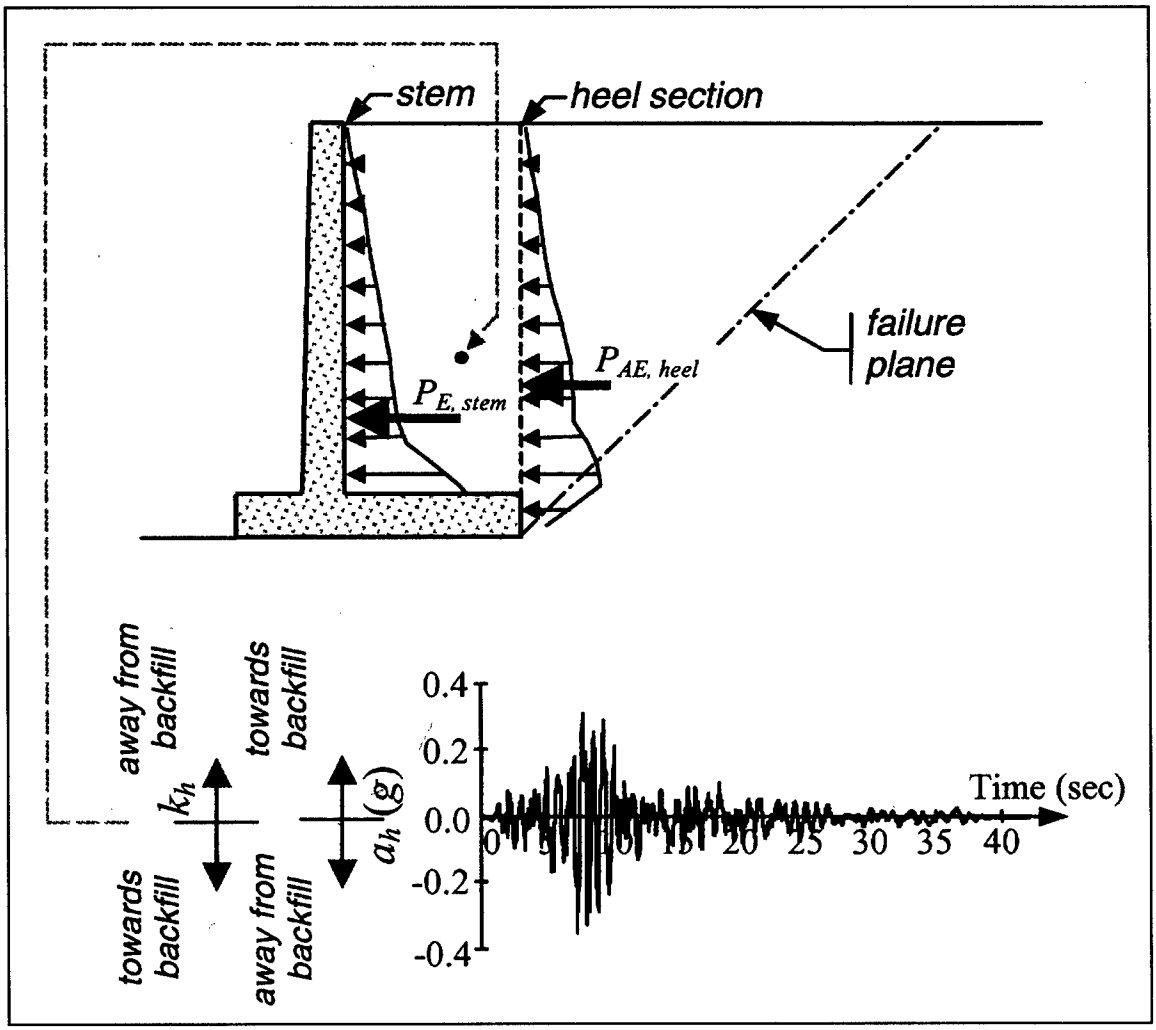

The contents of this report are not to be used for advertising, publication, or promotional purposes. Citation of trade names does not constitute an official endorsement or approval of the use of such commercial products.

The findings of this report are not to be construed as an official Department of the Army position, unless so designated by other authorized documents.

PRINTED ON RECYCLED PAPER

Earthquake Engineering Research Program

ERDC/ITL TR-02-3
September 2002

Seismic Analysis of Cantilever Retaining Walls, Phase I

by Russell A. Green

Department of Civil and Environmental Engineering
University of Michigan
Ann Arbor, MI 48109-2125

Robert M. Ebeling

Information Technology Laboratory
U.S. Army Engineer Research and Development Center
3909 Halls Ferry Road
Vicksburg, MS 39180-6199

Final report

Prepared for U.S. Army Corps of Engineers
Washington, DC 20314-1000

Under Work Unit 387-9456h

Contents

List of Figures

Preface

The study documented herein was undertaken as part of Work Unit 387-9456h, "Seismic Design of Cantilever Retaining Walls," funded by the Headquarters, U.S. Army Corps of Engineers (HQUSACE) Civil Works Earthquake Engineering Research Program (EQEN) under the purview of the Geotechnical and Structures Laboratory (GSL), Vicksburg, MS, U.S. Army Engineer Research and Development Center (ERDC). Technical Director for this research area was Dr. Mary Ellen Hynes, GSL. The HQUSACE Program Monitor for this work was Ms. Anjana Chudgar. The principal investigator (PI) for this study was Dr. Robert M. Ebeling, Computer-Aided Engineering Division (CAED), Information Technology Laboratory (ITL), Vicksburg, MS, ERDC, and Program Manager was Mr. Donald E. Yule, GSL. The work was performed at University of Michigan, Ann Arbor, and at ITL. The effort at the University of Michigan was funded through response to the ERDC Broad Agency Announcement FY01, BAA# ITL-1, "A Research Investigation of Dynamic Earth Loads on Cantilever Retaining Walls as a Function of the Wall Geometry, Backfill Characteristics, and Numerical Modeling Technique."

This research was performed and the report prepared by Dr. Russell A. Green of the Department of Civil and Environmental Engineering, University of Michigan, and by Dr. Ebeling under the direct supervision of Mr. H. Wayne Jones, CAED, and Dr. Jeffery P. Holland, Director, ITL. The work was performed during the period December 2001 to August 2002 by Dr. Green and Dr. Ebeling. This report summarizes the results of the first phase of a research investigation examining the seismic loads induced on the stem of a cantilever retaining wall. This investigation marks the first use of the computer program FLAC (Fast Lagrangian Analysis of Continua) for analyzing the dynamic response of a Corps earth retaining structure, with the emphasis of the investigation being on the details of numerical modeling with FLAC, as well as the results of the analyses. Further analyses are required to confirm the identified trends in the results of the analyses and to formulate design recommendations for Corps earth retaining structures. During the course of this research investigation, the authors had numerous discussions with other FLAC users. Of particular note were the lengthy conversations with Mr. Guney Olgun, Virginia Polytechnic and State University, Blacksburg, which were instrumental in completing Phase 1 of this research investigation. Others who provided valuable insight into the workings of FLAC were Mr. Nason McCullough and Dr. Stephen Dickenson, Oregon State University, Corvallis; Dr. N. Deng and Dr. Farhang Ostadan, Bechtel Corporation, San Francisco, CA; Mr. Michael R. Lewis, Bechtel

Savannah River, Inc., Aiken, SC; Dr. Peter Byrne and Dr. Mike Beaty, University of British Columbia, Vancouver; and Dr. Marte Gutierrez, Virginia Tech.

At the time of publication of this report, Dr. James R. Houston was Director, ERDC, and COL John W. Morris III, EN, was Commander and Executive Director.

1 Introduction

1.1 Introduction

This report presents the results of the first phase of a research investigation into the seismic response of earth retaining structures and the extension of the displacement controlled design procedure, as applied to the global stability assessment of Corps retaining structures, to issues pertaining to their internal stability. It is intended to provide detailed information leading to refinement of the Ebeling and Morrison (1992) simplified seismic engineering procedure for Corps retaining structures. Specific items addressed in this Phase 1 report deal with the seismic loads acting on the stem portion of cantilever retaining walls. A typical Corps cantilever retaining wall is shown in Figure 1-1. It is envisioned that this information will be used in the development of a refined engineering procedure of the stem and base reinforced concrete cantilever wall structural members for seismic structural design.

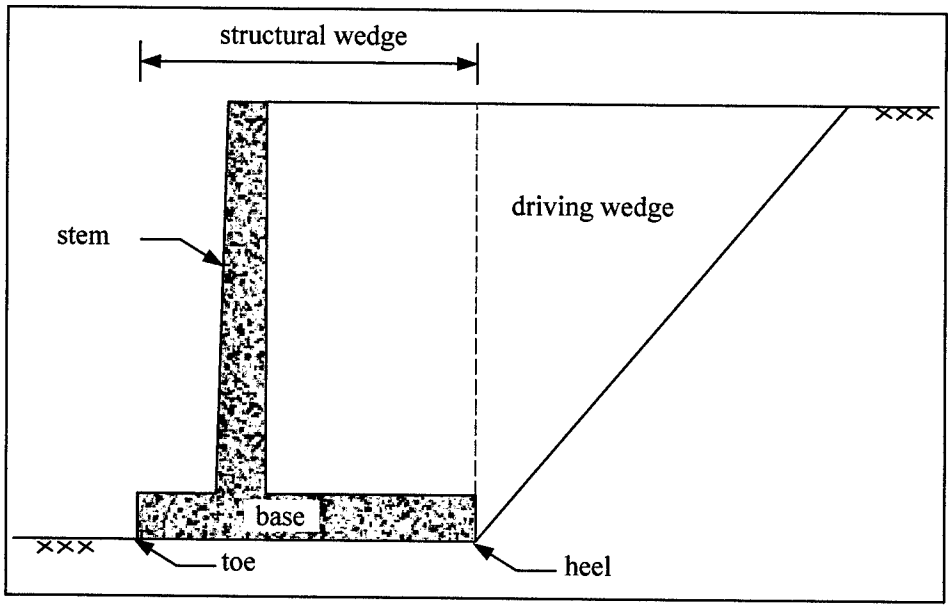

Figure 1-1. Typical Corps cantilever wall, including structural and driving wedges

1.2 Background

Formal consideration of the permanent seismic wall displacement in the seismic design process for Corps-type retaining structures is given in Ebeling and Morrison (1992). The key aspect of this engineering approach is that simplified procedures for computing the seismically induced earth loads on retaining structures are dependent upon the amount of permanent wall displacement that is expected to occur for each specified design earthquake. The Corps uses two design earthquakes as stipulated in Engineer Regulation (ER) 1110-2-1806 (Headquarters, U.S. Army Corps of Engineers (HQUSACE) 1995): the Operational Basis Earthquake (OBE)[1] and the Maximum Design Earthquake (MDE). The retaining wall would be analyzed for each design case. The load factors used in the design of reinforced concrete hydraulic structures are different for each of these two load cases.

The Ebeling and Morrison simplified engineering procedures for Corps retaining structures, as described in their 1992 report, are geared toward hand calculations. However, research efforts are currently underway at the U.S. Army Engineer Research and Development Center (ERDC) to computerize these engineering procedures and to make possible the use of acceleration time-histories in these design/analysis processes when time-histories are made available on Corps projects. In the Ebeling and Morrison simplified seismic analysis procedure two limit states are established for the backfill; the first corresponds to walls retaining yielding backfill, while the second corresponds to walls retaining nonyielding backfill. Examples of Corps retaining walls that typically exhibit these two conditions in seismic evaluations are shown in Figure 1-2. In this figure F_V and F'_H are the vertical and horizontal components, respectively, of the resultant force of the stresses acting on imaginary sections *A-A* and *B-B*, and T and N' are the shear and normal reaction forces, respectively, on the bases of the walls.

It is not uncommon for retaining walls of the type shown in Figure 1-2a, i.e., soil-founded cantilever retaining walls, to have sufficient wall movement away from the backfill during a seismic event to mobilize the shear strength within the backfill, resulting in active earth pressures acting on the structural wedge (as delineated from the driving wedge by imaginary section A-A extending vertically from the heel of the wall up through the backfill). Figure 1-2b shows a wall exemplifying the second category, walls retaining a nonyielding backfill. For a massive concrete gravity lock wall founded on competent rock with high base interface and rock foundation shear strengths (including high- strength rock joints, if present, within the foundation), it is not uncommon to find that the typical response of the wall during seismic shaking is the lock wall rocking upon its base. For this case, wall movements in sliding are typically not sufficient to mobilize the shear strength in the backfill.

[1] For convenience, symbols and unusual abbreviations are listed and defined in the Notation (Appendix E).

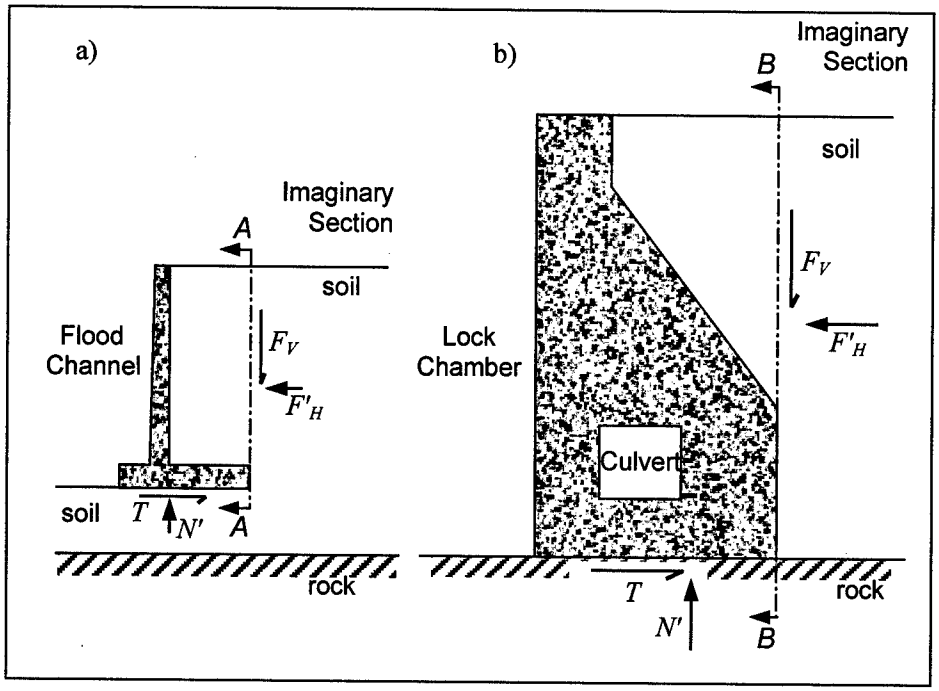

Figure 1-2. Earth retaining structures typical of Corps projects: (a) soil-founded, cantilever floodwall retaining earthen backfill; (b) rock-founded, massive concrete lock wall retaining earthen backfill

Yielding backfills assume that the shear strength of the backfill is fully mobilized (as a result of the wall moving away from the backfill during earthquake shaking), and the use of seismically induced active earth pressure relationships (e.g., Mononobe-Okabe) is appropriate. A calculation procedure first proposed by Richards and Elms (1979) for walls retaining "dry" backfills (i.e., no water table) is used for this limit state. Ebeling and Morrison (1992) proposed engineering calculation procedures for "wet" sites (i.e., sites with partially submerged backfills and for pools of standing water in the chamber or channel) and developed a procedure to compute the resultant active earth pressure force acting on the structural wedge using the Mononobe-Okabe relationship. (Most Corps sites are "wet" since the Corps usually deals with hydraulic structures.) The simplified Ebeling and Morrison engineering procedure recommends that a Richards and Elms type displacement-controlled approach be applied to the earth retaining structure, as described in Section 6.3 of Ebeling and Morrison (1992) for Corps retaining structures. It is critical to the calculations that partial submergence of the backfill and a standing pool of water in the chamber (or channel) are explicitly considered in the analysis, as given by the Ebeling and Morrison simplified computational procedure. Equations developed by Ebeling and Morrison to account for partial submergence of the backfill in the Mononobe-Okabe resultant active earth pressure force computation is given in Chapter 4 of their report. A procedure for assigning the corresponding earth pressure distribution was developed by Ebeling and Morrison for a partially submerged backfill and is described using Figures 7.8, 7.9, and 7.10 of their report.

Key to the categorization of walls retaining yielding backfills in the Ebeling and Morrison simplified engineering procedure for Corps retaining structures is

the assessment by the design engineer of the minimum seismically induced wall displacements to allow for the full mobilization of the shear resistance of the backfill and, thus, the appropriate use of the Mononobe-Okabe active earth pressure relationship in the computations. Ebeling and Morrison made a careful assessment of the instrumented dynamic earth pressure experiments available in the technical literature prior to their publication in 1992. The results of this assessment are described in Chapter 2 of Ebeling and Morrison (1992). Ebeling and Morrison concluded that the minimum wall displacement criteria developed by Clough and Duncan (1991) for the development of "active" static earth pressure are also reasonable guidance for the development of seismically induced active earth pressure. This guidance for engineered backfills is given in Table 1 of Ebeling and Morrison (1992). Minimum permanent seismically induced wall displacements away from the backfill are expressed in this table as a fraction of the height of backfill being retained by the wall. The value for this ratio is also a function of the relative density of the engineered backfill. Thus, prior to accepting a permanent seismic wall displacement prediction made following the simplified displacement-controlled approach for Corps retaining structures (Section 6.3 of Ebeling and Morrison 1992), the design engineer is to check if his computed permanent seismic wall displacement value meets or exceeds the minimum displacement value for active earth pressure given in Table 1 of Ebeling and Morrison (1992). This ensures that the use of active earth pressures in the computation procedure is appropriate.

In the second category of walls retaining nonyielding backfills (Figure 1-2b), Ebeling and Morrison recommend the use of at-rest type, earth pressure relationship in the simplified hand calculations. Wood's (1973) procedure is used to compute the incremental pseudo-static seismic loading, which is superimposed on the static, at-rest distribution of earth pressures. Wood's is an expedient but conservative computational procedure (Ebeling and Morrison (1992), Chapter 5). (A procedure to account for wet sites with partially submerged backfills and for pools of standing water in the chamber or channel was developed by Ebeling and Morrison (1992) and outlined in Chapter 8 of their report.) It is Ebeling's experience with the type lock walls shown in Figure 1-2b of dimensions that are typical for Corps locks that seismically induced sliding is an issue only with large ground motion design events and/or when a weak rock joint or a poor lock-to-foundation interface is present.

After careful deliberation, Ebeling and Morrison in consultation with Whitman[1] and Finn[2] judged the simplified engineering procedure for walls retaining nonyielding backfills applicable to walls in which the wall movements are small, less than one-fourth to one-half of the Table 1 (Ebeling and Morrison 1992) active displacement values. Recall that the Ebeling and Morrison engineering procedure is centered on the use of one of only two simplified hand-computational procedures.

---

[1] Dr. Robert V. Whitman, 1992, Professor Emeritus, Massachusetts Institute of Technology, Boston.

[2] Dr. W. D. Liam Finn, 1992, Professor Emeritus, University of British Columbia, Vancouver.

Rotational response of the wall (compared to sliding) is beyond the scope of the Ebeling and Morrison (1992) simplified engineering procedures for Corps retaining structures. This 1992 pioneering effort for the Corps dealt only with the sliding mode of permanent displacement during seismic design events. It is recognized that the Corps has some retaining structures that are more susceptible to rotation-induced (permanent) displacement during seismic events than to (permanent) sliding displacement. To address this issue, Ebeling is currently conducting research at ERDC leading to the development of a simplified engineering design procedure for the analysis of retaining structures that are constrained to rotate about the toe of the wall during seismic design events (Ebeling and White, in preparation).

1.3 Research Objective

The Ebeling and Morrison (1992) simplified seismic engineering procedures for Corps retaining structures did not address issues pertaining to the structural design of cantilever retaining walls. The objective of the research described in this report is to fill this knowledge gap and determine the magnitude and distribution of the seismic loads acting on cantilever retaining walls for use in the design of the stem and base reinforced concrete cantilever wall structural members.

1.4 Research into the Seismic Response of a Cantilever Retaining Wall

The seismic loads acting on the *structural wedge* of a cantilever retaining wall are illustrated in Figure 1-3. The structural wedge consists of the concrete wall and the backfill above the base of the wall (i.e., the backfill to the left of a vertical section through the heel of the cantilever wall). The resultant force of the static and dynamic stresses acting on the vertical section through the heel (i.e., heel section) is designated as $P_{AE,\,heel}$, and the normal and shear base reactions are N' and T, respectively. Seismically induced active earth pressures on the heel section, $P_{AE,\,heel}$, are used to evaluate the global stability of the structural wedge of a cantilever retaining wall, presuming there is sufficient wall movement away from the backfill to fully mobilize the shear resistance of the retained soil. The relative slenderness of the stem portion of a cantilever wall requires structural design consideration. In Figure 1-3 the seismically induced shear and bending moments on a section of the stem are designated as s and m, respectively. The resultant force of the static and dynamic stresses acting on the stem of the wall shown in Figure 1-3 is designated as $P_{E,\,stem}$. The A is not included in the subscript because the structural design load is not necessarily associated with active earth pressures.

A dry site (i.e., no water table) will be analyzed in this first of a series of analyses of cantilever retaining walls using FLAC (Fast Lagrangian Analysis of Continua). This allows the researchers to gain a full understanding of the dynamic behavior of the simpler case of a cantilever wall retaining dry backfill

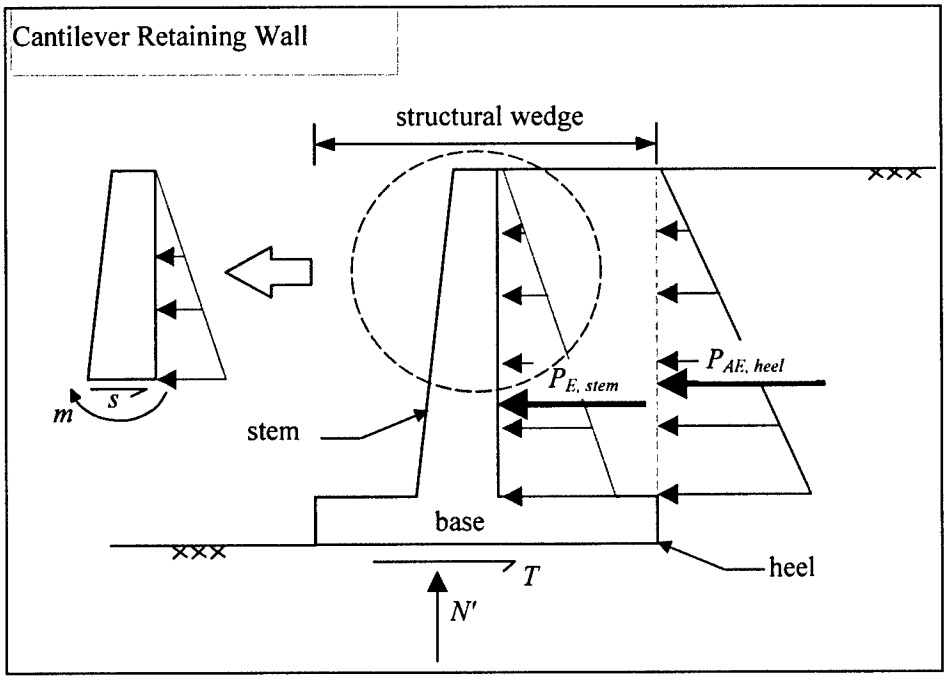

Figure 1-3. Loads acting on the structural wedge of a cantilever retaining wall

before adding the additional complexities associated with submerged or partially submerged backfills.

This report summarizes the results of detailed numerical analyses performed on a cantilever wall proportioned and structurally detailed per Corps guidelines given in Engineer Manuals (EM) 1110-2-2104 (HQUSACE 1992) and 1110-2-2502 (HQUSACE 1989)) for global stability and structural strength under static loading. The objective of the analyses was to identify trends and correlations between $P_{AE,\ heel}$ and $P_{E,\ stem}$ and their respective points of application. The identification of such trends allows the displacement-controlled design procedure, which can be used to estimate $P_{AE,\ heel}$, to be extended to estimate $P_{E,\ stem}$, which is required for the structural design of the stem.

The detailed numerical analyses were performed using the commercially available computer program FLAC. The nonlinear constitutive models, in conjunction with the explicit solution scheme, in FLAC give stable solutions to unstable physical processes, such as the sliding or overturning of a retaining wall. FLAC allows permanent displacements to be modeled, which is inherently required by the displacement-controlled design procedure. The resultant forces acting on the heel sections and their points of applications as determined from the FLAC analyses were compared with values computed using the Mononobe-Okabe equations in conjunction with the displacement-controlled design procedure (e.g., Ebeling and Morrison 1992).

1.5 Organization of Report

The organization of the report follows the sequence in which the work was performed. Chapter 2 outlines the process of selecting the ground motions (e.g., acceleration time-histories) used in the FLAC analyses. Chapter 3 gives a brief overview of the numerical algorithms in FLAC and outlines how the various numerical model parameters were determined. Chapter 4 describes the data reduction and interpretation of the FLAC results, followed by the References. Appendix A provides detailed calculation of the geometry and structural design for static loading of the wall analyzed dynamically. Appendix B reviews the sign convention and notation used in this report and also presents the Mononobe-Okabe earth pressure equations (e.g., Ebeling and Morrison 1992, Chapter 4). Appendix C is a brief overview of the displacement-controlled procedure for global stability of retaining walls. Finally, Appendix D summarizes a parameter study performed to determine how best to specify ground motions in FLAC.

1.6 Future Work

This report presents the results of the first phase of an ongoing research investigation. Additional FLAC analyses are planned to determine if the observed trends presented in Chapter 4 of this report are limited to the wall geometry and soil conditions analyzed, or whether they are general trends that are applicable to other wall geometries and soil conditions. Additionally, the same walls analyzed using FLAC will be analyzed using the computer program FLUSH. FLUSH solves the equations of motions in the frequency domain and uses the equivalent linear algorithm to account for soil nonlinearity. The advantages of FLUSH are that it is freely downloadable from the Internet and has considerably faster run times than FLAC. However, the major disadvantage of FLUSH is that it does not allow for permanent displacement of the wall. FLUSH accounts for the nonlinear response of soils during earthquake shaking through adjustments of the soil (shear) stiffness and damping parameters (as a function of shear strain) that develop in each element of the finite element mesh. The FLAC and FLUSH results will be compared.

2 Selection of Design Ground Motion

2.1 Selection Criteria

The selection of an earthquake acceleration time-history for use in the numerical analyses was guided by the following criteria:

a. A real earthquake motion was desired, not a synthetic motion.

b. The earthquake magnitude and site-to-source distance corresponding to the motion should be representative of design ground motions.

c. The motion should have been recorded on rock or stiff soil.

These criteria were used to assemble a list of candidate acceleration time-histories, while additional criteria, discussed in Section 2.3, were used to select one time-history from the candidate list. Because the response of a soil-structure system in a linear dynamic analysis is governed primarily by the spectral content of the time-history and because it is possible to obtain a very close fit to the design spectrum using spectrum-matching methods, it is sufficient to have a single time-history for each component of motion for each design earthquake. However, because the nonlinear response of a soil-structure system may be strongly affected by the time-domain character of the time-histories even if the spectra of different time-histories are nearly identical, at least five time-histories (for each component of motion) should be used for each design earthquake (Engineering Circular (EC) 1110-2-6051 (HQUSACE 2000)). More time-histories are required for nonlinear dynamic analyses than for linear analyses because the dynamic response of a nonlinear structure may be importantly influenced by the time domain character of the time-history (e.g., shape, sequence, and number of pulses), in addition to the response spectrum characteristics. However, for the first phase of this research investigation, only one time-history was selected for use in the dynamic analyses.

2.1.1 Real versus synthetic earthquake motion

Because the numerical analyses performed in the first phase of this research investigation involve permanent displacement of the wall and plastic deformations in the soil (i.e., nonlinearity), it was decided that a real motion should be

used. The rationale for this decision was to avoid potential problems of developing a synthetic motion that appropriately incorporates all the factors that may influence the dynamic response of a nonlinear system.

2.1.2 Representative magnitude and site-to-source distance

As stated in Chapter 1, the objective of this study is to determine the seismic structural design loads for the stem portion of a cantilever retaining wall. Accordingly, the magnitude M and site-to-source distance R of the ground motion used in the numerical analyses should be representative of an actual design earthquake, which will depend on several factors including geographic location and consequences of failure. In an effort to select a "representative" M and R for a design event, the deaggregated hazard of five cities located in the western United States (WUS) were examined: San Francisco, Oakland, Los Angeles, San Diego, and Salt Lake City. Deaggregation of the seismic hazard is a technique used in conjunction with probabilistic seismic hazard analyses (PSHA) (EM 1110-2-6050 (HQUSACE 1999)) to express the contribution of various M and R combinations to the overall seismic hazard at a site. The deaggregation results are often described in terms of the mean magnitude $\overline{M}$ and mean distance $\overline{R}$ for various spectral frequencies (Frankel et al. 1997). It is not uncommon to set the design earthquake magnitude and distance equal to the values of $\overline{M}$ and $\overline{R}$ corresponding to the fundamental frequency of the system being designed.

Table 2-1 lists the $\overline{M}$ and $\overline{R}$ for the peak ground acceleration *pga* and 1-hz spectral acceleration for the five WUS cities. These ground motions have average return periods of about 2500 years (i.e., 2 percent probability of exceedance in 50 years). From the deaggregated hazards, representative M and R for the design ground motions were selected as 7.0 and 25 km, respectively.

Table 2-1
Mean Magnitudes and Distances for Five WUS Cities for the 2500-year Ground Motion

WUS City	$\overline{M}_{pga}$	$\overline{R}_{pga}$, km	$\overline{M}_{1hz}$	$\overline{R}_{1hz}$, km
San Francisco, CA	7.8	25.0	7.9	25.0
Oakland, CA	7.2	25.0	7.3	25.4
Los Angeles, CA	6.8	25.2	7.0	27.1
San Diego, CA	7.0	25.0	7.0	25.1
Salt Lake City, UT	7.1	25.1	7.3	25.1

2.1.3 Site characteristics of motion

The amplitude and frequency content, as well as the phasing of the frequencies, of recorded earthquake motions are influenced by the source mechanism (i.e., fault type and rupture process), travel path, and local site conditions, among other factors. Because the selected ground motion ultimately is to be specified as a base rock motion in the numerical analyses, the site condition for the selected ground motions is desired to be as close as possible to the base rock conditions

underlying the profile on which the cantilever wall is located. This avoids additional processing of the recorded motion to remove the site effects on which it was recorded (e.g., deconvolving the record to base rock). Accordingly, motions recorded on rock or stiff soil profiles were desired for this study.

2.2 List of Candidate Motions

Based on the selection criteria, the motions listed in Table 2-2 were considered as candidates for use in the numerical analyses.

Table 2-2
Candidate Motions

Earthquake	Station	Record	*pga*, g
Cape Mendocino *M7.1, Ms7.1*	89530 Shelter Cove Airport *Closest to fault rupture: 33.8 km* *Closest to surface projection of rupture: 32.6 km*	SHL-UP SHL000 SHL090	0.054 0.229 0.189
Duzce, Turkey *M7.1, Ms7.3*	1058 Lamont *Closest to fault rupture: 0.9 km* *Closest to surface projection of rupture: 0.9 km*	1058-E 1058-N 1058-V	0.111 0.073 0.07
Duzce, Turkey *M7.1, Ms7.3*	1061 Lamont *Closest to fault rupture: 15.6 km* *Closest to surface projection of rupture: 15.6 km*	1061-E 1061-N 1061-V	0.134 0.107 0.048
Loma Prieta *M6.9, Ms7.1*	57383 Gilroy Array #6 *Closest to fault rupture: 19.9 km* *Closest to surface projection of rupture: 19.9 km*	G06-UP G06000 G06000	0.101 0.126 0.1
Loma Prieta *M6.9, Ms7.1*	47189 SAGO South-surface *Closest to fault rupture: 34.7 km* *Closest to surface projection of rupture: 34.1 km*	SG3-UP SG3261 SG3351	0.06 0.073 0.067

Note: Ms = surface wave magnitude of earthquake; M = moment magnitude of earthquake.

These records were obtained by searching the Strong Motion Database maintained by the Pacific Earthquake Engineering Research (PEER) Center (http://peer.berkeley.edu/smcat/).

2.3 Characteristics of Ground Motion Selected

As stated previously, at least five time-histories (for each component of motion) meeting the selection criteria should be used in nonlinear dynamic analyses (EC 1110-2-6051 (HQUSACE 2000)). However, for the first phase of this study, only SG3351 was used, which was recorded during the 1989 Loma Prieta earthquake in California. The basis for selecting SG3351 was that it was estimated, using CWROTATE (Ebeling and White, in preparation), to induce the greatest permanent relative displacement of the wall. The numerical formulation in CWROTATE is based on the Newmark sliding block procedure outlined in Ebeling and Morrison (1992), Section 6.3, and is discussed further in Appendix C.

SG3351 is plotted in Figure 2-1, as well as the corresponding 5 percent damped, pseudo-acceleration response spectrum, scaled to 1 g *pga*. Additionally,

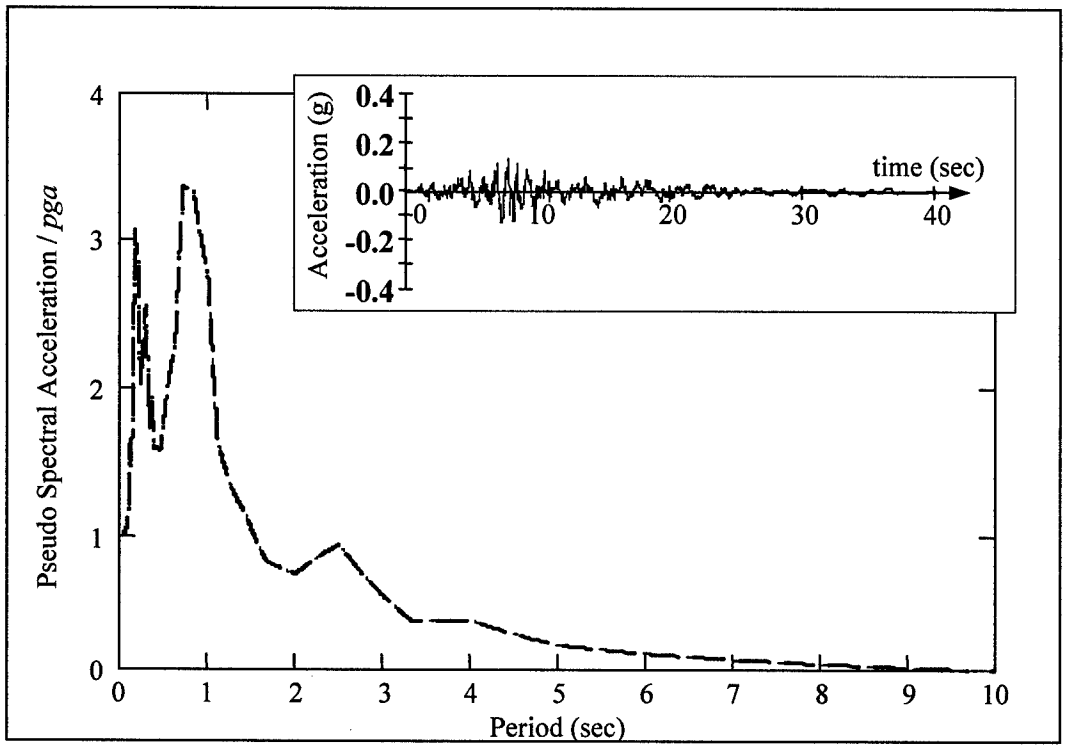

Figure 2-1. Acceleration time-history and 5 percent damped pseudo-acceleration spectrum, scaled to 1-g *pga*

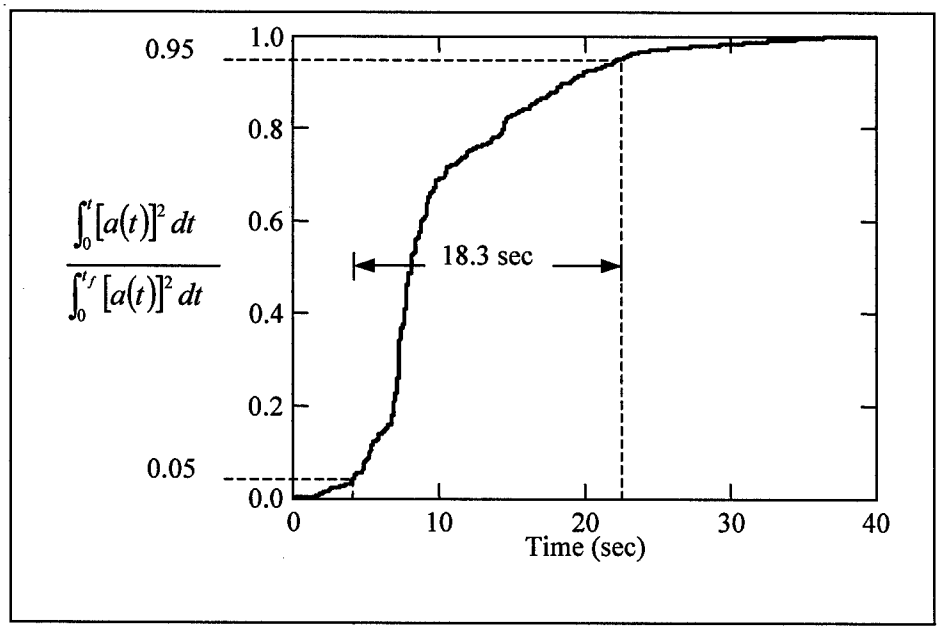

Figure 2-2. Husid plot of SG3351 used for determining duration of strong shaking, 18.3 sec ($a(t)$ is the acceleration at time t and t_f is the total duration of the acceleration time-history)

a Husid plot of the motion is shown in Figure 2-2, which was used to compute duration of strong shaking (EC 1110-2-6051 (HQUSACE 2000)), 18.3 sec.

2.4 Processing of the Selected Ground Motion

Although motion SG3351 met the selection criteria, several stages of processing were required before it could be used as an input motion in the FLAC analyses. The first stage was simply scaling the record. As a general rule, ground motions can be scaled upward by a factor of two without distorting the realistic characteristics of the motion (EC 1110-2-6051 (HQUSACE 2000)). The upward scaling was desired because although the motion induced the largest permanent relative displacement d_r of the candidate records, the induced displacement was still too small to ensure active earth pressures were achieved. For the retaining wall system being modeled in this first phase (i.e., wall height: 20 ft (6 m); backfill: medium-dense, compacted) $d_r \geq 0.5$ in. (12.7 mm) is required for active earth pressures (Ebeling and Morrison, 1992, Table 1, as adapted from values presented in Clough and Duncan 1991).

The second processing stage involved filtering high frequencies and computing the corresponding interlayer motion, both of which are required for either finite element or finite difference analyses. As discussed subsequently in detail in Chapter 3, in the finite element and finite difference formulations, the element dimension in the direction of wave propagation, as well as the propagation velocity of the material, limits the maximum frequency which the element can accurately transfer. For most soil systems and most earthquake motions, the removal of frequencies above 15 hz (i.e., low-pass cutoff frequency) will not influence the dynamic response of the system. However, caution should be used in selecting the low-pass cutoff frequency, especially when the motions are being used in dynamic soil-structure-interaction analyses where the building structure may have a high natural frequency, such as nuclear power plants. Next, SG3351 was recorded on the ground surface, and the corresponding interlayer motion needed to be computed for input into the base of the FLAC model. A modified version of the computer program SHAKE91 (Idriss and Sun 1992) was used both to remove the high frequencies and compute the interlayer motion. Figure 2-3 shows the recorded SG3351 and the processed record used as input at the base of the FLAC model.

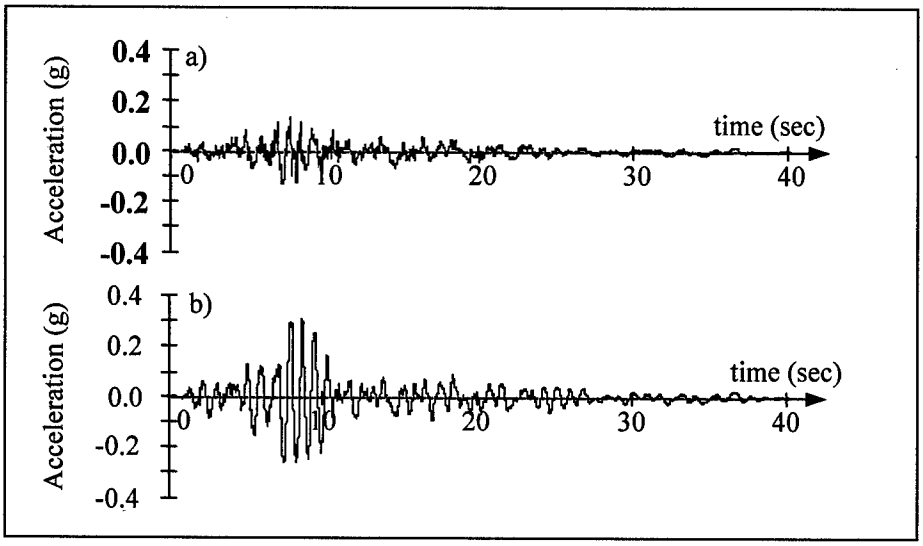

Figure 2-3. Selected ground motion (a) recorded motion SG3351and (b) the processed motion used as input into the base of the FLAC model

3 Numerical Analysis of Cantilever Retaining Wall

3.1 Overview of FLAC

As stated in Chapter 1, the detailed numerical analyses of the cantilever retaining walls were performed using FLAC, a commercially available, two-dimensional, explicit finite difference program, which was written primarily for geotechnical engineering applications. The basic formulation of FLAC is plane-strain, which is the condition associated with long structures perpendicular to the analysis plane (e.g., retaining wall systems). The following is a brief overview of FLAC and is largely based on information provided in the FLAC manuals (Itasca Consulting Group, Inc., 2000). The reader is referred to these manuals for additional details.

Because it is likely that most readers are more familiar with the finite element method (FEM) than with the finite difference method (FDM), analogous terms of the two methods are compared as shown:

Finite Element		Finite Difference
element	⇔	*zone*
node	⇔	*grid point*
mesh	⇔	*grid*

In places of convenience, these terms are used interchangeably in this report. For example, the terms structural elements and interface elements are used in this report, as opposed to structural zones and interface zones. Both FEM and FDM translate a set of differential equations into matrix equations for each element, relating forces at nodes to displacements at nodes. The primary difference between FLAC and most finite element programs relates to the explicit, Lagrangian calculation scheme used in FLAC, rather than the differences between the FEM and FDM. However, neither the Lagrangian formulation nor the explicit solution scheme is inherently unique to the FDM and may be used in the FEM.

Dynamic analyses can be performed with FLAC using the optional dynamic calculation module, wherein user-specified acceleration, velocity, or stress time-histories can be input as an exterior boundary condition or as an interior excitation. FLAC allows energy-absorbing boundary conditions to be specified, which limits the numerical reflection of seismic waves at the model perimeter.

FLAC has ten built-in constitutive models, including a null model, and allows user-defined models to be incorporated. The null model is commonly used in simulating excavations or construction, where the finite difference zones are assigned no mechanical properties for a portion of the analysis. The explicit solution scheme can follow arbitrary nonlinear stress-strain laws with little additional computational effort over linear stress-strain laws. FLAC solves the full dynamic equations of motion, even for essentially static systems, which enables accurate modeling of unstable processes (e.g., retaining wall failures). The explicit calculation cycle used in FLAC is illustrated in Figure 3-1.

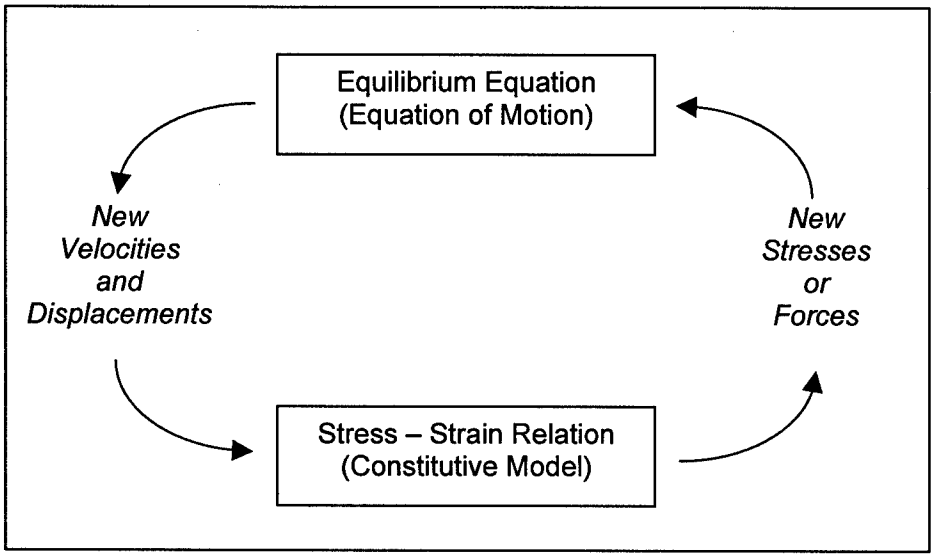

Figure 3-1. Basic explicit calculation cycle used in FLAC (adapted from Itasca Consulting Group, Inc., 2000, Theory and Background Manual)

Referring to Figure 3-1, beginning with a known stress state, the equation of motion is solved for the velocities and displacements for each element, while it is assumed that the stresses are *frozen*. Next, using the newly computed velocities and displacements, in conjunction with the specified stress-strain law, the stresses are computed for each element, while it is assumed that the velocities and displacements are *frozen*. The assumption of frozen velocities and displacements while stresses are computed and vice-versa can produce accurate results only if the computational cycle is performed for a very small increment in time (i.e., the "calculation wave speed" must always be faster than the physical wave speed). This leads to the greatest disadvantage of FLAC, long computational times, particularly when modeling stiff materials, which have large physical wave speeds. The size of the time-step depends on the dimension of the elements, the wave speed of the material, and the type of damping specified (i.e., mass

proportional or stiffness proportional), where stiffness proportional, to include Rayleigh damping, requires a much smaller time-step. The critical time-step for stability and accuracy considerations is automatically computed by FLAC, based on these factors listed. For those readers unfamiliar with the concept of critical time-step for stability and accuracy considerations in a seismic time-history engineering analysis procedure, please refer to Ebeling (1992), Part V, or to Ebeling, Green, and French (1997).

The Lagrangian formulation in FLAC updates the grid coordinates each time-step, thus allowing large cumulative deformations to be modeled. This is in contrast to the Eulerian formulation in which the material moves and deforms relative to a fixed grid, and is therefore limited to small deformation analyses.

3.2 Retaining Wall Model

The retaining wall-soil system analyzed in the first phase of this investigation is depicted in Figure 3-2. As shown in this figure, the FLAC model is only the top 30 ft (9 m) of a 225-ft (69-m) profile. Although the entire profile, to include the retaining wall, can be modeled in FLAC, the required computational time would be exorbitant, with little to no benefit added. To account for the influence of the soil profile below 30 ft (9 m), the entire profile without the retaining wall was modeled using a modified version of SHAKE91 (Idriss and Sun 1992), and the interlayer motion at the depth corresponding to the base of the FLAC model was computed. The input ground motion used in the SHAKE analysis was SG3351, the selection of which was discussed in Chapter 2. SG3351 was specified as a rock outcrop motion for the soil column. In this type of analysis the base of the soil column is modeled as a halfspace in the SHAKE model. In order to account for the site-specific *pga* value anticipated at this site for the specified design earthquake magnitude and specified site-to-source distance (discussed in Chapter 2), a scale factor of two was applied to SG3351 acceleration time-history. Based on the guidelines in EC 1110-2-6051 (HQUSACE 2000) allowing motions to be scaled upward by a factor less than or equal to two, this action was judged to be reasonable by this Corps criterion. The variation of the shear wave velocity as a function of depth in the profile is consistent with dense natural deposits beneath the base of the retaining wall and medium-dense compacted fill for the backfill.

The small strain natural frequency of the retaining wall-soil system in the FLAC model is estimated to be approximately 6.2 hz, as determined by the peak of the transfer function from the base of the model to the top of the backfill. At higher strains, it is expected that the natural period of the system will be less than 6.2 hz. The cutoff frequency in the SHAKE analysis was set at 15 hz. This value was selected based on both the natural frequency of the wall-soil system and the energies associated with the various frequencies in SG3351, and ensures proper excitation of the wall. Dimensioning of the finite difference zones to ensure proper transfer of frequencies up to 15 hz is discussed in Section 3.3.4.

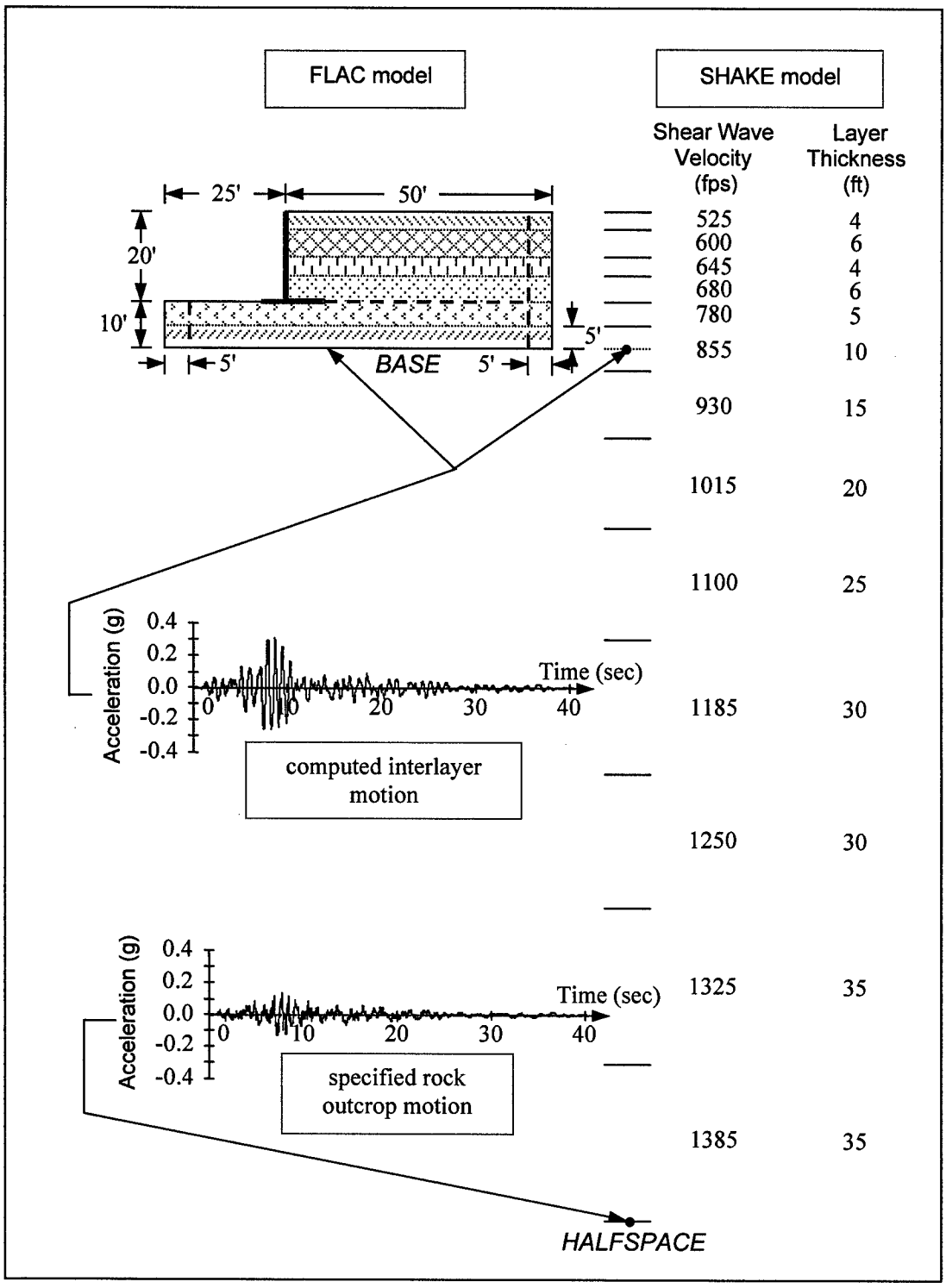

Figure 3-2. Numerical models used in the dynamic analysis of the cantilever retaining wall (To convert feet to meters, multiply by 0.3048)

The interlayer motion computed using SHAKE was specified as an acceleration time-history along the base of the FLAC model. Based on the results of a parametric study, outlined in Appendix D, specification of the ground motion in FLAC in terms of acceleration, as opposed to stress or velocity, gives the most accurate results for the profiles analyzed.

Figure 3-3 shows an enlargement of the retaining wall-soil system modeled in FLAC, as well as the finite difference grid. The FLAC model consists of four subgrids, labeled 1 through 4. Subgrids are used in FLAC to create regions of different shapes; there is no restriction on the variation of the material properties of the zones within a subgrid. The separation of the foundation soil and backfill into Subgrids 1 and 2 was required because a portion of the base of the retaining wall is inserted into the soil. Subgrid 4 was required because the free-field boundary conditions, an energy-absorbing boundary option in FLAC, cannot be specified across the interface of two subgrids. Subgrid 3 was included for symmetry. The subgrids were "attached" at the soil-to-soil interfaces, as depicted by the dashed red line in Figure 3-3a, and the yellow +'s in Figure 3-3b. The *attach* command welds the corresponding grid points of two subgrids together. Interface elements were used at the soil-structure interfaces, as depicted by green lines in Figure 3-3a, and discussed in more detail in Section 3.3.3.

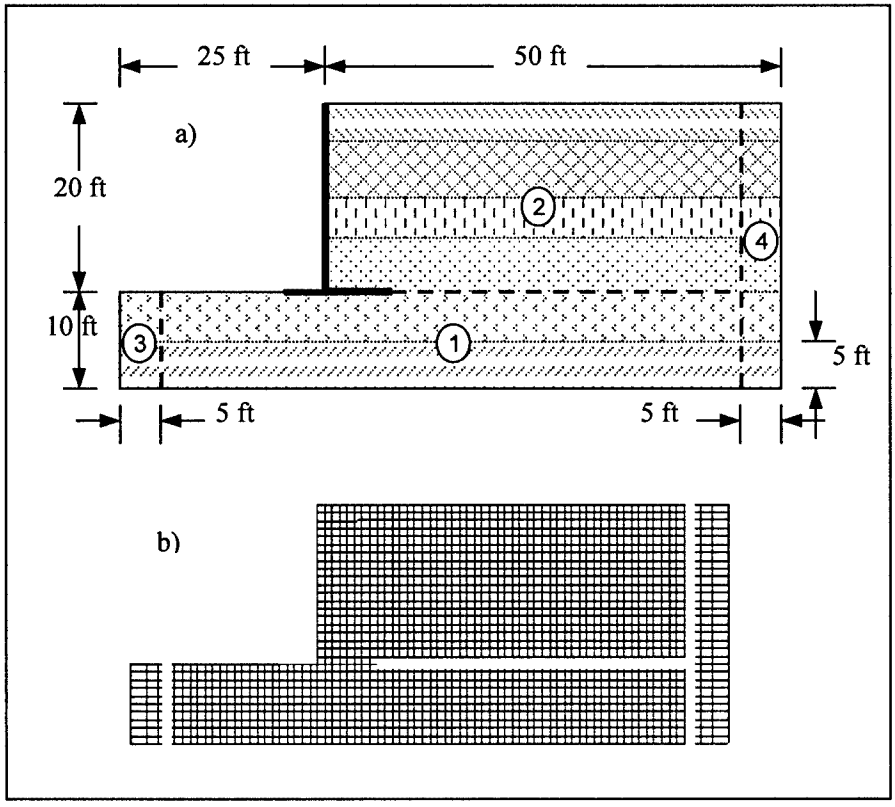

Figure 3-3. Retaining wall-soil system modeled in FLAC: (a) conceptual drawing showing dimensions and soil layering and (b) finite difference grid (To convert feet to meters, multiply by 0.348)

The retaining wall model was "numerically constructed" in FLAC similar to the way an actual wall would be constructed. The backfill was placed in 2-ft (0.6-m) lifts, for a total of ten lifts, with the model being brought to static equilibrium after the placement of each lift. This allowed realistic earth pressures to develop as the wall deformed and moved due to the placement of each lift. Figure 3-4 shows the deformed grid, magnified 75 times, after the construction of the wall and backfill placement to a height of 20 ft (6 m).

In the next section, an overview is given on how the numerical model parameters were determined.

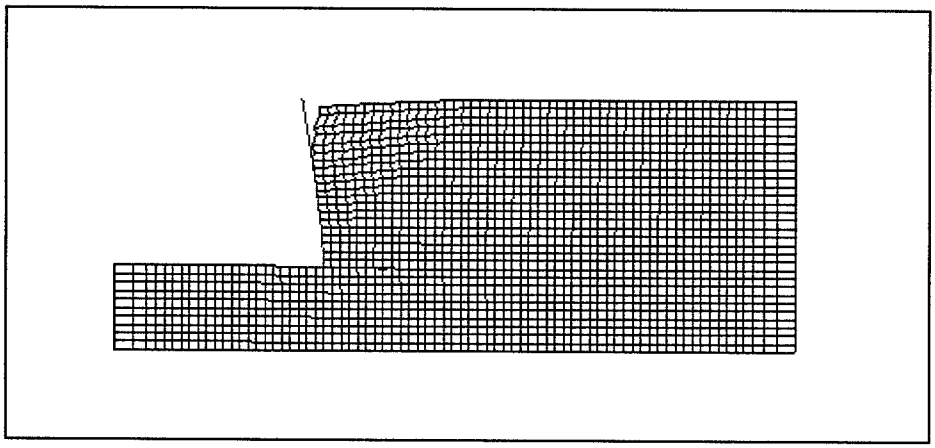

Figure 3-4. Deformed finite difference grid, magnified 75 times. The backfill was placed in ten 2-ft (0.6-m) lifts, with the model being brought to static equilibrium after the placement of each lift

3.3 Numerical Model Parameters

The previous section gave an overview of the physical system being analyzed and its numerical model counterpart. This section focuses on the specific constitutive models used for the soil, retaining wall, and their interface, with particular attention given to how to determine the various model parameters. An elastoplastic constitutive model, in conjunction with Mohr-Coulomb failure criteria, was used to model the soil. Elastic beam elements were used to model the concrete retaining wall, and interface elements were used to model the interaction between the soil and the structure. The following sections outline the procedures used to determine the various model parameters.

3.3.1 Mohr-Coulomb model

Four parameters are required for the Mohr-Coulomb model: internal friction angle ϕ; mass density ρ; shear modulus G; and bulk modulus K'. The first two parameters, ϕ and ρ, are familiar to geotechnical engineers, where mass density is the total unit weight of the soil γ_t divided by the acceleration due to gravity g, i.e., $\rho = \gamma_t / g$. ϕ for the foundation soil was set at 40 deg and to 35 deg for the

backfill. These values are consistent with dense natural deposits and medium-dense compacted fill. G and K' may be less familiar to geotechnical engineers, and therefore, their determination is outlined as follows.

Shear modulus G. Several correlations exist that relate G to other soil parameters. However, the most direct relation is between G and shear wave velocity v_s:

$$G = \rho \cdot v_s^2 \tag{3-1}$$

v_s may be determined by various types of site characterization techniques, such as cross hole or spectral analysis of surface waves (SASW) studies.

Bulk modulus K′. Values for K' are typically computed from G and Poisson's ratio ν using the following relation:

$$K' = \frac{2 \cdot G \cdot (1+\nu)}{3 \cdot (1-2 \cdot \nu)} \tag{3-2}$$

For natural deposits, ν may be estimated from the following expression:

$$\nu = \frac{1-\sin(\phi)}{2-\sin(\phi)} \tag{3-3}$$

This expression can be derived from the theory of elasticity (Terzaghi 1943) and the correlation relating at-rest earth pressure conditions K_o and ϕ proposed by Jaky (1944). However, for surficial compacted soil against a nondeflecting soil structure interface, Duncan and Seed (1986) proposed the following "empirically derived" expression for ν, which results in considerably higher values than that for natural soil deposits:

$$\nu = \frac{4-3 \cdot \sin(\phi)}{8-4 \cdot \sin(\phi)} \tag{3-4}$$

For the numerical analysis of a retaining wall with a compacted backfill, for which laboratory tests are not performed to determine ν, judgment should be used in selecting a value for ν, with a reasonable value being between those given by Equations 3-3 and 3-4:

$$\frac{1-\sin(\phi)}{2-\sin(\phi)} \le \nu \le \frac{4-3\cdot\sin(\phi)}{8-4\cdot\sin(\phi)} \tag{3-5}$$

3.3.2 Structural elements

The concrete retaining wall was modeled using elastic beam elements approximately 1 ft (0.3 m) long. In FLAC, four parameters are required to define the mechanical properties of the beam elements: cross-sectional area A_g; mass density ρ; elastic modulus E_c; and second moment of area I, commonly referred to as moment of inertia. The wall was divided into five segments having constant parameters, as illustrated in Figure 3-5, with each segment consisting of several 1-ft (0.3-m) beam elements. The number of segments used is a function of the variation of the mechanical properties in the wall. A wall having a greater taper or largely varying reinforcing steel along the length of the stem or base would likely require more segments.

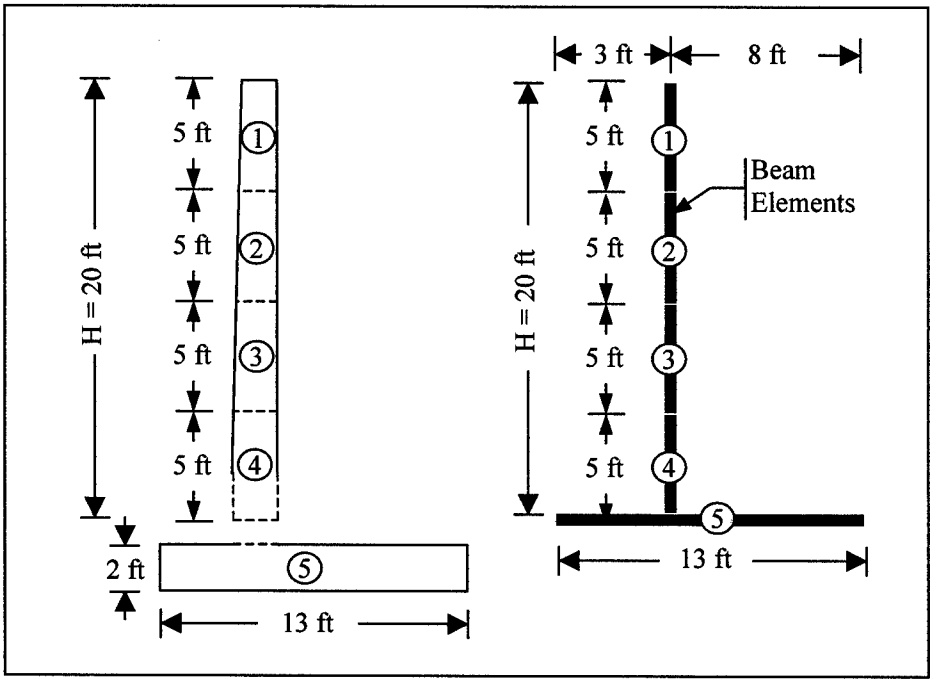

Figure 3-5. Subdivision of the cantilever wall into five segments, each having constant material properties (To convert feet to meters, multiply by 0.3048)

For each of the segments, A_g and ρ were readily determined from the wall geometry and the unit weight of the concrete (i.e., 150 lb/cu ft (2,403 kg/cu m)). A_g and ρ are used in FLAC to compute gravity and inertial forces.

E_c was computed using the following expression (MacGregor 1992):

$$E_c = 57,000 \cdot \sqrt{f'_c} \tag{3-6}$$

In this expression, f'_c is the compressive strength of the concrete (e.g., 4,000 psi (28 MPa) for the wall being modeled), and both E_c and f'_c are in psi. Because the structure is continuous in the direction perpendicular to the analysis plane, E_c needs to be modified using the following expression to account for plane-strain conditions, where 0.2 was assumed for Poisson's ratio for concrete (Itasca Consulting Group, Inc., 2000, FLAC Structural Elements Manual):

$$E_{c\ plane\ strain} = \frac{E_c}{(1-\nu^2)} \tag{3-7}$$

I is dependant on the geometry of the segments, the amount of reinforcing steel, and the amount of cracking in the concrete, where the latter is in turn a function of the static and dynamic loading imposed on the member. Table 3-1 presents values of I for the five wall segments assuming uncracked and fully cracked sectional properties. In dynamic analyses, it is difficult to state a priori whether use of sectional properties corresponding to uncracked, fully cracked, or some intermediate level of cracking will result in the largest demand on the structure. In this first phase of this research investigation, two FLAC analyses were performed assuming the extreme values for I (i.e., $I_{uncracked}$ and $I_{cracked}$). However, using $I = 0.4 \cdot I_{uncracked}$ is a reasonable estimate for the sectional properties for most cases (Paulay and Priestley 1992).

Table 3-1
Second Moment of Area for Wall Segments

Section	$I_{uncracked}$ (ft^4)	$I_{cracked}$ (ft^4)
1	0.339	0.094
2	0.439	0.121
3	0.557	0.152
4	0.694	0.186
5	0.701	0.174

Note: To convert ft^4 to m^4, multiply by 0.008631.

3.3.3 Interface elements

Interface elements were used to model the interaction between the concrete retaining wall and the soil. However, FLAC does not allow interface elements to be used at the intersection of branching structures (e.g., the intersection of the stem and base of the cantilever wall). Of the several attempts by the authors to circumvent this limitation in FLAC, the simplest and best approach found is illustrated in Figure 3-6. As shown in this figure, three very short beam elements, oriented in the direction of the stem, toe side of the base, and heel side of the base, were used to model the base-stem intersection. No interface elements were used on these three beam elements. However, interface elements were used along the other contact surfaces between the soil and wall, as depicted by the green lines in Figure 3-6.

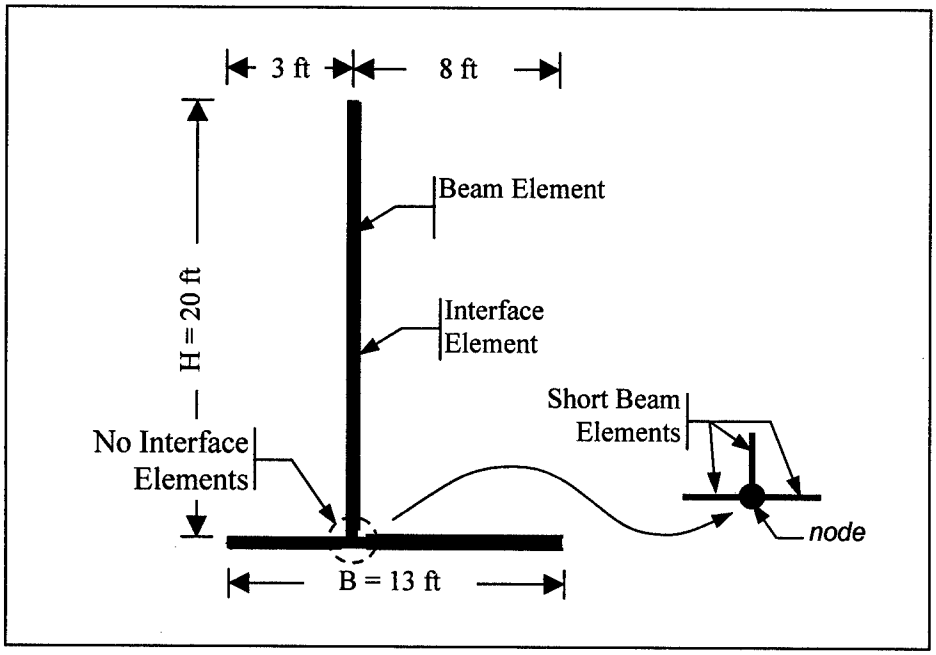

Figure 3-6. Approach to circumventing the limitation in FLAC of not allowing interface elements to be used at branching intersections of structural elements (To convert feet to meters, multiply by 0.3048)

A schematic of the FLAC interface element and the inclusive parameters is presented in Figure 3-7. The element allows permanent separation and slip of the soil and the structure, as controlled by the parameters tensile strength T' and slider S, respectively. For the analyses performed as part of this research investigation, $T' = 0$, thus modeling a cohesionless soil. S was specified as a function of the interface friction angle δ. Based on the values of δ for medium-dense sand against concrete given in Tables 3-7 and 3-8 of Gomez, Filz, and Ebeling (2000b), $\delta = 31$ deg was selected as a representative value.

Normal stiffness k_n. The FLAC manual (Itasca Consulting Group, Inc., 2000, Theory and Background Manual) recommends as a rule of thumb that k_n be set to ten times the equivalent stiffness of the stiffest neighboring zone, i.e.,

$$k_n \approx 10 \cdot \max\left[\frac{K' + \frac{4}{3} \cdot G}{\Delta z_{\min}}\right] \tag{3-8}$$

In this relation, Δz_{min} is the smallest width of a zone in the normal direction of the interfacing surface. The max[ ] notation indicates that the maximum value over all zones adjacent to the interface is used. The FLAC manual warns against using arbitrarily large values for k_n, as is commonly done in finite element analyses, as this results in an unnecessarily small time-step and therefore unnecessarily long computational times.

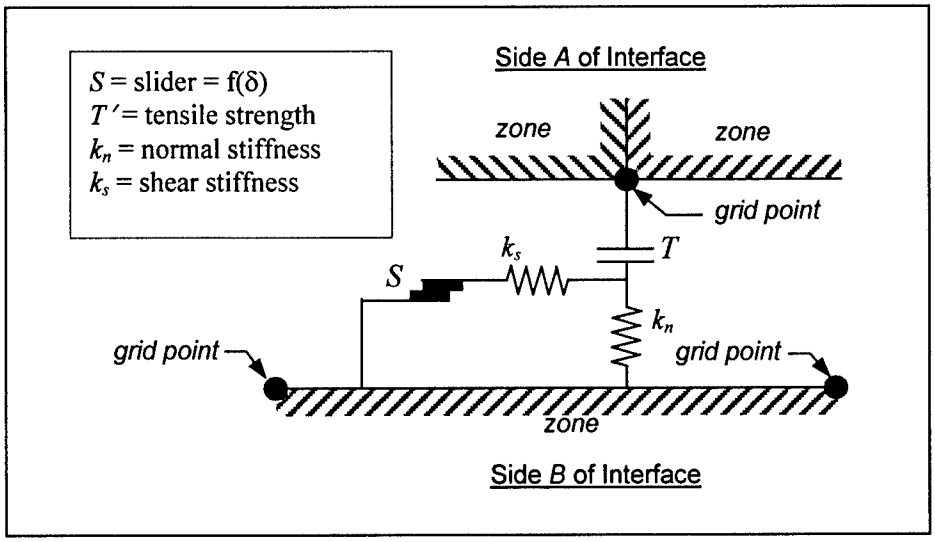

Figure 3-7. Schematic of the FLAC interface element (adapted from Itasca Consulting Group, Inc., 2000, Theory and Background Manual)

Shear stiffness k_s. The determination of k_s required considerably more effort than the determination of the other interface element parameters. In shear, the interface element in FLAC essentially is an elastoplastic model with an elastic stiffness of k_s and yield strength S. k_s values were selected such that the resulting elasto-plastic model gave an approximate fit of the hyperbolic-type interface model proposed by Gomez, Filz, and Ebeling (2000a,b). A comparison of the two models is shown in Figure 3-8 for initial loading (i.e., construction of the wall).

The procedure used to determine k_s values for initial loading is outlined in the following steps. See Gomez, Filz, and Ebeling (2000a,b) for more details concerning their proposed hyperbolic-type model.

a. Compute the reference displacement along the interface Δr using the following expression. Representative values for R_{fj}, K_I, n_j, and δ were obtained from Gomez, Filz, and Ebeling (2000a).

$$\Delta r = \frac{\tau_f}{R_{fj} \cdot K_{si}} \tag{3-9a}$$

where

$$\tau_f = \sigma_n \cdot \tan(\delta) \tag{3-9b}$$

$$K_{si} = K_I \cdot \gamma_w \cdot \left(\frac{\sigma_n}{P_a}\right)^{n_j} \tag{3-9c}$$

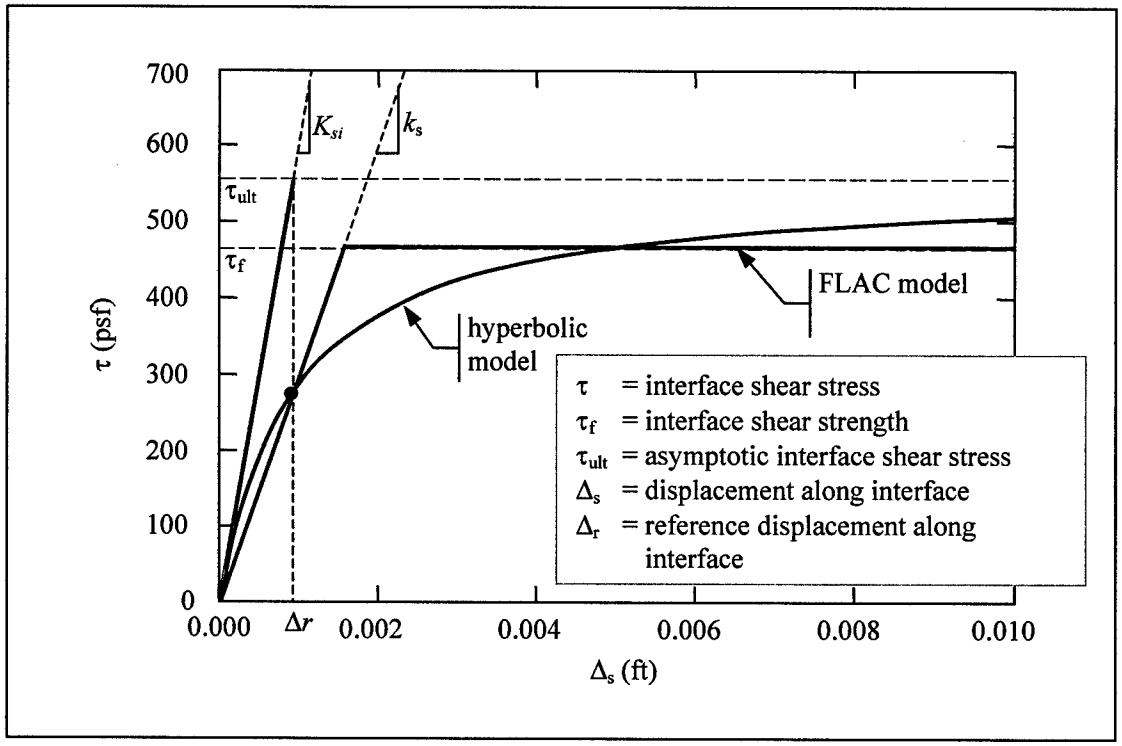

Figure 3-8. Comparison of the Gomez, Filz, and Ebeling (2000a,b) hyperbolic-type interface element model and the approximate-fit elastoplastic model (To convert pounds (force) per square foot to pascals, multiply by 47.88; to convert feet to meters, multiply by 0.3048)

R_{fj} = failure ratio = 0.84

K_{si} = initial shear stiffness of the interface

σ_n = normal stress acting on the interface, and determined iteratively in FLAC by first assuming a small value for k_s and then constructing the wall

δ = interface friction angle = 31 deg

K_I = dimensionless interface stiffness number for initial loading = 21000

γ_w = unit weight of water in consistent units as Δr (i.e., = 62.4 lb/cu ft (1,000 kg/cu m))

P_a = atmospheric pressure in the same units as σ_n

n_j = dimensionless stiffness exponent = 0.8

b. k_s is computed using the following expression:

$$k_s = \frac{1}{\frac{1}{K_I \cdot \gamma_w \cdot \left(\frac{\sigma_n}{P_a}\right)^{n_j}} + \frac{R_{fj} \cdot \Delta r}{\sigma_n \cdot \tan(\delta)}} \tag{3-10}$$

These computed k_s values were used only for the initial construction of the wall. After the construction of the wall and prior to the application of the earthquake loading the k_s values were changed to values consistent with the Gomez-Filz-Ebeling Version I load/unload/reload extended hyperbolic interface model (Gomez, Filz, and Ebeling 2000b). The procedure used to compute k_s for the cyclic loading is outlined in the following equations. Again, refer to Gomez, Filz, and Ebeling for more details concerning this model.

$$k_s = K_{urj} \cdot \gamma_w \cdot \left(\frac{\sigma_n}{P_a}\right)^{n_j} \tag{3-11a}$$

where

$$K_{urj} = C_k \cdot K_I \tag{3-11b}$$

$$C_k = 0.5 \cdot (1 + R_{fj})^2 \tag{3-11c}$$

and

K_{urj} = unload-reload stiffness number for interfaces

C_k = interface stiffness ratio

The interface stiffnesses were computed using Equations 3-8, 3-10, and 3-11 for the interface elements identified in Figure 3-9. The computed values are listed in Table 3-2. The normal stiffnesses were the same for both the initial loading and the unload-reload. However, the shear stiffnesses increased from the initial loading to the unload-reload.

3.3.4 Dimensions of finite difference zones

As mentioned previously, proper dimensioning of the finite difference zones is required to avoid numerical distortion of propagating ground motions, in addition to accurate computation of model response. The FLAC manual (Itasca Consulting Group, Inc., 2000, Optional Features Manual) recommends that the length of the element Δl be smaller than one-tenth to one-eighth of the wavelength λ associated with the highest frequency f_{max} component of the input

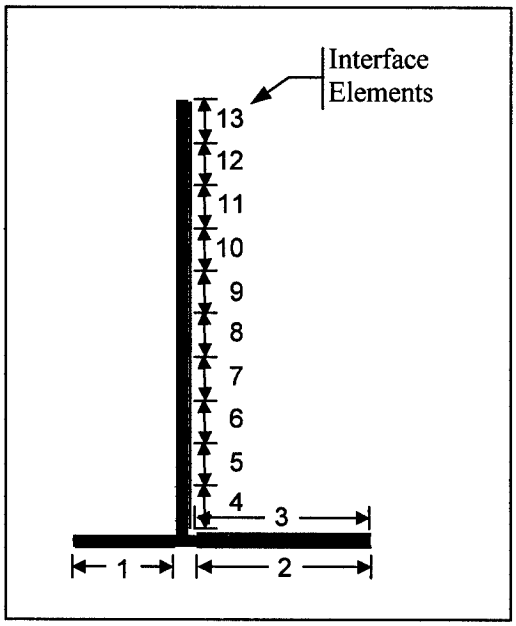

Figure 3-9. Interface element numbering

Table 3-2
k_n and k_s Initial and Unload-reload Values for Interface Elements

Interface Element Number	k_n lbf/ft²/ft	$k_{s\ initial\ loading}$ lbf/ft²/ft	$k_{s\ unload\text{-}reload}$ lbf/ft²/ft
1	1.203×10^{8}	7.875×10^{5}	2.666×10^{6}
2	1.203×10^{8}	6.709×10^{5}	2.379×10^{6}
3	1.073×10^{8}	9.967×10^{5}	3.374×10^{6}
4	1.073×10^{8}	9.012×10^{5}	3.051×10^{6}
5	1.073×10^{8}	3.056×10^{5}	1.035×10^{6}
6	1.073×10^{8}	2.647×10^{5}	8.963×10^{5}
7	9.657×10^{7}	2.255×10^{5}	7.634×10^{5}
8	9.657×10^{7}	1.827×10^{5}	6.185×10^{5}
9	8.356×10^{7}	1.491×10^{5}	5.050×10^{5}
10	8.356×10^{7}	1.214×10^{5}	4.110×10^{5}
11	8.356×10^{7}	7.971×10^{4}	2.699×10^{5}
12	6.398×10^{7}	4.641×10^{4}	1.571×10^{5}
13	6.398×10^{7}	2.465×10^{4}	8.345×10^{4}

Note: To convert lbf/ft²/ft to pascals per meter, multiply by 157.09

motion. The basis for this recommendation is a study by Kuhlemeyer and Lysmer (1973). Interestingly, the FLUSH manual (Lysmer et al. 1975) recommends Δl be smaller than one-fifth the λ associated with f_{max}, also referencing Kuhlemeyer and Lysmer (1973) as the basis for the recommendation, i.e.,:

FLAC	*FLUSH*	
$\Delta l \leq \frac{\lambda}{10}$	$\Delta l \leq \frac{\lambda}{5}$	(3-12)

λ is related to the shear wave velocity of the soil v_s and the frequency f of the propagating wave by the following relation:

$$\lambda = \frac{v_s}{f} \tag{3-13}$$

In a FLUSH analysis it is important to note that the v_s used in this computation is not that for small (shear) strains, such as measured in the field using cross-hole shear wave tests. In FLUSH, the v_s used to dimension the elements should be consistent with the earthquake-induced shear strains, frequently referred to as the "reduced" v_s by FLUSH users. Assuming that the response of the retaining wall will be dominated by shear waves, substitution of Equation 3-13 into the FLAC expression for Δl in Equation 3-12 gives:

$$\Delta l \leq \frac{v_s}{10 \cdot f_{\max}} \tag{3-14a}$$

$$f_{\max} \leq \frac{v_s}{10 \cdot \Delta l} \tag{3-14b}$$

As may be observed from these expressions, the finite difference zone with the lowest v_s and a given Δl will limit the highest frequency that can pass through the zone without numerical distortion. For the FLAC analyses performed in Phase 1 of this investigation, 1-ft by 1-ft (0.3-m by 0.3-m) zones were used in subgrids 1 and 2 (Figure 3-3). The top layer of the backfill has the lowest v_s (i.e., 525 fps (160 m/sec)). Using these expressions and Δl = 1 ft (0.3 m), the finite difference grid used in the FLAC analyses should adequately propagate shear waves having frequencies up to 52.5 hz. This value is well above the 15-hz cutoff frequency used in the SHAKE analysis to compute the input motion for the FLAC analysis and well above the estimated fundamental frequency of the retaining wall-soil system being modeled.

3.3.5 Damping

An elastoplastic constitutive model in conjunction with the Mohr-Coulomb failure criterion was used to model the soil in FLAC. Inherent in this model is the characteristic that once the induced dynamic shear stresses exceed the shear strength of the soil, the plastic deformation of the soil introduces considerable hysteretic damping. However, for dynamic shear stresses less than the shear strength of the soil, the soil behaves elastically (i.e., no damping), unless additional mechanical damping is specified. FLAC allows mass proportional, stiffness proportional, and Rayleigh damping to be specified, where the latter provides relatively constant level of damping over a restricted range of

frequencies. Use of either stiffness proportional or Rayleigh damping results in considerably longer run times than when either no damping or mass proportional damping is specified.

For the FLAC analyses performed, Rayleigh damping was specified, for which the critical damping ratio ξ may be determined by the following relation:

$$\xi = \frac{1}{2} \cdot \left(\frac{\alpha}{\omega} + \beta \cdot \omega \right) \tag{3-15}$$

where

α = the mass-proportional damping constant

β = the stiffness-proportional damping constant

ω = angular frequency associated with ξ

For Rayleigh damping, the damping ratio and the corresponding central frequency need to be specified. Judgment is required in selecting values for both parameters. A lower bound for the damping ratio is 1 to 2 percent. This level helps reduce high-frequency spurious noise. However, considerable high-frequency noise will still exist even when 1 to 2 percent Rayleigh damping is specified; this is an inherent shortcoming of an explicit solution algorithm. The damping levels in the last iteration of SHAKE analysis used to compute the FLAC input motion may be used as an upper bound of the values for Rayleigh damping. The central frequency corresponding to the specified damping ratio is typically set to either the fundamental period of the system being modeled (an inherent property of the soil-wall system) or predominant period of the system response (an inherent property of the soil-wall system and the ground motion). For the FLAC analyses performed as part of the first phase of this investigation, the SHAKE computed damping ratios were used and the central frequency was set equal to the fundamental frequency of the retaining wall-soil system. In future FLAC analyses, the damping ratios will be set to half the values from the SHAKE analysis.

3.4 Summary

When a physical system is modeled numerically, considerable judgment is required in selecting appropriate values for the model parameters. This chapter provided an overview of the models used in the FLAC analyses of the cantilever retaining wall and discussed approaches for selecting values for the various model parameters. In the next chapter, the results from the FLAC analyses are presented and put into perspective of the current Corps design procedure, as presented in Ebeling and Morrison (1992).

4 FLAC Data Reduction Discussion of Results

In the previous chapter, an overview was given of the numerical model used to analyze the cantilever retaining wall. In this chapter an overview is given on how the FLAC data were reduced, followed by a presentation and discussion of the reduced data. Two FLAC analyses were performed as part of the first phase of this research effort, one using the uncracked properties of the concrete wall, and the other using the fully cracked properties (refer to Table 3-1 for the listing of the respective properties). The results from the two analyses were similar. However, more information was computed in the FLAC analysis of the fully cracked wall (i.e., additional acceleration time-histories in the foundation and backfill soil and displacement time-histories along the wall were requested in the FLAC input file for the cracked wall). Accordingly, the results of the FLAC analysis of the cracked wall are primarily discussed in this chapter.

4.1 Data Reduction

Time-histories for the lateral stresses acting on the elements composing the stem and heel section were computed by FLAC, as well as acceleration time-histories at various places in the foundation soil and backfill and displacement time-histories at various places on the wall. The stresses computed by FLAC are averages of the stresses acting across the elements, which is similar to using constant strain triangular elements in the FEM. From the FLAC computed stresses, the resultant forces and the points of applications were computed for both the stem and heel sections. The resultant force and its point of application on the stem are needed for the structural design of the stem, while the resultant force and its point of application on the heel section are required for the global stability of the structural wedge.

Two approaches were used to determine the resultant forces acting on the stem and heel sections from the FLAC computed stresses. In the first approach, constant stress distributions across the elements were assumed, while in the second approach, linearly varying stress distributions were assumed. The details of the approaches are discussed in the following subsections.

4.1.1 Determination of forces assuming constant-stress distribution

The first approach used to determine the forces acting on the stem and heel section assumed constant stress distributions across the elements, as illustrated in Figure 4-1 for three of the beam elements used to model a portion of the stem.

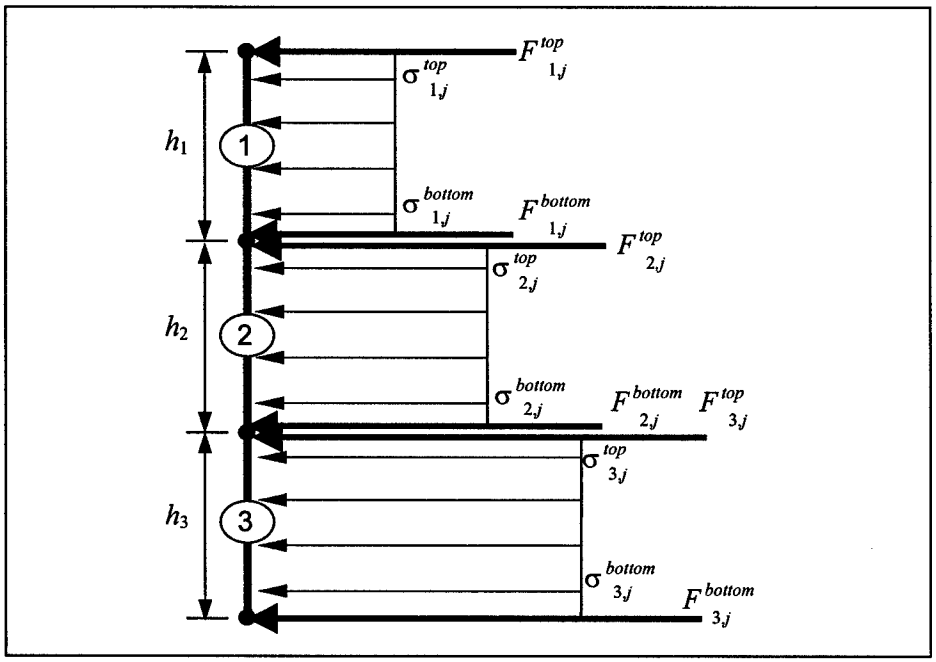

Figure 4-1. Assumed constant stress distribution across elements, at time t_j, used to compute the forces acting on the stem and heel section in the first approach

For the assumed constant stress distributions, the forces acting on the top and bottom nodes of each beam element, shown as red dots in Figure 4-1, were computed using the following expressions:

$$F_{i,j}^{top} = \frac{1}{2} \cdot h_i \cdot \sigma_{i,j}^{top} = \frac{1}{2} \cdot h_i \cdot \sigma_{i,j} \tag{4-1a}$$

$$F_{i,j}^{bottom} = \frac{1}{2} \cdot h_i \cdot \sigma_{i,j}^{bottom} = \frac{1}{2} \cdot h_i \cdot \sigma_{i,j} \tag{4-1b}$$

where

$F_{i,j}^{top}$ = force acting on the top node of element i and at time increment j

h_i = length of element i

$\sigma_{i,j}^{top}$ = lateral stress acting on the top of element i and at time increment j

$\sigma_{i,j}$ = average lateral stress acting on element i and at time increment j

$F_{i,j}^{bottom}$ = force acting on the bottom node of element i and at time increment j

$\sigma_{i,j}^{bottom}$ = lateral stress acting on the bottom of element i and at time increment j

The total force acting on the stem or heel section P_j at time increment j was determined by:

$$P_j = \sum_i \left(F_{i,j}^{top} + F_{i,j}^{bottom} \right) = \sum_i h_i \cdot \sigma_{i,j} \tag{4-2}$$

4.1.2 Determination of forces assuming linearly varying stress distribution

In the second approach used to determine the forces acting on the stem and heel sections, linearly varying stress distributions across the elements were assumed, as illustrated in Figure 4-2. This approach is analogous to using a first-order shape function in the FEM. To apply this approach, the only actual nodes considered were the nodes at the top and bottom of the wall, shown as red dots in Figure 4-2. In addition to these two actual nodes, the centers of the elements were treated as nodes, shown as green dots in Figure 4-2. The magnitudes of the stresses on the green nodes were assumed equal to the average stresses computed by FLAC for the corresponding elements. The magnitudes of the stresses acting on the red nodes were determined by linearly extrapolating the stresses from the neighboring green nodes. In Figure 4-2, newly defined "elements" and "nodes" are numbered with primes (e.g., 3′) to distinguish them from the actual nodes and elements shown in Figure 4-1. Additionally, for comparison, the constant stress distribution assumed in the previous approach is shown as a dashed gray line in Figure 4-2, as well as the linearly varying stress distributions (blue lines), assumed in the current approach.

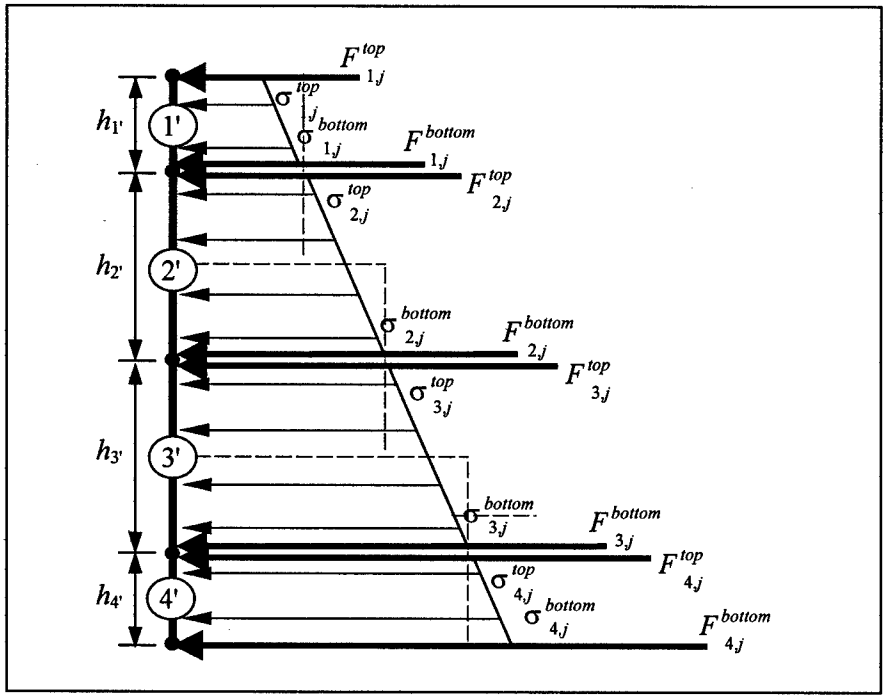

Figure 4-2. Assumed linearly varying stress distribution across elements, at time t_j, used to compute forces on stem and heel sections in the second approach

For the assumed linearly varying stress distribution, the forces acting on the top and bottom nodes of the newly designated elements shown in Figure 4-2 were computed using the following expressions.

$$F^{top}_{i',j} = h_{i'} \cdot \left(\frac{\sigma^{top}_{i',j}}{3} + \frac{\sigma^{bottom}_{i',j}}{6} \right) \tag{4-3a}$$

$$F^{bottom}_{i',j} = h_{i'} \cdot \left(\frac{\sigma^{top}_{i',j}}{6} + \frac{\sigma^{bottom}_{i',j}}{3} \right) \tag{4-3b}$$

The total force acting on a node is the sum of *bottom* force from the element above and the *top* force from the element below, i.e., $F^{bottom}_{i',j}$ and $F^{top}_{i'+1,j}$, respectively. The total force acting on the stem and heel section were computed using the following expressions:

$$\begin{aligned} P_j &= \sum_{i'} \left(F^{bottom}_{i',j} + F^{top}_{i'+1,j} \right) \\ &= \sum_{i'} \left\{ h_{i'} \cdot \left(\frac{\sigma^{top}_{i',j}}{6} + \frac{\sigma^{bottom}_{i',j}}{3} \right) + h_{i'+1} \cdot \left(\frac{\sigma^{top}_{i'+1,j}}{3} + \frac{\sigma^{bottom}_{i'+1,j}}{6} \right) \right\} \end{aligned} \tag{4-4}$$

The resultant forces computed assuming the constant and linearly varying stress distributions were essential identical.

4.1.3 Incremental dynamic forces

In addition to computing the total resultant forces acting on the stem and heel sections, the incremental dynamic forces ΔP_j at time increment j were computed. ΔP_j is the difference between the total resultant force P_j at time increment j minus the total resultant force prior to shaking (i.e., P_j at $j = 0$, designated as P_{static}):

$$\Delta P_j = P_j - P_{static} \tag{4-5}$$

Because P_j values computed assuming constant and linearly varying stress distributions were essentially identical, ΔP_j was computed only using P_j for the constant stress distribution.

4.1.4 Reaction height of forces

The points of application of the total and incremental dynamic resultant forces were computed for the stem and heel sections in terms of their vertical distances above the base of the wall. For the total resultant forces, the vertical distances Y were computed using the following relation:

$$Y_j = \frac{\sum_i h_i \cdot \sigma_{i,j} \cdot y_i}{\sum_i h_i \cdot \sigma_{i,j}} \tag{4-6}$$

where

Y_j = vertical distance from the base of the retaining wall to the point of application of the total resultant force acting on the stem or heel section at time increment j

y_i = vertical distance from the base of the retaining wall to the center of element i

The vertical distances ΔY from the base of the retaining wall to the points of application of ΔP_j acting on the stem or heel section were computed using the following relation:

$$\Delta Y_j = \frac{P_j \cdot Y_j - P_{static} \cdot Y_{static}}{\Delta P_j} \tag{4-7}$$

In this equation, Y_{static} is the vertical distance from the base of the retaining wall to the point of application of the total resultant force acting on the stem or heel section prior to the shaking (i.e., Y_j at $j = 0$).

4.2 Presentation and Discussion of Reduced Data

Using the procedures described in the preceding section, the total and dynamic incremental resultant forces acting on the stem and heel sections were determined from the FLAC computed stresses, as well as the corresponding vertical distance above the base at which the resultant forces act. Additionally, the permanent relative displacements of the wall computed in the FLAC analysis are compared with those predicted using a Newmark sliding block-type analysis procedure, e.g., CWROTATE (Ebeling and White, in preparation). Finally, a brief discussion is given concerning the deformed shape of the wall-soil system at the end of shaking.

4.2.1 Total resultant forces and points of action

The horizontal acceleration a_h and the corresponding dimensionless horizontal inertial coefficient k_h at approximately the middle of the backfill portion of the structural wedge were computed during the FLAC analyses, as shown in Figure 4-3. Appendix B gives the appropriate sign convention related to a_h and k_h. In this figure, the potential active and passive failure planes are shown for illustration only. The k_h time-history shown in this figure is that to which reference is made during the remainder of this chapter, unless otherwise noted.

The k_h time-history shown in Figure 4-3 is repeated in Figure 4-4a and in Figure 4-4b for reference purposes (i.e., the time-histories in Figures 4-3, 4-4a, and 4-4b are identical). Assuming constant stress distributions across the elements, Equation 4-2 was used to compute the time-histories of the resultant forces acting on the stem and heel sections (P_{stem} and P_{heel}, respectively), presented as Figures 4-4c and d, respectively. Equation 4-6 was used to compute time-histories of the vertical distances from the base of the wall to the point of application of the resultant forces acting on the stem and heel sections (Y_{stem} and Y_{heel}, respectively). These time-histories are presented, normalized by the height of the wall H, in Figures 4-4e and f. Finally, the time-histories of the resultant forces multiplied by the corresponding vertical distances above the base at which they act for the stem and heel sections ($(Y \cdot P)_{stem}$ and $(Y \cdot P)_{heel}$, respectively) are presented in Figures 4-4g and h, respectively.

Several interesting trends may be observed from the time-histories presented in Figure 4-4. First, P_{stem} and P_{heel} are essentially at active earth pressure conditions K_A prior to shaking, which is somewhat unexpected. The factor of safety against sliding in the static design of the wall, per Corps design procedures (refer to Appendix A), precludes the required movements to develop active

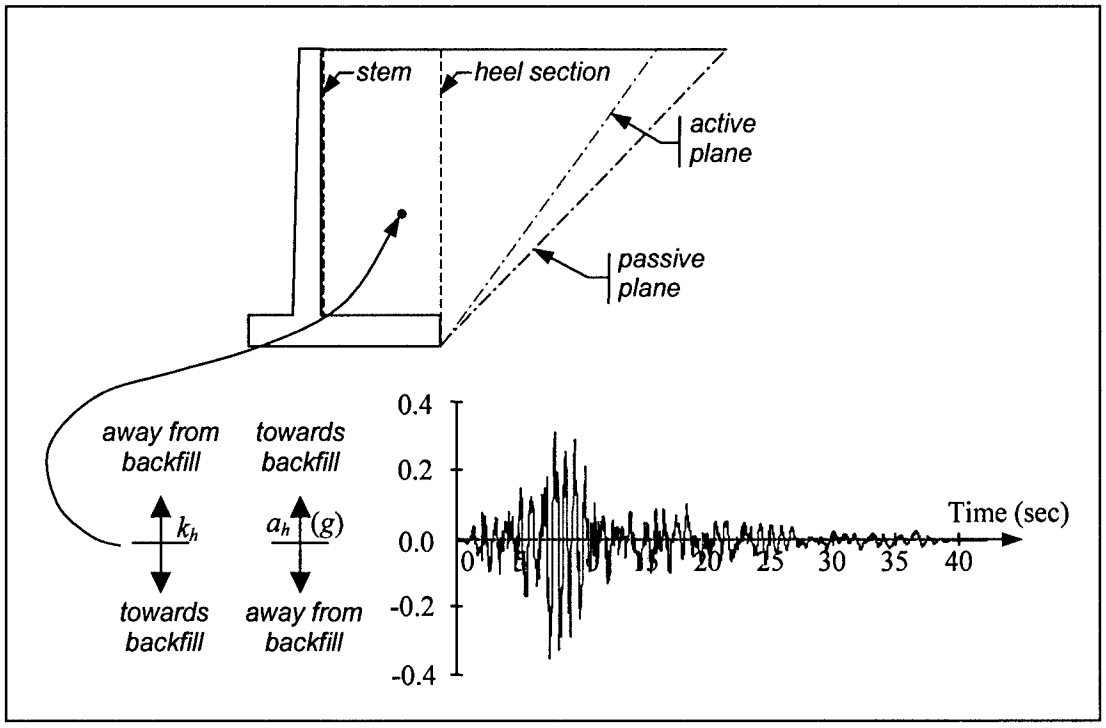

Figure 4-3. Horizontal acceleration a_h, and corresponding dimensionless horizontal inertial coefficient k_h, of a point in the backfill portion of the structural wedge

conditions under static loading. Subsequent FLAC analyses of the "numerical construction" phase of the wall will be performed to more fully understand this stress condition. Another observation concerning the lateral earth pressures is that at the end of shaking, the residual earth pressures are approximately equal to at-rest K_o conditions for both the stem and heel sections. Similar increases in the earth pressures were found in other studies, both numerical and laboratory (i.e., centrifuge and shake table), as outlined in Whitman (1990). Additionally, the maximum value of P_{heel} is larger than the maximum value of P_{stem}, while P_{stem} shows a much larger cyclic fluctuation and at several points dips slightly below initial K_A conditions. Although difficult to see from Figure 4-4 due to the scales, P_{stem} is in phase with k_h, while P_{heel} is out of phase with k_h (i.e., the peaks in one time-history coincide with the troughs of the other time-history). Trends in the relative magnitude of the resultant forces acting on the stem and heel sections, and their phasing with k_h, can be more easily observed when presented in terms of the lateral earth pressure coefficients K. The following expression relates P and K at a given time increment j:

$$K_j = \frac{2 \cdot P_j}{\gamma_t \cdot H^2 \cdot (1 - k_{v\,j})} \tag{4-8}$$

where k_{vj} is the vertical inertial coefficient at time increment j (assumed to be zero).

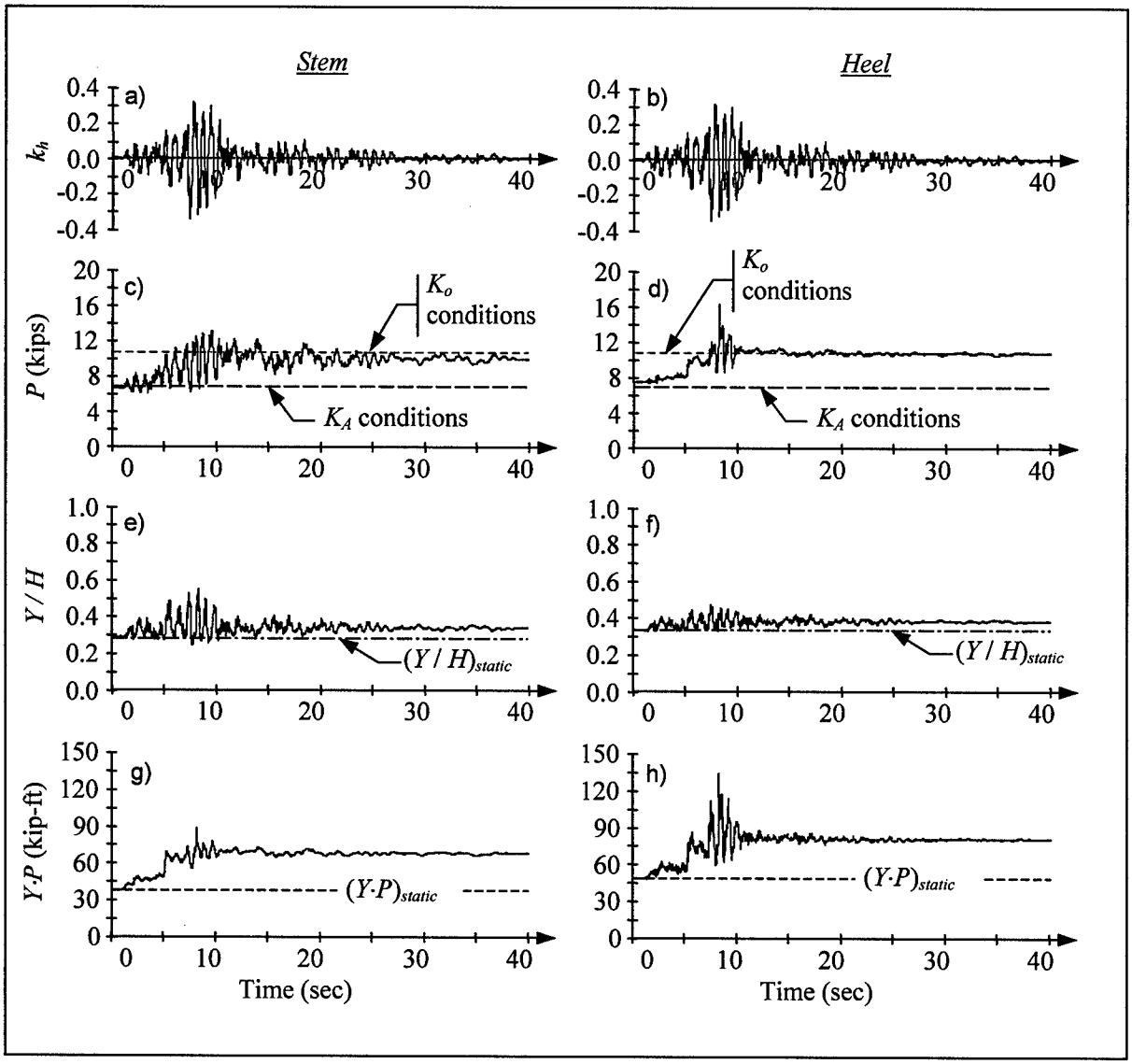

Figure 4-4. Time-histories of *P*, *Y/H* and *Y·P* for the stem and heel sections (To convert kip-feet to Newton-meters, multiply by 1,355.8; to convert kips to newtons, multiply by 4,448)

Using this expression, K values were computed for the stem and heel sections at the peaks and troughs during the strong motion portion of the k_h time-history (i.e., 5-10 sec, approximately). The K values thus computed are plotted as functions of their corresponding absolute values of k_h in Figure 4-5. Additionally, the active and passive dynamic earth pressure coefficients (K_{AE} and K_{PE}, respectively) computed using the Mononobe-Okabe expressions given in Appendix B are shown in Figure 4-5.

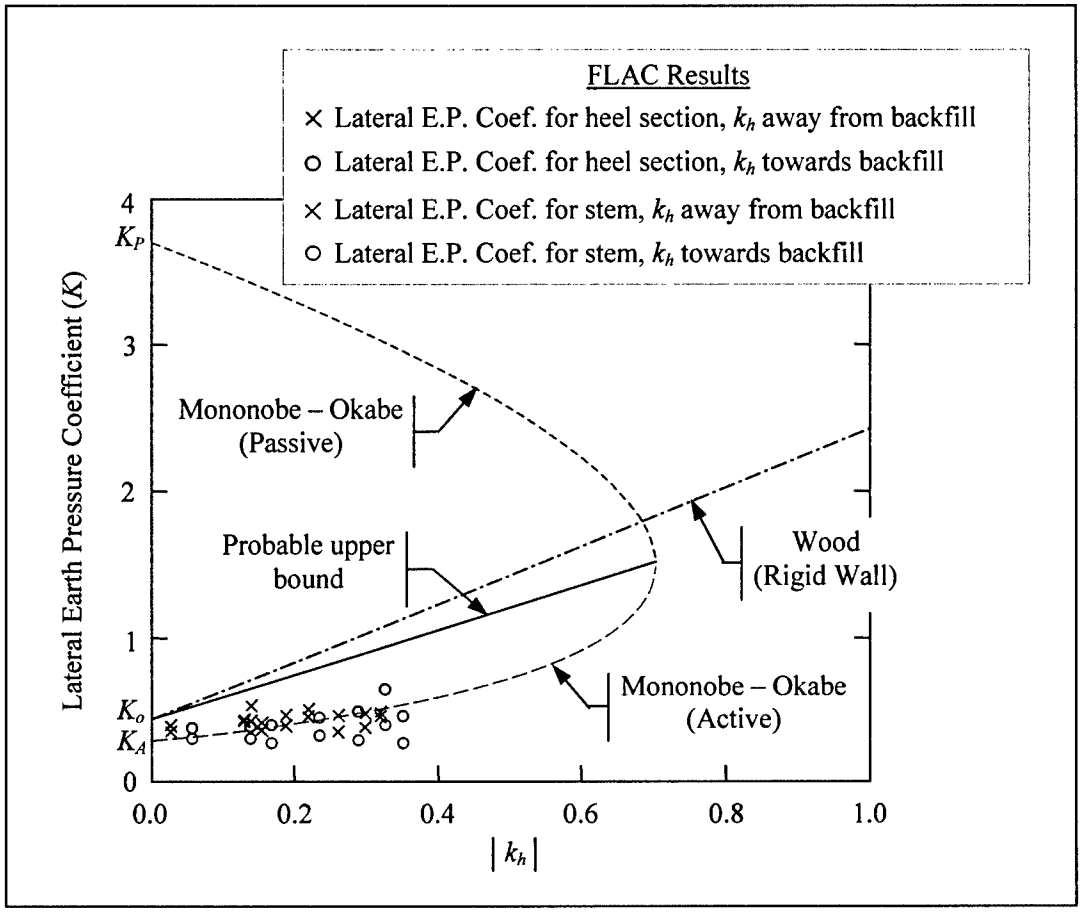

a. Entire range of interest

Figure 4-5. Comparison of lateral earth pressure coefficients computed using the Mononobe-Okabe active and passive expressions (yielding backfill), Wood expression (non-yielding backfill), and FLAC (Continued)

A portion of the plot in Figure 4-5a is enlarged in Figure 4-5b. Additionally the k_h time-history is given with the peaks and troughs identified that correspond to the computed K values. Several distinct trends may be observed from Figure 4-5:

a. $K_{heel} > K_{stem}$ when $k_h < 0$ (i.e., when k_h is directed toward the backfill).

b. $K_{stem} > K_{heel}$ when $k_h > 0$ (i.e., when k_h is directed away from the backfill).

c. The largest K_{stem} occurs when $k_h > 0$ (i.e., when k_h is directed away from the backfill).

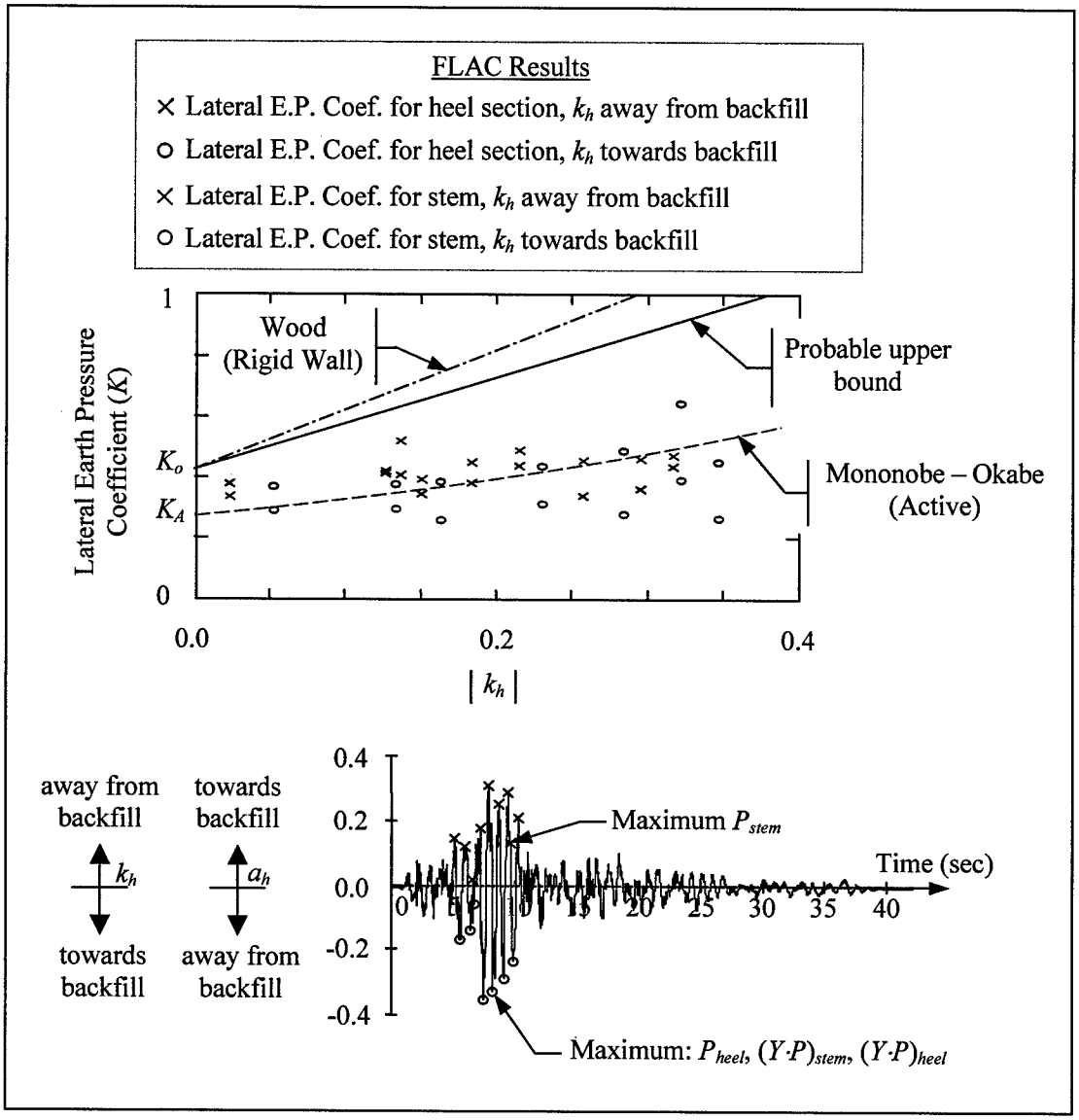

b. Enlargement of range of FLAC computed values

Figure 4-5. (Concluded)

d. The largest K_{heel} occurs when $k_h < 0$ (i.e., when k_h is directed toward the backfill).

e. The computed K values show a general scatter around the curve for the Mononobe-Okabe dynamic active earth pressure curve.

The shape of the Mononobe-Okabe active and passive dynamic earth pressure curves warrant discussion. As k_h increases, K_{AE} increases, while K_{PE} decreases. For the conditions examined (i.e., horizontal backfill, vertical wall, zero interface friction between the structural and driving wedges, $k_v = 0$), K_{AE} and

K_{PE} reach the same limiting value. The limiting K value occurs when the angles of the active and passive failure planes (which are assumed to be planar in the Mononobe-Okabe formulation) become horizontal; refer to Appendix B for expressions for angles of the failure planes.

For comparison purposes, the earth pressure coefficient for nonyielding backfills is also plotted in Figure 4-5. A wall retaining a nonyielding backfill does not develop the limiting dynamic active or passive earth pressures because sufficient wall movements do not occur to mobilize the full shear strength of the backfill, such as is the case with massive concrete gravity retaining walls founded on firm rock. Wood (1973) developed a procedure, which was simplified in Ebeling and Morrison (1992), Section 5.2, to determine the lateral dynamic earth pressures on structures with nonyielding backfills. The following expression is from Ebeling and Morrison (1992), Equation 68:

$$F_{sr} = \gamma \cdot H^2 \cdot k_h \tag{4-9}$$

where

F_{sr} = lateral seismic force component

γ = unit weight of the soil

By treating F_{sr} as the dynamic incremental force, the equivalent earth pressure coefficient was computed by substituting F_{sr} into Equation 4-8 for P and adding K_o to the result. The resulting curve, shown in Figure 4-5, will likely be a conservative upper bound of the earth pressures that will occur on the heel section of a cantilever wall. However, a more probable upper bound is that formed by a line drawn from K_o pressure for $k_h = 0$ and the intersection of K_{AE} and K_{PE} at their limiting values. Further FLAC analyses will be performed to verify this hypothesized upper bound.

Similar to the trends in P_{stem} and P_{heel}, Y/H for the stem and heel sections (i.e., Y/H_{heel} and Y/H_{stem}, respectively) also show increasing trends as the shaking progresses, with Y/H_{stem} having greater cyclic fluctuation than Y/H_{heel}. Of particular note is that Y/H_{stem} is out of phase with both k_h and P_{stem}, while Y/H_{heel} is out of phase with k_h, but in phase with P_{heel}. As a result of the phasing, $(Y \cdot P)_{heel}$ has considerably larger cyclic fluctuations and peak value than $(Y \cdot P)_{stem}$.

The magnitudes of Y_{stem} and Y_{heel} are directly related to the distribution of stresses along the stem and heel sections, respectively. The stress distributions, resultant forces, and deformed shape of the cantilever wall corresponding to maximum values of P_{stem}, P_{heel}, $(Y \cdot P)_{stem}$, and $(Y \cdot P)_{heel}$ are shown in Figure 4-6, where the maximum values for P_{heel}, $(Y \cdot P)_{stem}$, and $(Y \cdot P)_{heel}$ all occur at the same instant in time. The maximum value of P_{stem} occurs while $k_h > 0$ (i.e., k_h is

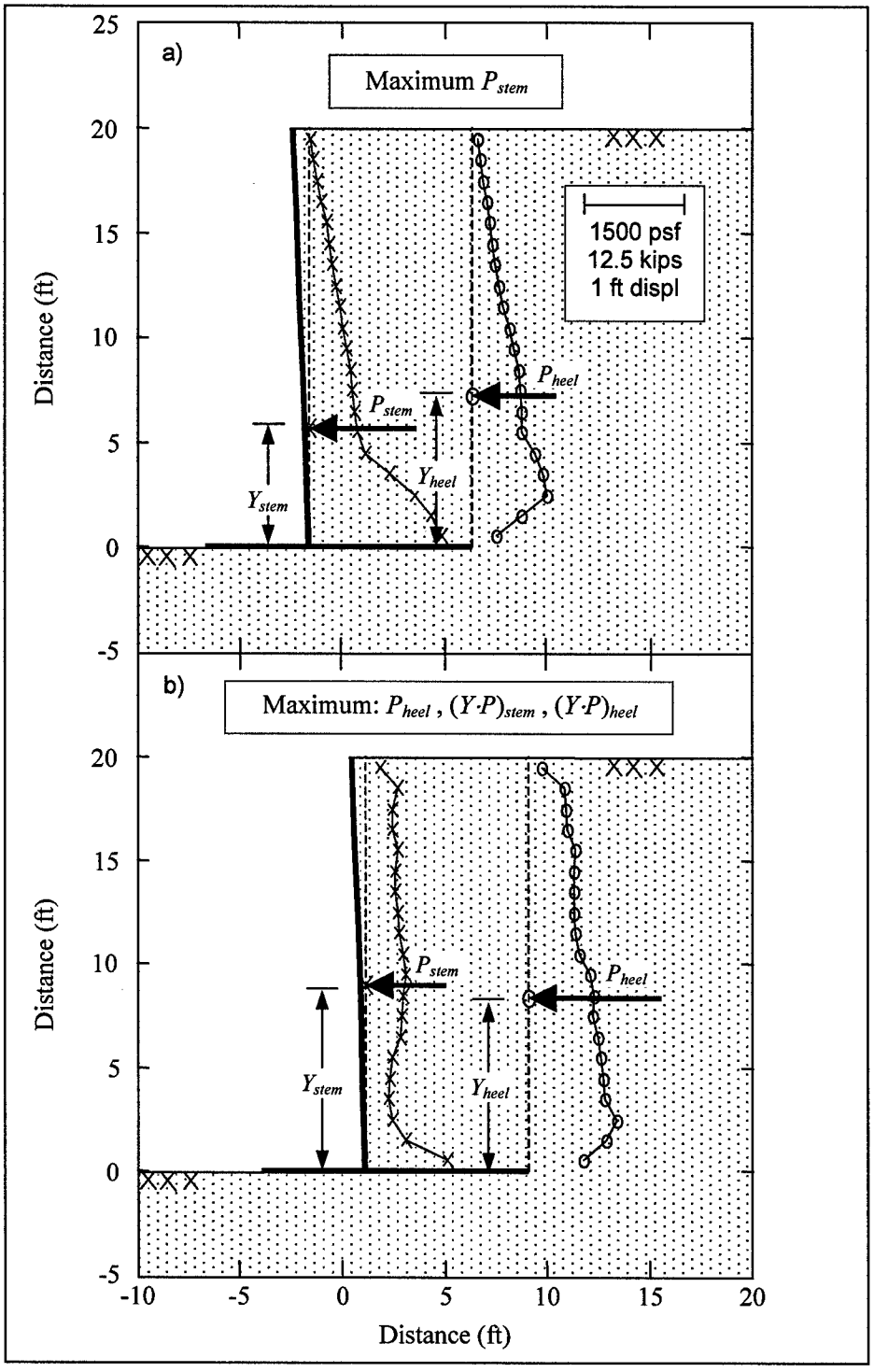

Figure 4-6. Stress distributions and total resultant forces on the stem and heel sections at times corresponding to the following: (a) maximum value for P_{stem} and (b) the maximum values for P_{heel}, $(Y{\cdot}P)_{stem}$, and $(Y{\cdot}P)_{heel}$ (To convert feet to meters, multiply by 0.3048; to convert psf to pascals, multiply by 47.88; to convert kips to newtons, multiply by 4,448)

directed away from the backfill); refer to the k_h time-history in Figure 4-5b. The relatively triangular-shaped stress distributions on the stem and heel sections shown in Figure 4-6a are characteristic of those occurring at the peaks in the k_h time-history. The points of action of the resultant forces on stem and heel sections are approximately equal to those prior to the start of the shaking.

The maximum values of P_{heel}, $(Y{\cdot}P)_{stem}$, and $(Y{\cdot}P)_{heel}$ occur while $k_h < 0$ (i.e., k_h is directed toward the backfill); again, refer to the k_h time-history in Figure 4-5b. The relatively uniform stress distributions on the stem and heel sections shown in Figure 4-6b are characteristic of those occurring at the troughs in the k_h time-history. The points of action of the resultant forces on stem and heel sections are approximately at midheight of the wall, and therefore higher than the static values.

4.2.2 Ratio of total resultant forces and points of action

Given the difference in the phasing of the stem and heel section time-histories, it is only of limited value to examine the ratios of the respective time-histories for the stem and heel sections, which are presented in Figure 4-7. For example, from examination of Figure 4-7b, P_{stem}/P_{heel}, one might conclude that the maximum value for P_{stem} is larger than the maximum value for P_{heel}, which is clearly not the case, as may be seen from Figure 4-4c and d. Similar misinterpretations can be made in relation to the ratios of the other time-histories presented in Figure 4-7.

4.2.3 Incremental resultant forces and points of action

As an alternate to presenting the total resultant force of the lateral earth pressures, Seed and Whitman (1970) expressed the resolved lateral earth pressures in terms of a static active resultant (P_{static}) and a dynamic incremental resultant (ΔP), as discussed previously in Section 4.1.3. Seed and Whitman's (1970) procedure is outlined in Ebeling and Morrison (1992), Section 4.2.2.

Using Equations 4-5 and 4-7, time-histories for ΔP acting on the stem and heel sections and their corresponding height ΔY above the base of the wall were determined from the FLAC computed stresses. The computed time-histories for ΔP and $\Delta Y{\cdot}\Delta P$ are shown in Figure 4-8. P_{static} is included in Figure 4-8c and d for reference purposes only. The computed time-histories of ΔY were not included in this figure because the extreme ranges of the ΔY values and the erratic characteristics of the time-histories made them impossible to present in an intelligible manner.

In addition to the results computed from the FLAC stresses, the simplified procedure proposed by Seed and Whitman (1970), and outlined in Ebeling and Morrison (1992), Section 4.2.2, was used to compute ΔP, ΔY, and $\Delta P{\cdot}\Delta Y$, i.e.,:

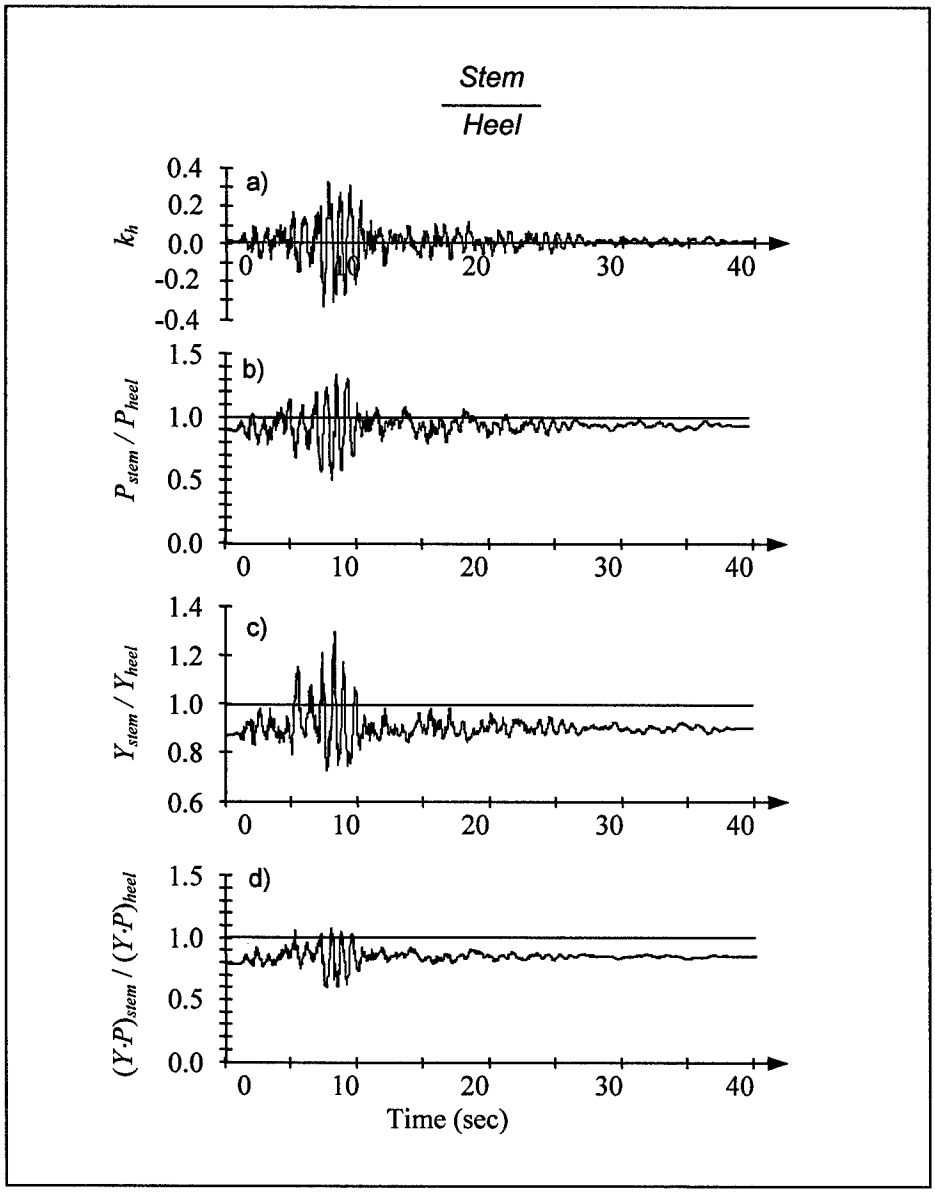

Figure 4-7. Time-histories of P_{stem} / P_{heel}, Y_{stem} / Y_{heel}, and $(Y \cdot P)_{stem} / (Y \cdot P)_{heel}$

$$\Delta P_{Seed\ and\ Whitman} = \frac{3}{8} \cdot k_h \cdot \gamma_t \cdot H^2 \tag{4-10a}$$

$$\Delta Y_{Seed\ and\ Whitman} = 0.6 \cdot H \tag{4-10b}$$

$$(\Delta P \cdot \Delta Y)_{Seed\ and\ Whitman} = 0.225 \cdot k_h \cdot \gamma_t \cdot H^3 \tag{4-10c}$$

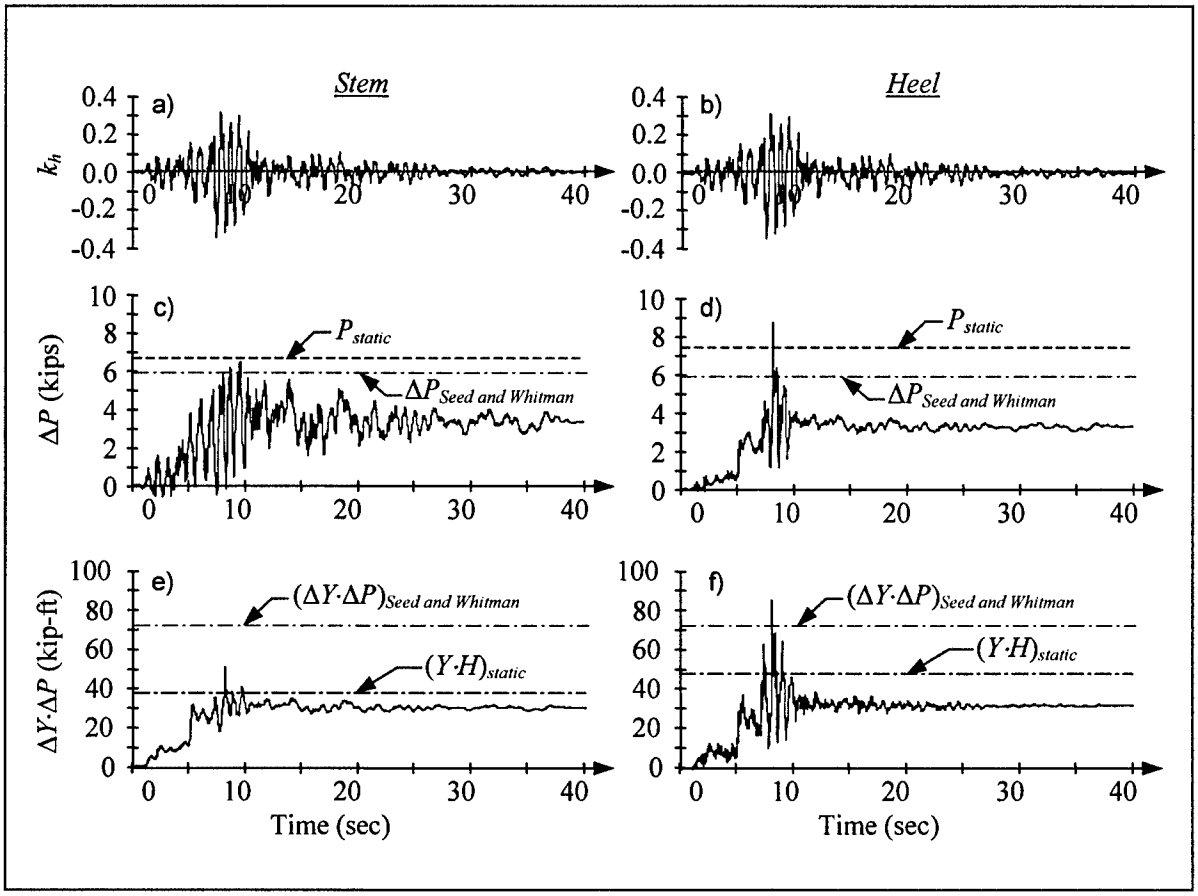

Figure 4-8. Time-histories of ΔP and $\Delta Y \cdot \Delta P$ for the stem and heel sections (To convert kips to newtons, multiply by 4,448; to convert kip-feet to newton-meters, multiply by 1,355.8)

The validity of these expressions is limited to specific values of ϕ, θ, δ, and β (the refer to Appendix B for definitions of these variables). More general expressions for ΔP and ΔY, which are likely more applicable to most Corps projects, are given in Ebeling and Morrison (1992), Section 4.2.2.

Setting k_h equal to the maximum peak value (i.e., $k_h = 0.32$), $\Delta P_{Seed\ and\ Whitman}$, $\Delta Y_{Seed\ and\ Whitman}$, and $(\Delta Y \cdot \Delta P)_{Seed\ and\ Whitman}$ were computed using Equations 4-10a, b, and c; and $\Delta P_{Seed\ and\ Whitman}$ and $(\Delta Y \cdot \Delta P)_{Seed\ and\ Whitman}$ are presented in Figure 4-8. As may be observed in Figure 4-8c, $\Delta P_{Seed\ and\ Whitman}$ is very close to the maximum value of ΔP_{stem} from the FLAC results. However, this may be coincidental given that ΔP_{stem} does not coincide with the maximum peak in the k_h time-history. $\Delta P_{Seed\ and\ Whitman}$ is less than maximum value of ΔP_{heel}, which is associated with a high frequency spike. Most notable of the observed trends in Figure 4-8 is that the maximum value of $(\Delta Y \cdot \Delta P)_{stem}$ is considerably less than the maximum value of $(\Delta Y \cdot \Delta P)_{heel}$ and $(\Delta Y \cdot \Delta P)_{Seed\ and\ Whitman}$. In regard to the comparison of the maximum values of $(\Delta Y \cdot \Delta P)_{stem}$ and $(\Delta Y \cdot \Delta P)_{heel}$, the difference is due largely to

the phasing of the respective ΔY and ΔP time-histories, where ΔY_{stem} and ΔP_{stem} are out of phase with each other, while ΔY_{heel} and ΔP_{heel} are in phase.

Analogous to Figure 4-6, P_{static} and ΔP for the stem and heel sections are shown in Figure 4-9 superimposed on the stress distributions and deformed shape of the cantilever wall at times corresponding to maximum values of P_{stem}, P_{heel}, $(Y \cdot P)_{stem}$, and $(Y \cdot P)_{heel}$. Of particular note are heights above the base at which ΔP on the stem and heel sections act (i.e., ΔY_{stem} and ΔY_{heel}, respectively). For the condition where P_{stem} is maximum, ΔY_{stem} is approximately equal to Y_{static}, which is about $0.3 \cdot H$. However, ΔY_{heel} is closer to $0.5 \cdot H$. For the condition when P_{heel}, $(Y \cdot P)_{stem}$, and $(Y \cdot P)_{heel}$ are maximum, ΔY_{stem} is just over $0.75 \cdot H$, while ΔY_{heel} remains at approximately $0.5 \cdot H$. Figure 4-9 also illustrates the phasing of the various parameters. For the condition where P_{stem} is maximum, ΔP_{stem} is large, while ΔY_{stem} and ΔP_{heel} are relatively small. For the condition where P_{heel}, $(Y \cdot P)_{stem}$, and $(Y \cdot P)_{heel}$ are maximum, ΔP_{stem} is small, while ΔY_{stem} and ΔP_{heel} are relatively large.

4.2.4 Permanent relative displacement of the wall

Using an acceleration time-history computed by FLAC at approximately middepth of the backfill and located near the free-field boundary in the FLAC model, a Newmark sliding block-type analysis was performed on the structural wedge. This analysis was similar to those performed using CWROTATE (Ebeling and White, in preparation) with the SHAKE computed time-histories, which are presented in Appendix C. The results from the sliding block-type analysis were compared to wall movements computed by FLAC.

The FLAC computed free-field acceleration time-history used in the sliding block analysis is shown in Figure 4-10a. Also shown in Figure 4-10a is the acceleration time-history of the structural wedge, as determined by sliding block analysis. Relative movement of the soil and the structural wedge occurs when the free-field acceleration exceeds the maximum transmissible acceleration $(N^* \cdot g)$ of the structural wedge, where $N^* \cdot g$ was determined to be $0.22g$ in Appendix C. Figure 4-11a shows an enlargement of the region where the two acceleration time-histories differ; Figure 4-11b, c, and d show the progression of the steps used to compute the permanent relative displacement using a Newmark sliding block-type analysis. Figure 4-10b shows a comparison of the FLAC computed permanent relative displacement time-history with that computed in the sliding block analysis. The magnitude and the occurrence times of the slips are very similar for both analyses. However, the FLAC results have what is believed to be a "numerical creep" prior to approximately 7 sec and after approximately 20 sec. This numerical creep is likely due to precision error that occurs when the displacement experienced during one time increment is

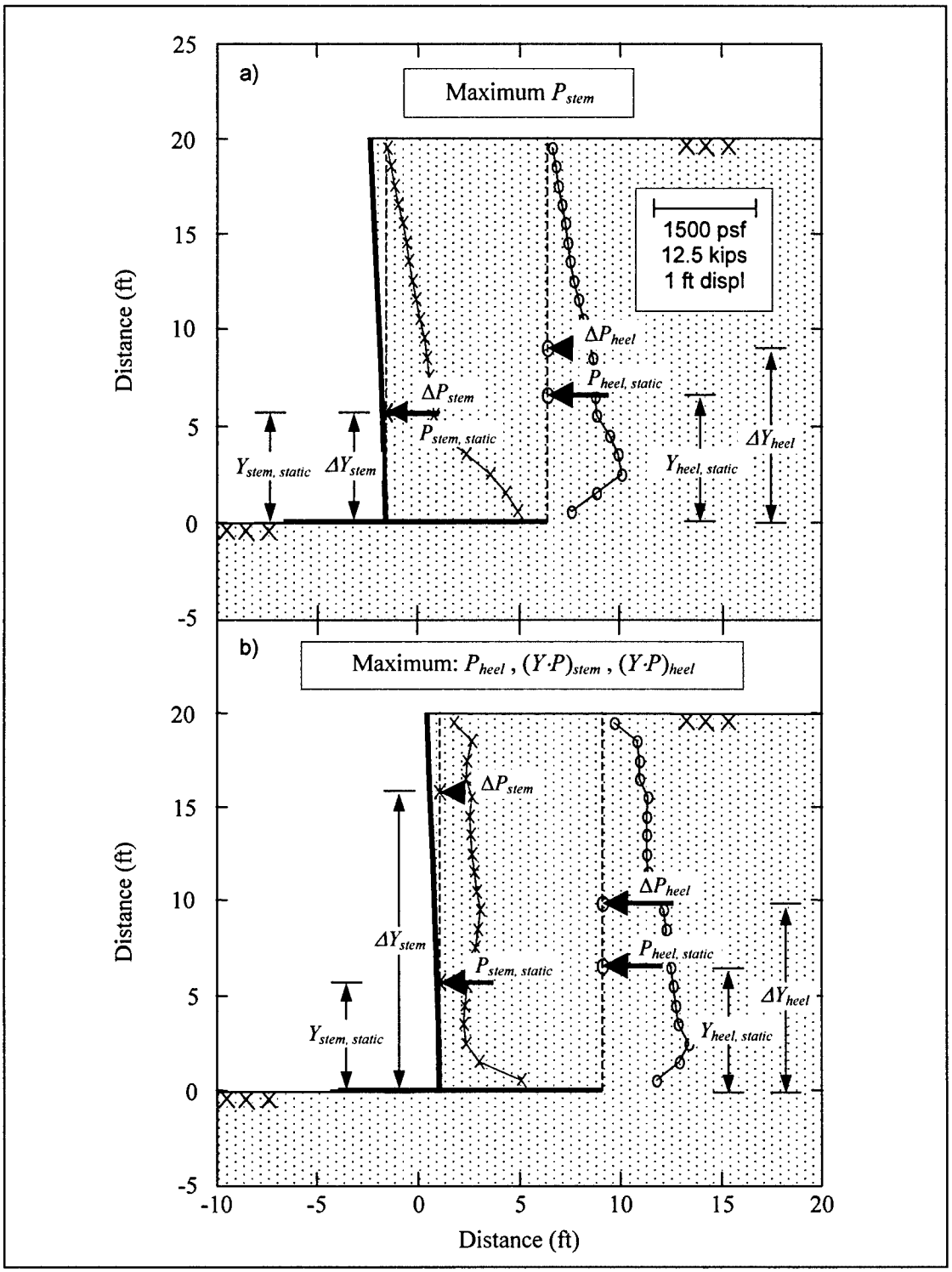

Figure 4-9. Stress distributions, static and incremental dynamic resultant forces on the stem and heel sections at times corresponding to the following: (a) maximum value for P_{stem}, and (b) the maximum values for P_{heel}, $(Y \cdot P)_{stem}$, and $(Y \cdot P)_{heel}$ (To convert feet to meters, multiply by 0.3048; to convert psf to pascals, multiply by 47.88; to convert kips to newtons, multiply by 4,448)

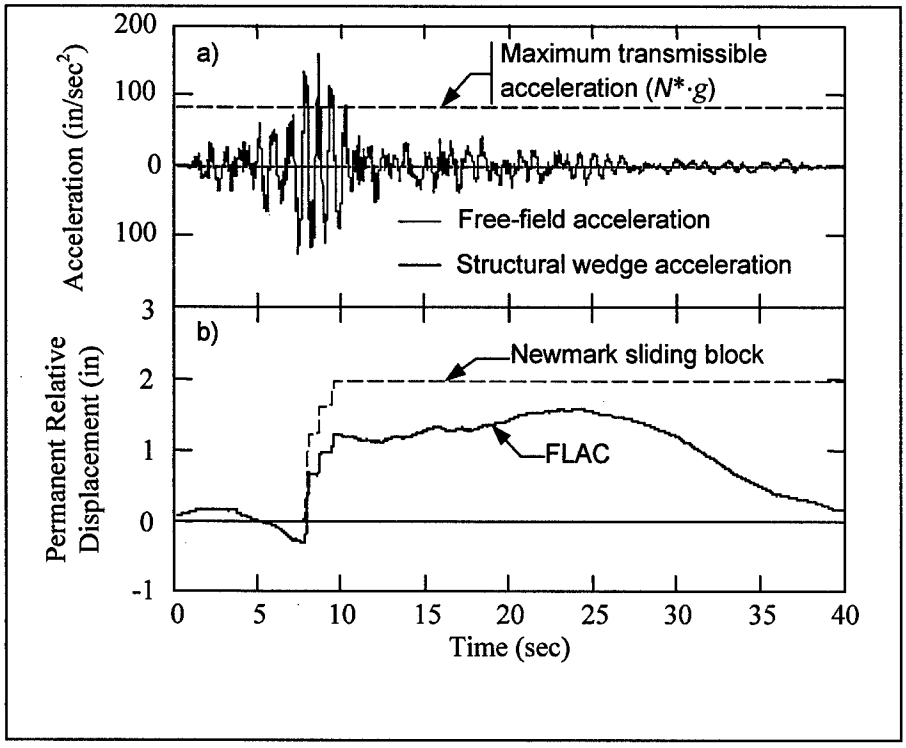

Figure 4-10. Comparison of the permanent relative displacements predicted by a Newmark sliding block-type analysis and by FLAC: (a) k_h time-history used in the analysis, (b) sliding block and FLAC results (To convert inches to millimeters, multiply by 25.4)

relatively small compared with the cumulative total displacement.[1] In cases where higher accuracy is required in the cumulative relative displacement, rather than just the magnitude of the slip increments, the double precision version of FLAC should be used.

4.2.5 Deformed grid of the wall-soil system, post shaking

Figure 4-12 shows the deformed grid of the wall-soil system after the completion of the earthquake shaking, magnified by a factor of ten. Two interesting observations may be made concerning this figure. First, the interface between the structural and driving wedges does not appear to be vertical, as is often assumed in simplified analysis procedures. The practical significance of this needs to be explored further.

A second observation is that as opposed to one distinct failure plane running from the heel of the wall up through the backfill to the right, multiple failure planes or shear bands are observed. The range of the shear bands is highlighted

[1] N. McCullough, 2002, Personal communication regarding FLAC modeling, Department of Civil, Construction, and Environmental Engineering, Oregon State University, Corvallis, OR.

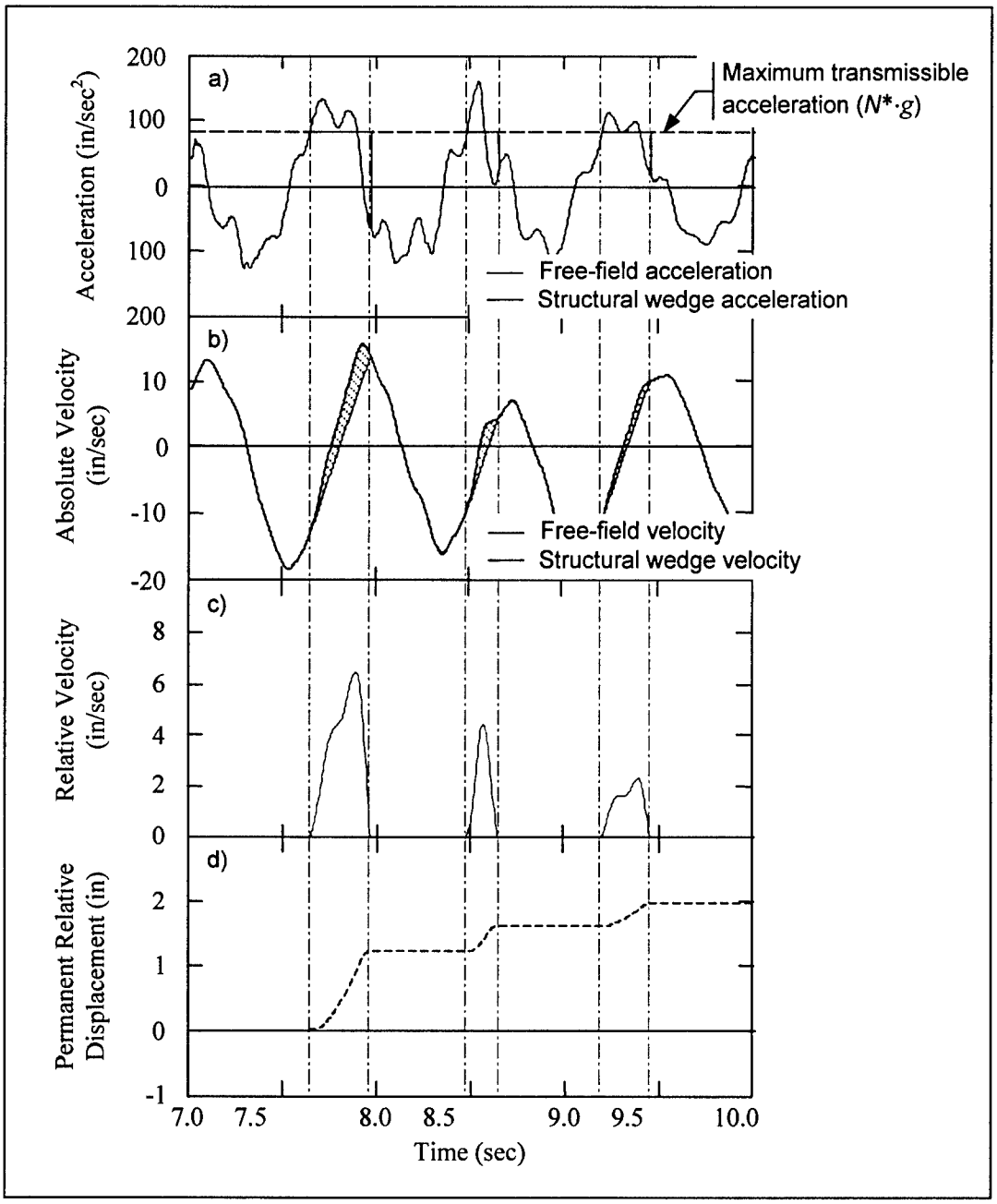

Figure 4-11. Results from the Newmark sliding block-type analysis of the structural wedge: (a) acceleration time-histories of the soil and structural wedge, (b) absolute velocity time-histories of the soil and structural wedge, (c) relative velocity of the soil and structural wedge, and d) permanent relative displacement of the structural wedge (To convert inches to millimeters, multiply by 25.4)

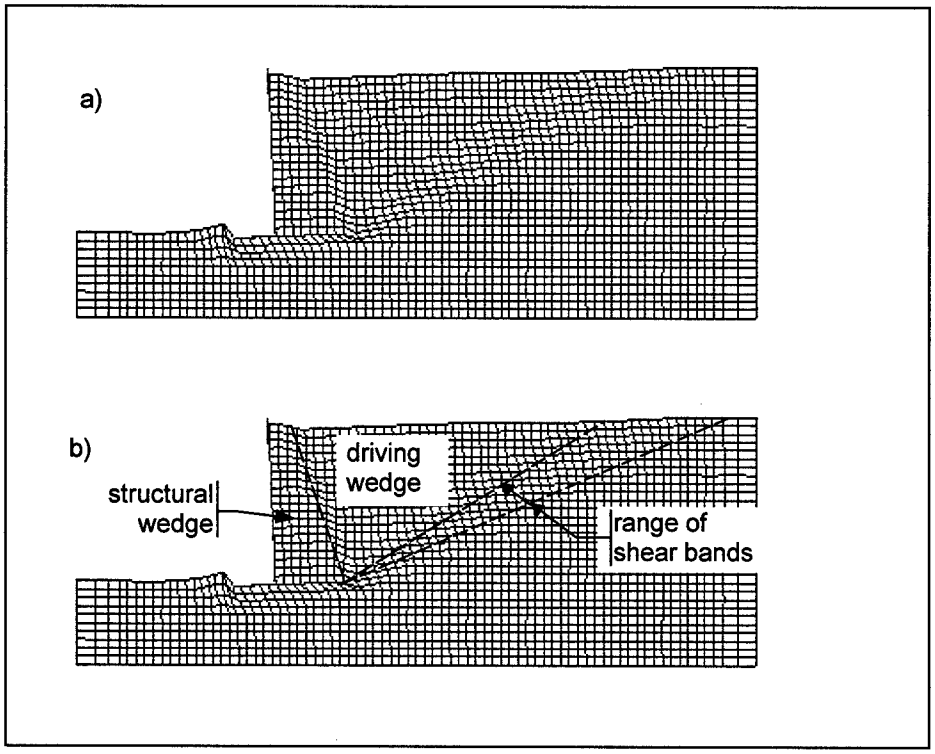

Figure 4-12. Deformed grid of the wall-soil system, post shaking, magnification × 10: (a) without markups, (b) with markups

in Figure 4-12b. The formation of multiple failure planes is consistent with Equation B-5a, which predicts the angle of inclination of the failure plane to flatten as k_h increases. Accordingly, it would be expected that a range of failure to plane would form during the random shaking of earthquake motions. Figure 4-13 presents model wall tests performed on a shake table. Multiple failure planes are clearly identifiable in these photographs. However, the formation of multiple failure planes is not always observed in laboratory studies. For dilative soils, the formation of one failure plane may be favored over the formation of multiple failure planes.

4.3 Conclusions

In the preceding sections, the procedures used to reduce the FLAC data were presented for this, the first FLAC analysis of a Corps type retaining wall. Additionally, the reduced data were presented and preliminary interpretation given. Further studies are required to determine whether the trends identified in the first phase of this study are general in nature, or limited to certain wall configurations, assumed wall and soil properties, and soil conditions.

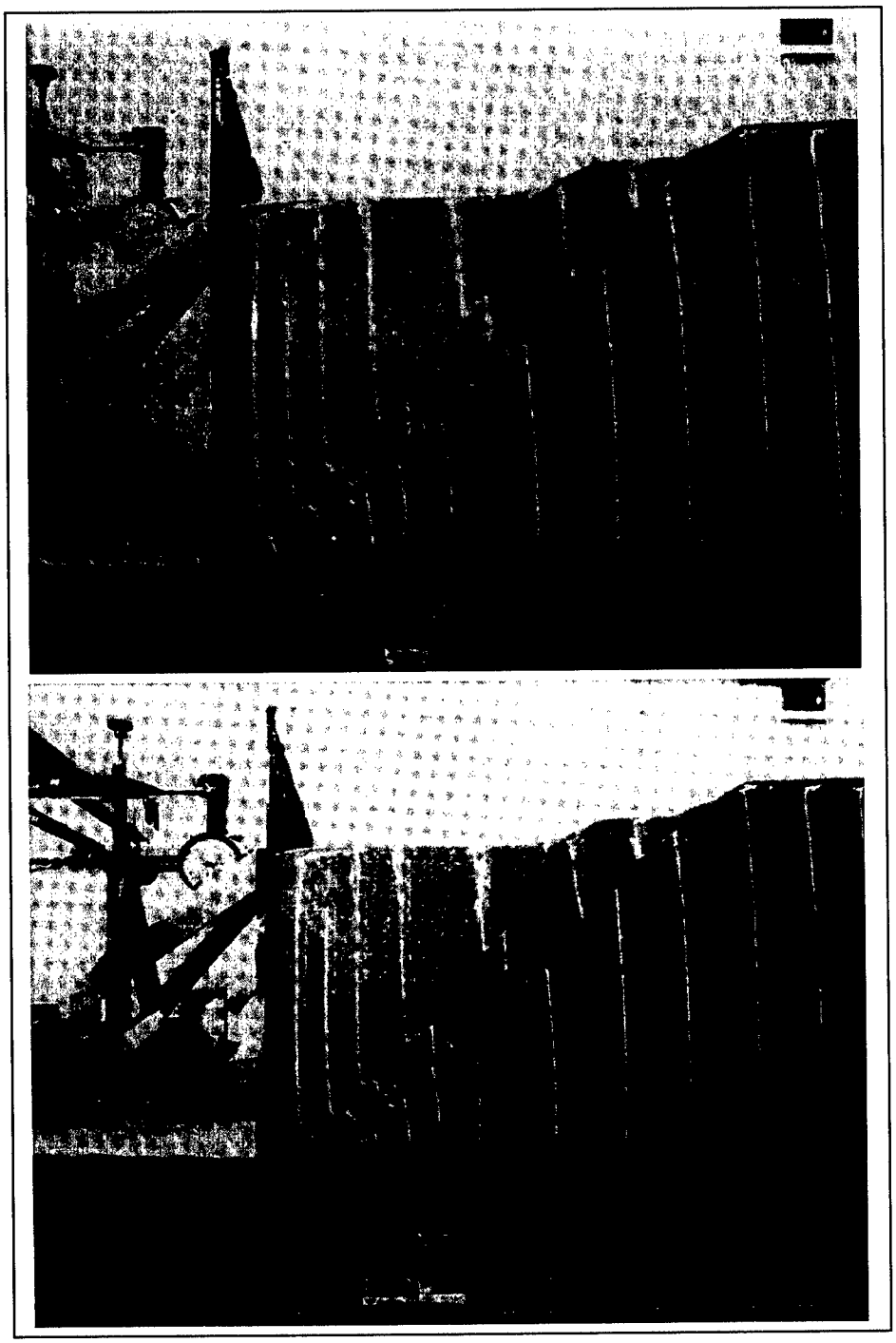

Figure 4-13. Shake table tests performed on scale models of retaining wall. Note the multiple failure planes in the backfill (from Aitken, Elms, and Berrill 1982)

References

American Concrete Institute. (2002). "Building code requirements for reinforced concrete and commentary," ACI 318-02, Detroit, MI.

Aitken, G. H., Elms, D. G., and Berrill, J. B. (1982). "Seismic response of retaining walls," Research Report 82-5, Department of Civil Engineering, University of Canterbury, Christchurch, New Zealand, 87 pp.

Clough, G. W., and Duncan, J. M. (1991). "Earth pressures." *Foundation engineering handbook.* 2nd ed., H.Y. Fang, ed., Van Nostrand Reinhold, New York, Chapter 6, 223-235.

Davies, T. G., Richards, R., and Chen, K. -H. (1986). "Passive pressure during seismic loading," *Journal of Geotechnical Engineering*, 112(4), 479-483.

Duncan, J. M., and Seed, R. B. (1986). "Compaction-induced earth pressures under K_o-conditions," *Journal of Geotechnical Engineering,* 112(1), 1-22.

Ebeling, R. M. (1992). "Introduction to the computation of response spectrum for earthquake loading," Technical Report ITL-92-4, U.S. Army Engineer Waterways Experiment Station, Vicksburg, MS.

Ebeling, R. M., and Morrison, E. E. (1992). "The seismic design of waterfront retaining structures," U.S. Army Technical Report ITL-92-11, U.S. Navy Technical Report NCEL TR-939, U.S. Army Engineer Waterways Experiment Station, Vicksburg, MS.

Ebeling, R. M., and White, B. C. "$C_{orps}W_{all}$ROTATE-"Dry": A computer program to perform a rotating or sliding analysis of a retaining wall for a specified earthquake acceleration time history" (in preparation), U.S. Army Engineer Research and Development Center, Vicksburg, MS.

Ebeling, R. M., Green, R. A., and French, S. E. (1997). "Accuracy of response of single-degree-of-freedom systems to ground motion," Technical Report ITL-97-7, U.S. Army Engineer Waterways Experiment Station, Vicksburg, MS.

Frankel, A., Harmsen, S., Mueller, C., Barnhard, T., Leyendecker, E.V., Perkins, D., Hanson, S., Dickman, N., and Hopper, M. (1997). "USGS National Seismic Hazard Maps: Uniform hazard spectra, de-aggregation, and uncertainty." *Proceedings of FHWA/NCEER Workshop on the National Representation of Seismic Ground Motion for New and Existing Highway Facilities*. I. M. Friedland, M. S. Power, and R. L. Mayes, ed., NCEER Technical Report 97-0010, National Center for Earthquake Engineering Research, Buffalo, NY, 39-73.

Gomez, J. E., Filz, G. M., and Ebeling, R. M. (2000a). "Development of an improved numerical model for concrete-to-soil interfaces in soil-structure interaction analyses; Report 2, Final study," ERDC/ITL TR-99-1, U.S. Army Engineer Research and Development Center, Vicksburg, MS.

_____. (2000b). "Extended load/unload/reload hyperbolic model for interfaces: Parameter values and model performance for the contact between concrete and coarse sand," ERDC/ITL TR-00-7, U.S. Army Engineer Research and Development Center, Vicksburg, MS.

Headquarters, U.S. Army Corps of Engineers. (1989). "Retaining and flood walls," EM 1110-2-2502, Washington, DC.

_____. (1992). "Strength design for reinforced-concrete hydraulic structures," EM 1110-2-2104, Washington, DC.

_____. (1995). "Earthquake design and evaluation of civil works projects," ER 1110-2-1806, Washington, DC.

_____. (1999). "Response spectra and seismic analysis for concrete hydraulic structures," EM 1110-2-6050, Washington, DC.

_____. (2000). "Time-history dynamic analysis of concrete hydraulic structures," EC 1110-2-6051, Washington, DC.

Idriss, I. M., and Sun, J. I. (1992). "User's manual for SHAKE91: A computer program for conducting equivalent linear seismic response analyses of horizontally layered soil deposits," Center for Geotechnical Modeling, Department of Civil and Environmental Engineering, University of California, Davis, CA.

Itasca Consulting Group, Inc. (2000). FLAC (Fast Lagrangian Analysis of Continua) user's manuals, Minneapolis, MN.

Jaky, J. (1944). "The coefficient of earth pressure at rest." *Magyar Menok es Epitesz Kozloi (Journal of the Society of Hungarian Architects and Engineers).*

Kuhlemeyer, R. L., and Lysmer, J. (1973). "Finite element method accuracy for wave propagation problems," *Journal of the Soil Mechanics and Foundations Division* 99(SM5), 421-427.

Lysmer, J., Udaka, T., Tsai, C. -F., and Seed, H. B. (1975). "FLUSH: A computer program for approximate 3-D analysis of soil-structure interaction problems," EERC Report No. EERC-75-30, Earthquake Engineering Research Center, University of California, Berkeley, CA.

MacGregor, J. G. (1992). *Reinforced concrete mechanics and design.* Prentice-Hall, Englewood Cliffs, NJ, 848 pp.

Mononobe, N., and Matsuo, H. (1929). "On the determination of earth pressures during earthquakes." *Proceedings, World Engineering Congress* 9, 177-185.

Okabe, S. (1926). "General theory of earth pressures," *Journal Japan Society of Civil Engineering* 12(1).

Pace, M. E. (1994). "User's guide to CTWALL-A microcomputer program for the analysis of retaining and flood walls," Instruction Report ITL-94-7, U.S. Army Engineer Waterways Experiment Station, Vicksburg, MS.

Paulay, T., and Priestley, M. J. N. (1992). *Seismic design of reinforced concrete and masonry buildings.* John Wiley and Sons, Inc., New York, 744 pp.

Richards, R., and Elms, D. G. (1979). "Seismic behavior of gravity retaining walls," *Journal of the Geotechnical Engineering Division* 105(GT4), 449-464.

Seed, H. B., and Whitman, R.V. (1970). "Design of earth retaining structures for dynamic loads, in lateral stresses in the ground and design of earth-retaining structures." *ASCE Specialty Conference.* 103-147.

Terzaghi, K. (1943). *Theoretical soil mechanics.* John Wiley and Sons, Inc., New York, 510 pp.

Whitman, R.V. (1990). "Seismic design and behavior of gravity retaining walls, design and performance of earth retaining structures," ASCE Geotechnical Special Publication No. 25, 817-842.

Whitman, R.V., and Liao, S. (1985). "Seismic design of gravity retaining walls," Miscellaneous Paper GL-85-1, U.S. Army Engineer Waterways Experiment Station, Vicksburg, MS.

Wood, J. H. (1973). "Earthquake-induced soil pressures on structures," Report No. EERL 73-05, California Institute of Technology, Pasadena, CA.

Zarrabi-Kashani, K. (1979). "Sliding of gravity retaining wall during earthquakes considering vertical acceleration and changing inclination of failure surface," S. M. Thesis, Department of Civil Engineering, Massachusetts Institute of Technology, Cambridge, MA.

Appendix A
Static Design of the Cantilever Retaining Wall

A.1 Introduction

This appendix illustrates the sizing and structural design for usual loading (i.e., static) of the 20-ft-high[1] cantilever retaining wall that is analyzed dynamically in the main body of this report. The wall design is performed in two stages. The first stage consists of sizing the wall to satisfy global stability requirements, in general accordance with Engineer Manual (EM) 1110-2-2502 (Headquarters, U.S. Army Corps of Engineers (HQUSACE) 1989).[2] The global stability requirements are expressed in terms of the factor of safety against sliding; the factor of safety against bearing capacity failure; and the percentage of the base area in compression, with the latter quantifying the overturning stability of the wall.

The second stage of the wall design entails the dimensioning of the components of the concrete wall (i.e., stem and base slab, toe and heel elements) and detailing of the reinforcing steel, in general accordance with EM 1110-2-2104 (HQUSACE 1992). Each of the three structural elements is designed by the strength-design method as a cantilever, one-way slab for flexure and shear loadings. The design loads are those determined in the first design stage, with appropriate dead, live, and hydraulic load factors applied, thus ensuring that the Corps strength and serviceability requirements are satisfied.

The notation used in this appendix is generally consistent with that used by the Corps. However, both structural and geotechnical calculations are presented in this appendix, and the notation between the two disciplines is somewhat ambiguous (e.g., ϕ is used in both concrete design and geotechnical engineering, with very distinct meanings). Accordingly, rather than giving a compiled list of variable definitions used in this appendix, variables are defined mathematically and illustratively as they are presented in the calculations.

[1] Conversion factors for non-SI units of measurement used in this appendix are given in Table A-1.

[2] References cited in this appendix are included in the References section at the end of the main text.

A.2 Stage 1: Sizing of the Cantilever Retaining Wall

As stated previously, the first design stage consists of sizing the cantilever wall such that global stability requirements are satisfied (i.e., sliding, overturning, and bearing capacity), in general accordance with EM 1110-2-2502 (HQUSACE 1989). The structural wedge of the proposed wall and backfill is shown in Figure A-1, as well as the backfill and foundation material properties.

To assess the global stability of the wall, the external forces and corresponding points of action acting on the structural wedge need to be determined. The external forces include the resultant of the lateral earth pressure and reactionary forces acting along the base of the wall. However, before the reactionary forces can be determined, the weights and centers of gravity of the concrete and soil composing the structural wedge are required.

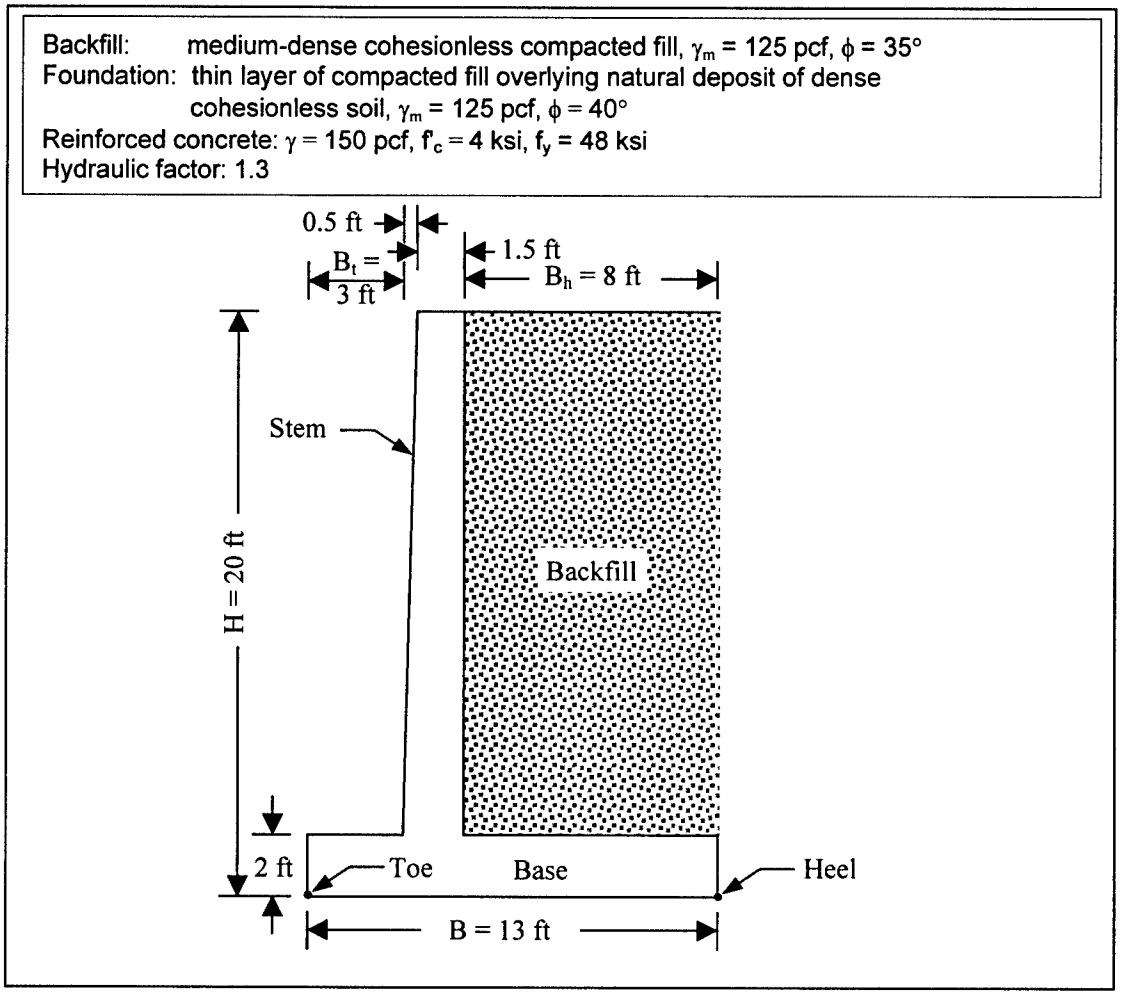

Figure A-1. Structural wedge of proposed wall, and backfill and foundation properties

To simplify the determination of the weight and center of gravity of the structural wedge, it is divided into subsections having uniform unit weights and simple geometries, as shown in Figure A-2. Once the weights and centers of gravity of each subsection are determined, the weight and center of gravity of the entire structural wedge are easily determined, as illustrated in the accompanying sketches.

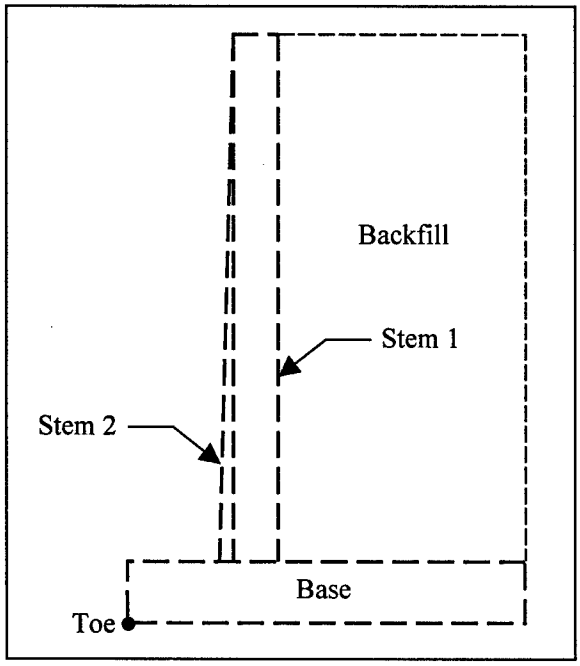

Figure A-2. Division of wall and backfill into sub-sections for determining internal forces and centroids of structural wedge

Backfill:

$W_s = 125\text{pcf} \times 8' \times 18'$

$= 18{,}000$ lbs

$\Delta x_{toe} \cdot W_s = 18{,}000 \text{ lbs} \times 9'$

$= 162{,}000$ ft-lbs

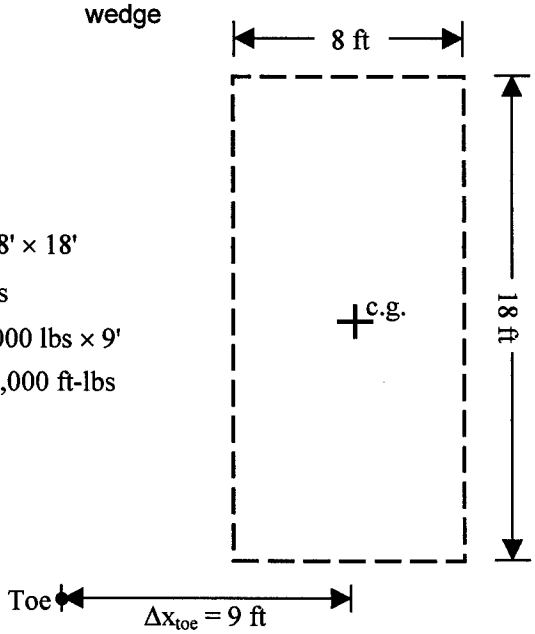

Stem 2:

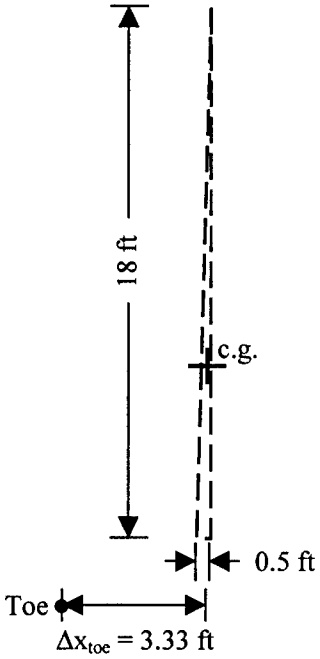

Stem 1:

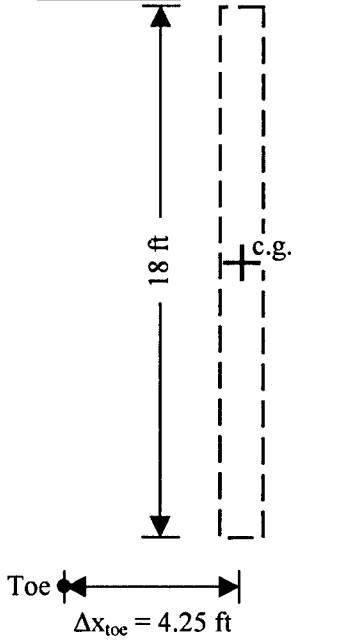

$W_{c\ stem\ 2} = 150pcf \times 0.5' \times 18' \times 0.5$

$= 675$ lbs

$\Delta x_{toe} \cdot W_{c\ stem\ 2} = 675$ lbs $\times 3.33'$

$= 2250$ ft-lbs

$W_{c\ stem\ 1} = 150pcf \times 1.5' \times 18'$

$= 4050$ lbs

$\Delta x_{toe} \cdot W_{c\ stem\ 1} = 4050$ lbs $\times 4.25'$

$= 17{,}212.5$ ft-lbs

Base:

$W_{c\ base} = 150pcf \times 2' \times 13'$

$= 3900$ lbs

$\Delta x_{toe} \cdot W_{c\ base} = 3900$ lbs $\times 6.5'$

$= 25{,}350$ ft-lbs

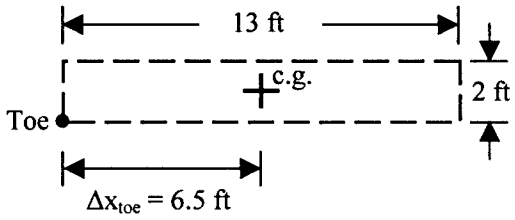

Weight of entire wall:

$$\sum_{i=1}^{3} W_{c,i} = 3900 \text{ lbs} + 4050 \text{ lbs} + 675 \text{ lbs}$$

$$= 8625 \text{ lbs}$$

Centroid of entire wall:

$$\sum_{i=1}^{3} W_{c,i} \cdot \Delta x_{toe,i} = 25{,}350 \text{ ft-lbs} + 17{,}212.5 \text{ ft-lbs} + 2250 \text{ ft-lbs}$$

$$= 44{,}812.5 \text{ ft-lbs}$$

$$\frac{\sum_{i=1}^{3} W_{c,i} \cdot \Delta x_{toe,i}}{\sum_{i=1}^{3} W_{c,i}} = 5.2 \text{ ft from the toe}$$

In a CTWALL analysis the retaining wall system is divided into two or three wedges: the structural wedge; the driving wedge; and the resisting wedge, when present (Pace 1994). Figure A-1 shows the structural wedge, which is defined by the outline of the cantilever retaining wall. The lateral extent of the structural wedge is defined by imaginary vertical sections made through the heel of the wall and the toe of the wall. The soil mass contained within this region is also considered part of the structural wedge. The driving soil wedge on the retained soil side (to the right of the Figure A-1 structural wedge and not shown in this figure) generates earth pressure forces tending to destabilize the structural wedge. No resisting wedge is present to the left of the Figure A-1 structural wedge in this case.

The general wedge method of analysis (EM 1110-2-2502 (HQUSACE 1989)) is used to calculate the lateral earth pressure force acting on the structural wedge. CTWALL (Pace 1994) performs the sliding and overturning stability analyses during execution. Forces computed during the CTWALL analysis of the user-specified wall geometry may be used to compute the factor of safety against a foundation bearing failure. This computation is made external to the CTWALL execution.

A sliding stability analysis using CTWALL (Pace 1994) follows Corps design criteria (EM 1110-2-2502). A sliding stability analysis is conducted of the driving wedge, structural wedge, and resisting wedge (when present) to determine a common factor of safety against sliding for the entire retaining structural system (of the three wedges). The procedure is a limit equilibrium

procedure and is iterative in nature. Critical failure angles for the driving side and resisting side (when present) potential planar slip planes are sought for an assumed sliding factor of safety value. The resulting earth forces are summed. If the sum is zero, the system is in equilibrium and the critical sliding factor of safety value has been found.

An overturning stability analysis using CTWALL (Pace 1994) follows Corps design criteria (EM 1110-2-2502). The program will calculate a percentage of the base in compression and report the location of the resultant of all forces applied to the structural wedge. The program will iterate, if necessary, to find the percent of the base in compression. Tension along the base is not allowed for these soil-founded walls. A linear base pressure distribution assumption is made by CTWALL (for the portion of the base in compression) in conjunction with the limit equilibrium procedure of analysis. The overturning analysis checks that a user-specified wall configuration satisfies Corps design criteria. These criteria are expressed in terms of base area in compression (versus computing the ratio of the stabilizing moment about the toe of the wall divided by the overturning moment). The overturning analysis uses an approximation for at-rest earth pressure forces in the driving wedge analysis to determine the earth force the driving wedge (i.e., the retained soil) exerts on the structural wedge. Per EM 11102-2502 (section 3-11), the shear mobilization factor (SMF) is set equal to 2/3. The SMF and factor of safety are inverses of each other. An SMF of 2/3 is equivalent to a factor of safety equal to 1.5. The determination of the lateral earth forces and pressures are illustrated in the following equations in simplified hand computations (and were used to check the CTWALL analyses for the final wall configuration):

$$SMF = 2/3 = 1/1.5$$

$$\tan(\phi'_{mob}) = SMF \cdot \tan(\phi')$$

$$= \frac{1}{1.5} \cdot \tan(35°)$$

$$\Rightarrow \quad \phi'_{mob} = 25°$$

In accordance with EM 1110-2-2502, the angle of friction alongside the structural wedge defined by the vertical section through the heel of the wall is assumed equal to zero (i.e., $\delta = 0°$). Thus, for the case being considered (i.e., homogenous backfill), the wedge analysis procedure reverts to the classical Rankine procedure, which is illustrated in the following sketches.

$$k_h = \tan^2(45° - \frac{\phi'_{mob}}{2})$$

$$= \tan^2(45° - \frac{25°}{2})$$

$$= 0.41$$

$$\sigma'_h = \gamma_{moist} \cdot H \cdot k_h$$

$$= 125 \text{ pcf} \cdot 20' \cdot 0.41$$

$$= 1013.8 \text{ psf}$$

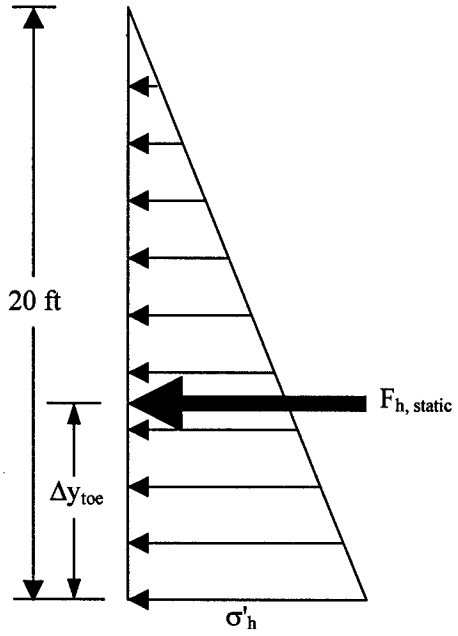

$$F_{h, static} = \frac{1}{2} \cdot \sigma'_h \cdot H$$

$$= \frac{1}{2} \cdot 1013.8 \text{ psf} \cdot 20'$$

$$= 10{,}137.5 \text{ lbs}$$

$$\Delta y_{toe} = \frac{H}{3}$$

$$= \frac{20'}{3}$$

$$= 6.667 \text{ ft}$$

$$F_{h, static} \times \Delta y_{toe} = 10{,}137.5 \text{ lbs} \cdot 6.667'$$

$$= 67{,}583 \text{ ft-lbs}$$

The remaining, yet-to-be-determined, forces acting on the structural wedge are the reactionary shear and normal forces (i.e., *T* and *N'*, respectively) acting on the base of the wall. Figure A-3 shows a free body diagram of the structural wedge with the known and unknown forces identified. As illustrated in the following equations, the magnitude of *T* and *N'* are determined by summing the forces in the horizontal and vertical directions, respectively, while the point at which *N'* acts is determined by summing the moments around the toe.

$$+\uparrow \sum F_v = 0$$

$$= N' - W_c - W_s$$

$$\Rightarrow N' = W_c + W_s$$

$$= 8625 \text{ lbs} + 18{,}000 \text{ lbs}$$

$$= 26{,}625 \text{ lbs}$$

$$\pm\rightarrow \sum F_h = 0$$

$$= T - F_{h, static}$$

$$\Rightarrow T = F_{h, static}$$

$$= 10{,}137.5 \text{ lbs}$$

$$\circlearrowleft_{+} \sum M_{toe} = 0$$

$$= x_{N'} \cdot N' + F_{h,\,static} \cdot \Delta y_{toe} - W_c \cdot \Delta x_{toe} - W_s \cdot \Delta x_{toe}$$

$$\Rightarrow x_{N'} \cdot N' = -F_{h,\,static} \cdot \Delta y_{toe} + W_c \cdot \Delta x_{toe} + W_s \cdot \Delta x_{toe}$$

$$\Rightarrow x_{N'} = \frac{-F_{h,\,static} \cdot \Delta y_{toe} + W_c \cdot \Delta x_{toe} + W_s \cdot \Delta x_{toe}}{N'}$$

$$= \frac{-10{,}137.5 \text{ lbs} \cdot 6.667' + 8625 \text{ lbs} \cdot 5.2' + 18{,}000 \text{ lbs} \cdot 9'}{26{,}625 \text{ lbs}}$$

= 5.23 ft from the toe

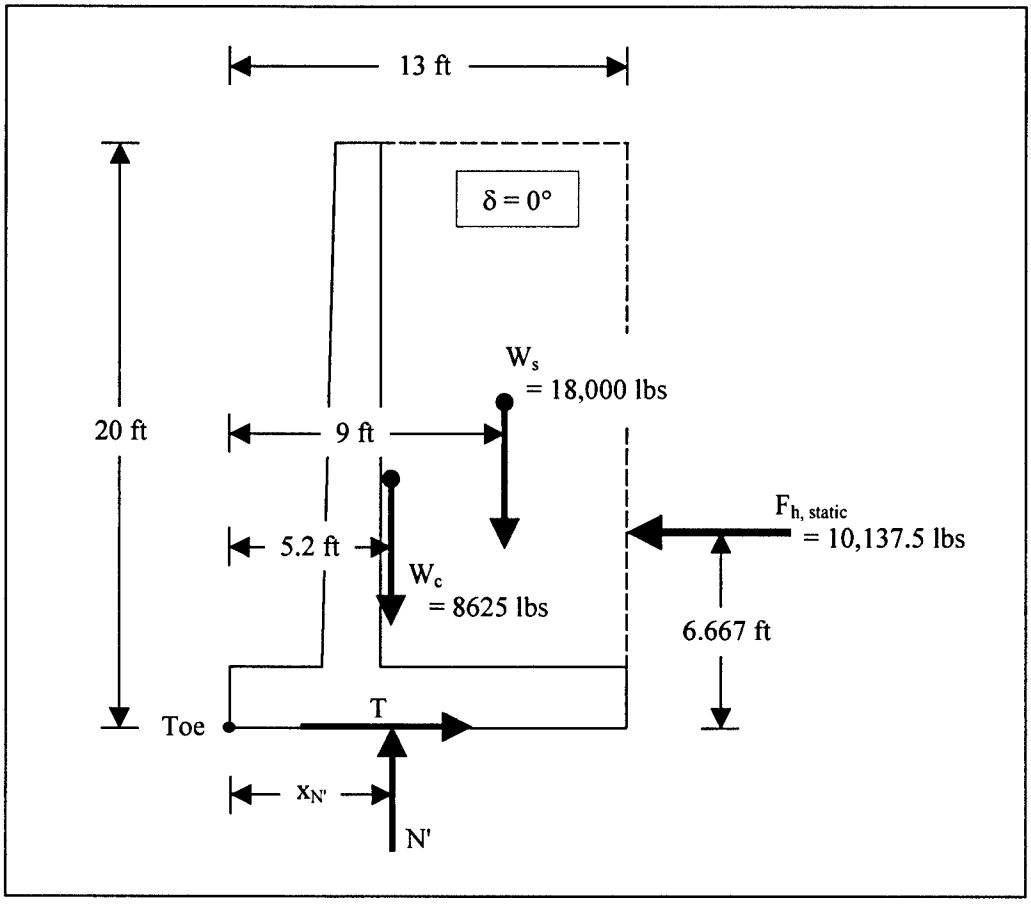

Figure A-3. Free body diagram of the structural wedge, with known forces (W_s, W_c, and $F_{h,\,static}$) and unknown forces (N' and T) identified

With all external forces acting on the structural wedge determined, the global stability of the wall is assessed by computing the factor of safety against sliding; the percentage of the base area in compression (overturning stability); and the factor of safety against bearing capacity failure.

A.2.1. Factor of safety against sliding

EM 1110-2-2502 requires the following minimum factors of safety against sliding ($FS_{sliding}$) for cantilever retaining walls:

a. 1.5: usual loadings.

b. 1.33: short-duration (unusual) loads, such as those that might occur during high winds, construction activities, or the Operational Basis Earthquake (OBE).

c. 1.1: extreme loads, such as those that might occur during the Maximum Design Earthquake (MDE).

The $FS_{sliding}$ for usual loadings is computed as follows:

$$T_{ult} = N' \cdot \tan(\delta_{base})$$

$$\delta_{base} = \phi_{base}$$

$$= 26{,}625 \text{ lbs} \cdot \tan(35°)$$

$$= 18{,}643 \text{ lbs}$$

$$FS_{sliding} = \frac{T_{ult}}{T}$$

$$= \frac{18{,}643 \text{ lbs}}{10{,}137.5 \text{ lbs}}$$

$$= 1.84 \geq 1.5 \quad \textit{okay}$$

Note: It is assumed that the wall sits on a thin layer of compacted fill. The internal friction angle of this thin layer is assumed equal to that of the compacted backfill (i.e., $\phi = 35°$).

A.2.2 Percentage of the base area in compression (i.e., overturning stability)

The global stability of cantilever retaining walls to overturning is quantified by the percentage of the base area in compression. EM 1110-2-2502 requires the following minimum percentages cantilever walls on soil foundations:

a. 100%: usual loadings.

b. 75%: unusual loadings.

c. Resultant within base: extreme loadings.

The percentage of the base area that is in compression for usual loadings is computed as follows:

$$e = \frac{B}{2} - x_{N'}$$

$$= \frac{13'}{2} - 5.23'$$

$$= 1.27'$$

$$\sigma_{max} = \frac{N'}{B} \cdot (1 + \frac{6\,e}{B})$$

$$= \frac{26{,}625 \text{ lbs}}{13'} \cdot (1 + \frac{6 \cdot 1.27'}{13'})$$

$$= 3249 \text{ psf}$$

$$\sigma_{min} = \frac{N'}{B} \cdot (1 - \frac{6\,e}{B})$$

$$= \frac{26{,}625 \text{ lbs}}{13'} \cdot (1 - \frac{6 \cdot 1.27'}{13'})$$

$$= 848 \text{ psf}$$

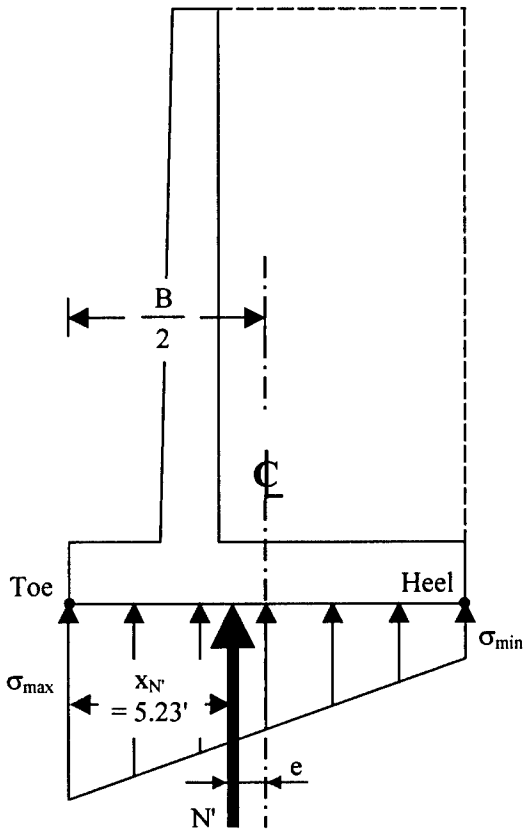

$\sigma_{min} \geq 0$ ∴ 100% base area in compression: *okay*

Note: Per Corps design criteria, a linear effective base pressure is assumed.

A.2.3 Factor of safety against bearing capacity failure

EM 1110-2-2502 requires the following minimum factors of safety against bearing capacity failure FS_{bc} for cantilever retaining walls:

a. 3.0: usual loadings.

b. 2.0: unusual loadings.

c. >1: extreme loadings.

EM 1110-2-2502 provides the following expression for the normal component to the base of the structure of the ultimate bearing capacity for strip footings:

$$Q = \overline{B}\,[(\xi_{cd} \cdot \xi_{ci} \cdot \xi_{ct} \cdot \xi_{cg} \cdot c \cdot N_c) + (\xi_{qd} \cdot \xi_{qi} \cdot \xi_{qt} \cdot \xi_{qg} \cdot q_o \cdot N_q) + \frac{(\xi_{\gamma d} \cdot \xi_{\gamma i} \cdot \xi_{\gamma t} \cdot \xi_{\gamma g} \cdot \overline{B} \cdot \gamma \cdot N_\gamma)}{2}]$$

However, for the wall being analyzed, only the last term is nonzero, and thus, this expression reduces to:

$$Q = \overline{B} \cdot \frac{(\xi_{\gamma d} \cdot \xi_{\gamma i} \cdot \xi_{\gamma t} \cdot \xi_{\gamma g} \cdot \overline{B} \cdot \gamma \cdot N_\gamma)}{2}$$

The FS_{bc} for usual loadings is computed as follows:

$$\overline{B} = B - 2e$$
$$= 13' - 2(1.27')$$
$$= 10.46'$$

$$\delta = \tan^{-1}\left(\frac{T}{N'}\right)$$
$$= \tan^{-1}\left(\frac{10{,}137.5 \text{ lbs}}{26{,}625 \text{ lbs}}\right)$$
$$= 20.8°$$

$$\xi_{\gamma i} = \left(1 - \frac{\delta}{\phi}\right)^2$$
$$= \left(1 - \frac{20.8°}{40°}\right)$$
$$= 0.23$$

$$\xi_{\gamma d} = \xi_{\gamma t} = \xi_{\gamma g} = 1$$

$$Q = \overline{B} \cdot \frac{(\xi_{\gamma d} \cdot \xi_{\gamma i} \cdot \xi_{\gamma t} \cdot \xi_{\gamma g} \cdot \overline{B} \cdot \gamma \cdot N_\gamma)}{2}$$

$$= 10.46' \cdot \frac{(1 \cdot 0.23 \cdot 1 \cdot 1 \cdot 10.46' \cdot 125\text{pcf} \cdot 93.69)}{2}$$

$$= 147{,}612 \text{ lbs}$$

$$FS_{bc} = \frac{Q}{N'}$$

$$= \frac{147{,}612 \text{ lbs}}{26{,}625 \text{ lbs}}$$

$$= 5.54 \textit{ okay}$$

Note: Although the wall sits on a thin layer of compacted fill having $\phi = 35°$, this layer will have little influence on bearing capacity, as the failure surfaces will primarily pass through the underlying denser natural deposit ($\phi = 40°$). This is contrary to the sliding mode of failure where the thin layer of compacted fill has significant influence, and accordingly, $\phi = 35°$ was used to compute $FS_{sliding}$.

A.3 Stage 2: Structural Design of Concrete Cantilever Retaining Wall

As stated in the introduction to this appendix, the second stage of the wall design entails the structural design of the concrete wall, to include the dimensioning of the concrete base slab (the toe and heel elements) and stem, and the detailing of the reinforcing steel. All reinforced-concrete hydraulic structures must satisfy both strength and serviceability requirements. In the strength design method, this is accomplished by multiplying the service loads by appropriate load factors and by a hydraulic factor. The hydraulic factor is used to improve

crack control in hydraulic structures by increasing reinforcement requirements, thereby reducing steel stresses at service loads. The service loads are those determined in the first design stage presented previously.

Each of the three structural elements is designed as a cantilever, one-way slab for flexure and shear loadings, in general accordance with EM 1110-2-2104 (HQUSACE 1992), with the exception of the grade steel of the reinforcing bars. The following example uses Grade 40 steel, which is in line with the design examples in EM 1110-2-2502 (HQUSACE 1989). However, EM 1110-2-2104 (Section 2-2) recommends that Grade 60 reinforcing steel be used. Four-inch cover is used in the example, per EM 1110-2-2104 (Section 2-6). Where design criteria is absent in EM 1110-2-2104 and EM 1110-2-2502, ACI 318 (American Concrete Institute 2002) was used. Figure A-4 shows the structural wedge and the externally imposed stresses determined in the first design stage. Also shown in Figure A-4 are the critical locations for evaluating shear and bending moment for the stem, heel, and toe elements.

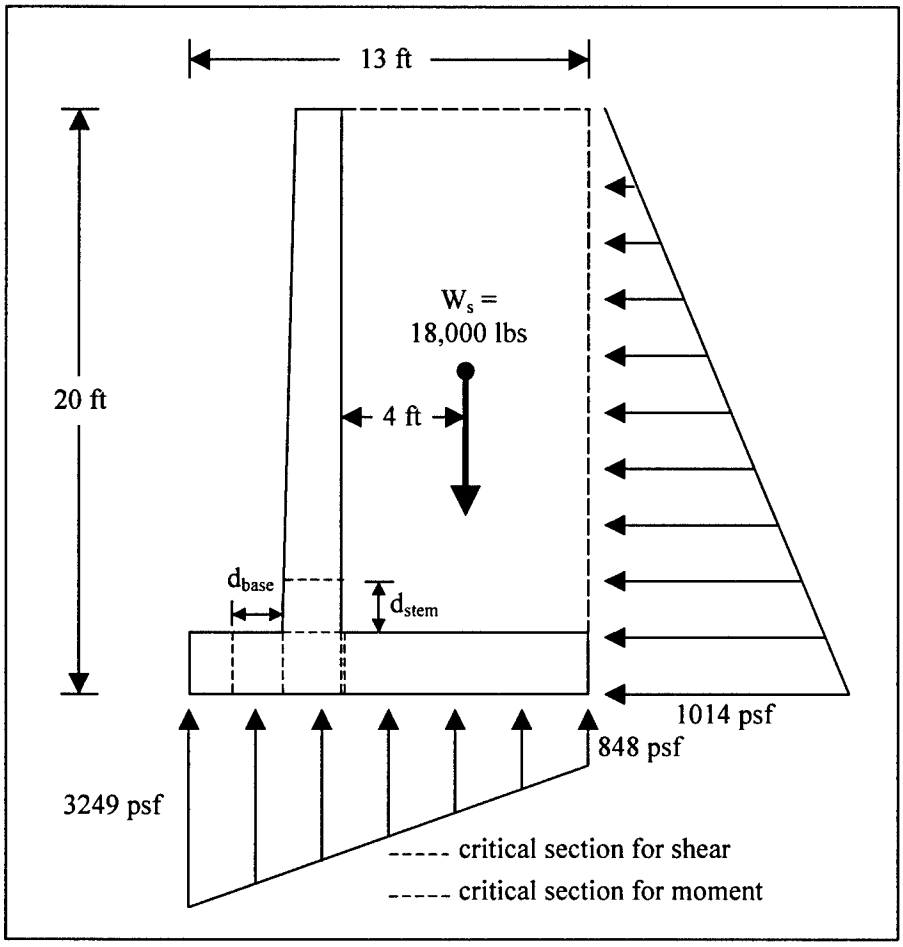

Figure A-4. Critical locations for shear and bending moment, per ACI 318 and EM 1110-2-2502

A.3.1 Moment capacity of the stem

The stem is analyzed as being singly reinforced with the critical section for moment capacity being at the base of the stem, as illustrated below.

$M_{stem} = 4.667' \cdot 8302.5 \text{ lbs}$

$= 38{,}748 \text{ ft-lbs}$

$M_u = 1.7 H_f (D + L)$

$= 1.7 \cdot 1.3 \cdot (38{,}748 \text{ ft-lbs})$

$= 85{,}633 \text{ ft-lbs}$

$$M_n = \frac{M_u}{\phi}$$

$$= \frac{85{,}633 \text{ ft-lbs}}{0.9}$$

$= 95{,}147 \text{ ft-lbs} = 1142 \text{ in-kips}$

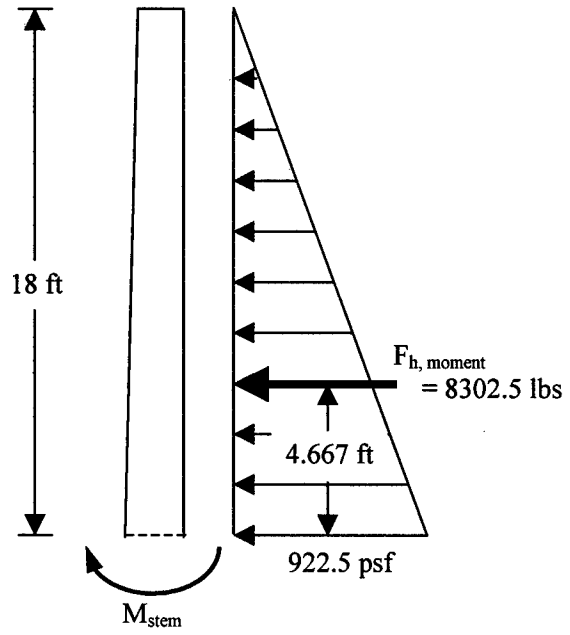

Minimum Effective Depth:

$$d_d = \sqrt{\frac{2.4956 \cdot M_n}{b}}$$

$$= \sqrt{\frac{2.4956 \cdot 1142 \text{ in-kips}}{12"}}$$

$= 15.4" < d$ *okay*

Minimum Required Reinforcing Steel:

$$k_u = 1 - \sqrt{1 - \frac{M_n + P_n \cdot (d - h/2)}{0.425 \cdot f'_c \cdot b \cdot d^2}}$$

$$= 1 - \sqrt{1 - \frac{1142 \text{ in-kips}}{0.425 \cdot 4 \text{ ksi} \cdot 12" \cdot (19.5")^2}}$$

$= 0.0765$

$$A_s = \frac{0.85 \cdot f'_c \cdot k_u \cdot b \cdot d}{f_y}$$

$$= \frac{0.85 \cdot 4 \text{ ksi} \cdot 0.0765 \cdot 12" \cdot 19.5"}{48 \text{ ksi}}$$

$= 1.27 \text{ in}^2$ per 1 ft width of wall

Use #11 @ 9" c-c (*conservative*)

$\Rightarrow A_s = 2.08 \text{ in}^2$ per ft of wall

Check Ductility Requirements:

$\rho_{min} \le \rho \le \rho_{max}$???

$$\rho_{min} = \frac{200}{f_y}$$

$$= \frac{200}{48{,}000}$$

$$= 0.00417$$

$$\rho_{max} = 0.375 \cdot \rho_b$$

$$= 0.375 \cdot 0.0388$$

$$= 0.0146$$

$$\rho_b = 0.85 \cdot \beta_1 \cdot \frac{f'_c}{f_y}\left(\frac{87{,}000}{87{,}000 + f_y}\right)$$

$$= 0.85 \cdot 0.85 \cdot \frac{4 \text{ ksi}}{48 \text{ ksi}}\left(\frac{87{,}000}{87{,}000 + 48{,}000}\right)$$

$$= 0.0388$$

$$\rho = \frac{A_s}{b \cdot d}$$

$$= \frac{2.08 \text{ in}^2}{12" \cdot 19.5"}$$

$$= 0.0089$$

$\rho_{min} \le \rho \le \rho_{max}$ *okay*

A.3.2 Shear capacity of the stem

The critical section for shear in the stem is taken as 19.5" above the interface of the base and stem, where 19.5" is *d* at the base of the stem. However, the *d* at the critical section is only 19", due to the taper of the wall.

$$V_u = 1.7 \cdot (D + L)$$

$$= 1.7 \cdot (6871 \text{ lbs})$$

$$= 11{,}681 \text{ lbs}$$

$$\phi \cdot V_c = \phi_{shear} \cdot 2 \cdot \sqrt{f'_c}\, b \cdot d$$

$$= 0.85 \cdot 2 \cdot \sqrt{4000 \text{ psi}}\ 12" \cdot 19"$$

$$= 24{,}514 \text{ lbs}$$

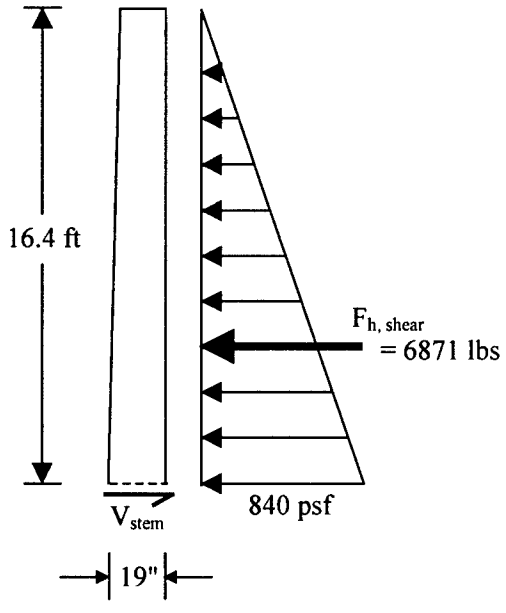

$$\phi \cdot V_s \geq 1.3 \cdot (V_u - \phi \cdot V_c)$$

$$1.3 \cdot (V_u - \phi \cdot V_c) = 1.3 \cdot (11{,}681 \text{ lbs} - 24{,}514 \text{ lbs})$$

$$< 0 \quad \textit{okay}$$

A.3.3 Moment and shear capacity of the heel

The heel is analyzed as being singly reinforced, with the steel along the top face and 4 in. coverage. The critical section for both moment and shear capacity in the heel is at the interface of the heel and the stem.

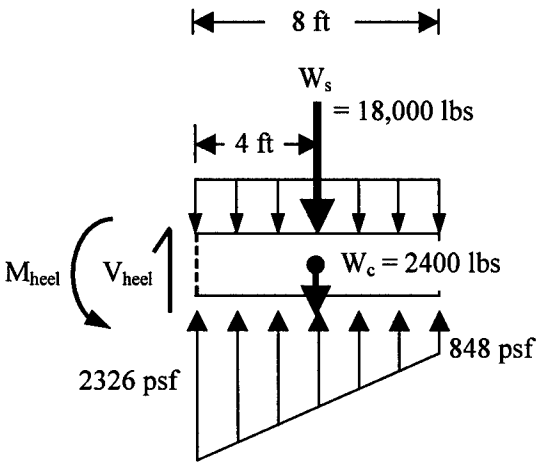

$$\circlearrowleft_{+} \sum M_{heel} = 0$$

$$\Rightarrow \quad 4' \cdot (18{,}000 \text{ lbs} + 2400 \text{ lbs}) - 3.38' \cdot (12{,}694 \text{ lbs}) - M_{heel} = 0$$

$$M_{heel} = 38{,}694 \text{ ft-lbs}$$

$$M_u = 1.7 H_f (D + L)$$

$$= 1.7 \cdot 1.3 \cdot (38{,}694 \text{ ft-lbs})$$

$$= 85{,}514 \text{ ft-lbs}$$

$$M_n = \frac{M_u}{\phi}$$

$$= \frac{85{,}514 \text{ ft-lbs}}{0.9}$$

$$= 95{,}016 \text{ ft-lbs} = 1140 \text{ in-kips}$$

Because the dimensions (i.e., *d*) for both the stem and heel and M_n are essentially the same, the reinforcement used for the stem is also used for the heel (i.e., #11 @ 9" c-c $\Rightarrow$ $A_s = 2.08$ in^2 per ft of wall).

Minimum Effective Depth:

$$d_d = \sqrt{\frac{2.4956 \cdot M_n}{b}}$$

$$= \sqrt{\frac{2.4956 \cdot 1140 \text{ in-kips}}{12"}}$$

$$= 15.4" < d \quad \textit{okay}$$

Shear Capacity of Heel:

$V_u = 1.7 \cdot (D + L)$

$= 1.7 \cdot (18{,}000 \text{ lbs} + 2400 \text{ lbs} - 12{,}694 \text{ lbs})$

$= 13{,}100 \text{ lbs}$

$\phi \cdot V_c = \phi_{shear} \cdot 2 \cdot \sqrt{f'_c}\, b \cdot d$

$= 0.85 \cdot 2 \cdot \sqrt{4000 \text{ psi}}\ 12" \cdot 19.5"$

$= 25{,}159 \text{ lbs}$

$\phi \cdot V_s \geq 1.3 \cdot (V_u - \phi \cdot V_c)$

$1.3 \cdot (V_u - \phi \cdot V_c) = 1.3 \cdot (13{,}100 \text{ lbs} - 25{,}159 \text{ lbs})$

$< 0 \quad \textit{okay}$

A.3.4 Shear capacity of the toe

The critical section for shear capacity in the toe is at a distance *d* from the interface of the toe and the stem, where $d = 19.5"$. Because the length of the toe is short, moment capacity is not checked.

$V_{toe} = 4293 \text{ lbs} - 413 \text{ lbs}$

$= 3880 \text{ lbs}$

$V_u = 1.7 \cdot (D + L)$

$= 1.7 \cdot (3880 \text{ lbs})$

$= 6596 \text{ lbs}$

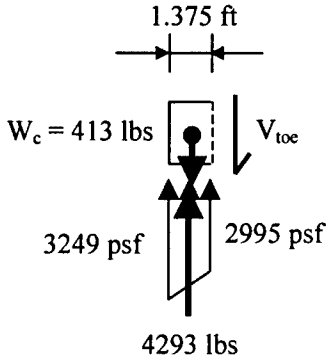

$$\phi \cdot V_c = \phi_{shear} \cdot 2 \cdot \sqrt{f'_c}\, b \cdot d$$

$$= 0.85 \cdot 2 \cdot \sqrt{4000\ psi}\ 12" \cdot 19.5"$$

$$= 25{,}159\ lbs$$

$$\phi \cdot V_s \geq 1.3 \cdot (V_u - \phi \cdot V_c)$$

$$1.3 \cdot (V_u - \phi \cdot V_c) = 1.3 \cdot (6596\ lbs - 25{,}159\ lbs)$$

$$< 0 \quad \textit{okay}$$

Use #11 @ 9" c-c $\Rightarrow$ $A_s = 2.08\ in^2$ per ft of wall

Figure A-5a shows the steel reinforcing detailing, determined previously (note: development lengths need to be checked), wherein the stem, heel, and toe were treated as singly reinforced members (i.e., reinforcement is only on one face of the member). However, good engineering judgment would dictate that the reinforcing steel in the toe and heel be continuous for the length of the base, such as shown in Figure A-5b. By doing so, any potential issues regarding development length of the base reinforcing are avoided, and additionally, the base would better withstand load reversals that might occur during the life of the wall.

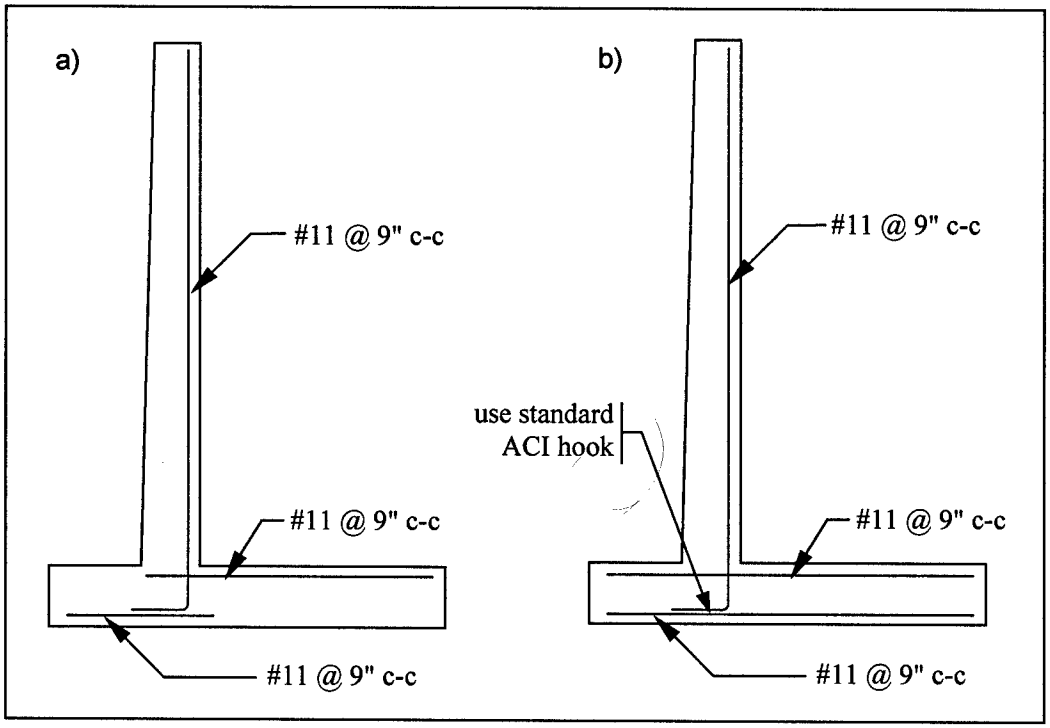

Figure A-5. Proposed steel reinforcement detailing. A minimum 4" cover is required

Notes: The primary purpose of the structural design computations presented previously was to ensure that the wall dimensioned for global stability was also feasible from a structural design standpoint. The structural design is not complete, and no attempts were made to optimize the design (i.e., refine the spacing of the reinforcing steel, or reduce the reinforcement in the upper portions of the stem).

Table A-1
Conversion Factors, Non-SI to SI Units of Measurement Used in This Appendix

Multiply	By	To Obtain
feet	0.3048	meters
foot-pounds	1.355818	joules
kips per square inch	6.894757	megapascals
inches	25.4	millimeters
inch-kips	112.9848	newton-meters
pounds (force) per square foot	47.88026	pascals
pounds (force) per square inch	0.006894757	megapascals
pounds (mass)	0.4535924	kilograms
pounds (mass) per cubic foot	16.01846	kilograms per cubic meter
square inches	645.16	square millimeters

Appendix B
Notation, Sign Convention, and Earth Pressure Expressions

The notation shown in Figure B-1 is used throughout this report. All the variables shown in this figure are presented in their positive orientation. Additionally, expressions for the classical Mononobe-Okabe active and passive dynamic earth pressures are presented (e.g., Ebeling and Morrison 1992, Chapter 4),[1] as well as expressions for the slope of the corresponding failure planes.

Notation:

a_h = horizontal acceleration

a_v = vertical acceleration

g = acceleration due to gravity

H = wall height

K_{AE} = active thrust coefficient

K_{PE} = passive resistance coefficient

k_h = horizontal inertial coefficient

k_v = vertical inertial coefficient

P_{AE} = active thrust of soil

P_{PE} = passive resistance of soil

W = weight of failure wedge

[1] References cited in this appendix are included in the References section at the end of the main text.

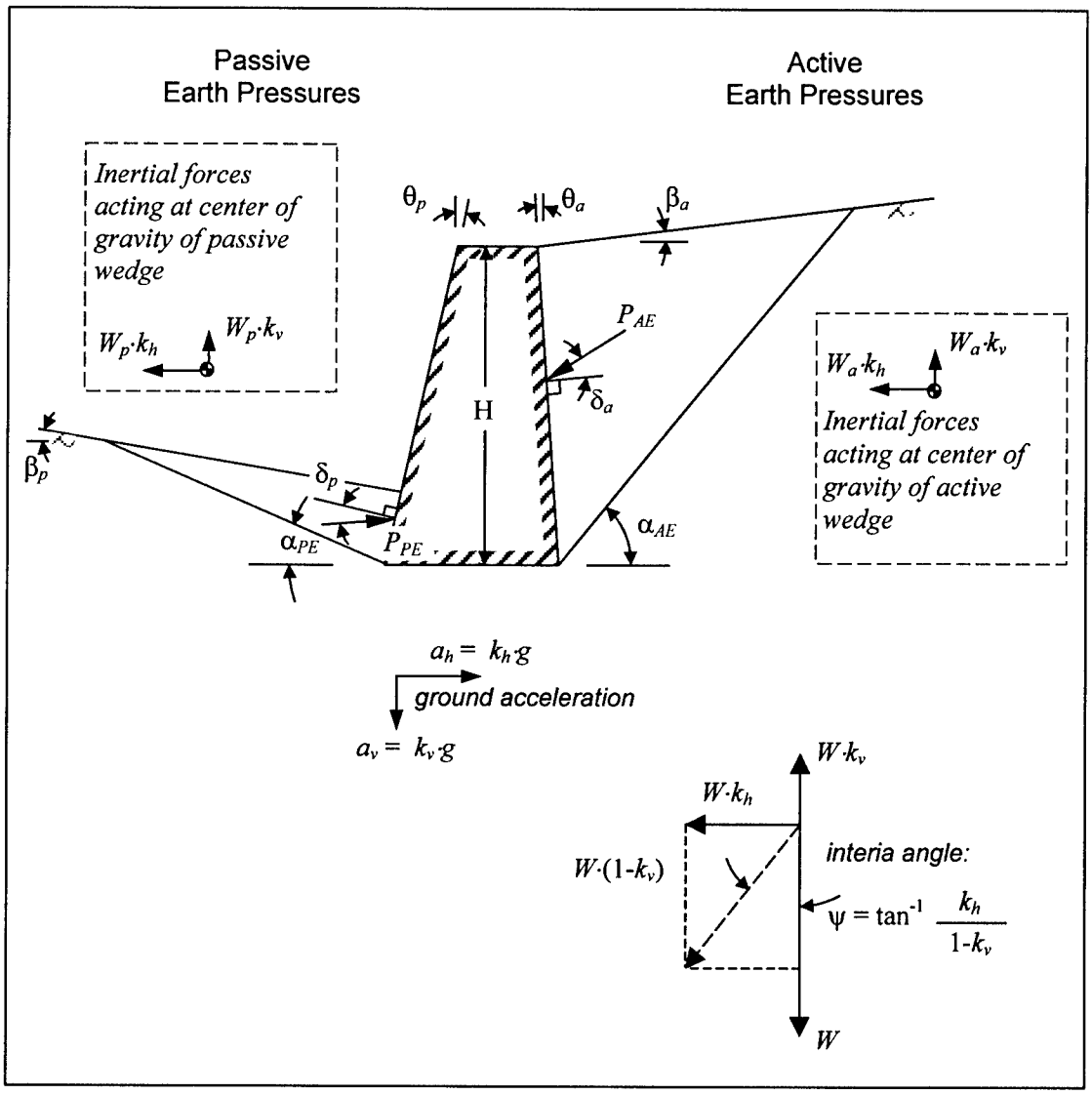

Figure B-1. Sign Convention. All quantities are shown in their positive orientation (adapted from Davies, Richards, and Chen 1986)

W_a = weight of active failure wedge

W_p = weight of passive failure wedge

α_{AE} = inclination to horizontal of failure plane, active case

α_{PE} = inclination to horizontal of failure plane, passive case

β_a = slope of backfill, active case

β_p = slope of backfill, passive case

δ_a = interface friction angle, active case

δ_p = interface friction angle, passive case

γ_t = total unit weight of soil

θ_a = wall batter angle, active case

θ_p = wall batter angle, passive case

ϕ = angle of internal friction of soil

ψ = seismic inertia angle

The following expressions are the classical Mononobe-Okabe active and passive dynamic earth pressure expressions (e.g., Ebeling and Morrison 1992). Mononobe and Matsuo (1929) and Okabe (1926) derived these expressions by modifying Coulomb's classical earth pressure expression to account for seismically induced horizontal and vertical inertia forces in the assumed failure wedge.

a. Active case:

$$P_{AE} = \frac{1}{2} \cdot \gamma_t \cdot H^2 \cdot (1 - k_v) \cdot K_{AE} \tag{B-1}$$

$$K_{AE} = \frac{\cos^2(\phi - \psi - \theta_a)}{\cos(\psi) \cdot \cos^2(\theta_a) \cdot \cos(\psi + \theta_a + \delta_a) \cdot \left[1 + \sqrt{\frac{\sin(\phi + \delta_a) \cdot \sin(\phi - \psi - \beta_a)}{\cos(\delta_a + \psi + \theta_a) \cdot \cos(\beta_a - \theta_a)}}\right]^2} \tag{B-2}$$

b. Passive case:

$$P_{PE} = \frac{1}{2} \cdot \gamma_t \cdot H^2 \cdot (1 - k_v) \cdot K_{PE} \tag{B-3}$$

$$K_{PE} = \frac{\cos^2(\phi - \psi + \theta_p)}{\cos(\psi) \cdot \cos^2(\theta_p) \cdot \cos(\psi - \theta_p + \delta_p) \cdot \left[1 - \sqrt{\frac{\sin(\phi + \delta_p) \cdot \sin(\phi - \psi + \beta_p)}{\cos(\delta_p + \psi - \theta_p) \cdot \cos(\beta_p - \theta_p)}}\right]^2} \tag{B-4}$$

The expressions for the angles of inclination of the failure planes with the horizontal originally derived by Zarrabi-Kashani (1979), active case, and Ebeling and Morrison (1992), passive case, and presented in Ebeling and Morrison (1992) as Equations 37 and 61, respectively, were determined to give erroneous results for $\phi \leq \psi + \theta$. Equations 37 and 61 in Ebeling and Morrison (1992) are valid when the wall batter angle is zero (i.e., $\theta = 0$), and for nonzero batter angles for most levels of shaking (i.e., $\phi > \psi + \theta$). The following expressions for active

and passive slip plane angles were derived by Michalowski[1] and numerically verified by the authors.

a. Active case:

$$\alpha_{AE} = \tan^{-1}\left[\frac{\sin(\beta_a + \psi)\cdot c_{AE} + \cos(\phi + \delta_a + \theta_a + \psi)}{\cos(\beta_a + \psi)\cdot c_{AE} - \sin(\phi + \delta_a + \theta_a + \psi)}\right] - \psi \qquad \text{(B-5a)}$$

$$c_{AE} = \sqrt{\frac{\sin(\phi + \delta_a)\cdot\cos(\theta_a + \delta_a + \psi)}{\sin(\phi - \beta_a - \psi)\cdot\cos(\theta_a - \beta_a)}} \qquad \text{(B-5b)}$$

b. Passive case:

$$\alpha_{PE} = \tan^{-1}\left[\frac{\sin(\beta_p - \psi)\cdot c_{PE} + \cos(\phi + \delta_p - \theta_p + \psi)}{\cos(\beta_p - \psi)\cdot c_{PE} + \sin(\phi + \delta_p - \theta_p + \psi)}\right] + \psi \qquad \text{(B-6a)}$$

$$c_{PE} = \sqrt{\frac{\sin(\phi + \delta_p)\cdot\cos(\theta_p - \delta_p - \psi)}{\sin(\phi + \beta_p - \psi)\cdot\cos(\theta_p - \beta_p)}} \qquad \text{(B-6b)}$$

[1] R. Michalowski, 2002, Personal communication regarding the derivation of the angle of inclination of active and passive failure planes under seismic loading, Department of Civil Engineering, University of Michigan, Ann Arbor, MI.

Appendix C
Displacement-Controlled Design Procedure

The displacement-controlled approach for design of earth retaining structures was originally proposed by Richards and Elms (1979)[1] and is further developed in Ebeling and Morrison (1992), Section 6.3. The approach builds off the Newmark sliding block analysis procedure and provides a method of assessing the global stability of retaining walls against sliding and overturning based on the explicit choice of an allowable permanent displacement.

During a seismic event, the maximum inertial load that can be sustained by the structural wedge (in the case of a cantilever retaining wall) is limited by the maximum transmissible acceleration ($N^*{\cdot}g$). $N^*{\cdot}g$ is the value of acceleration (with coefficient N^*) imparted to the driving wedge and structural wedge that results in a factor of safety against sliding equal to 1.0. Recall that the cantilever retaining wall, contained within the structural wedge, was sized for the normal, static load case using a factor of safety against sliding equal to 1.5 (calculations given in Appendix A). So the maximum transmissible acceleration is a value of acceleration, $N^*{\cdot}g$, when imparted to the center of mass of both the structural wedge and the driving wedge, that reduces the factor of safety against sliding from its static value of 1.5 down to a value of 1.0. The value of $N^*{\cdot}g$ is a function of the geometry of the cantilever retaining wall, the structural and driving wedges, unit weights of the reinforced concrete structural members, as well as the unit weight(s) of the soil(s), and the shear strengths of the backfill, the foundation, and the structure-to-foundation interface. Note that the value of $N^*{\cdot}g$ is not a function of the design ground motion. Also, consideration is given only to $N^*{\cdot}g$ corresponding to the movement of the wall away from the backfill, as this is generally less than $N^*{\cdot}g$ corresponding to the movement of the wall toward the backfill.

The underlying premise of the displacement-controlled procedure is presented in Figure C-1. As illustrated in Figure C-1 at time *a*, when the horizontal inertial coefficient $k_h = N^*$, sliding occurs. Relative movement of the wall and

[1] References cited in this appendix are included in the References section at the end of the main text.

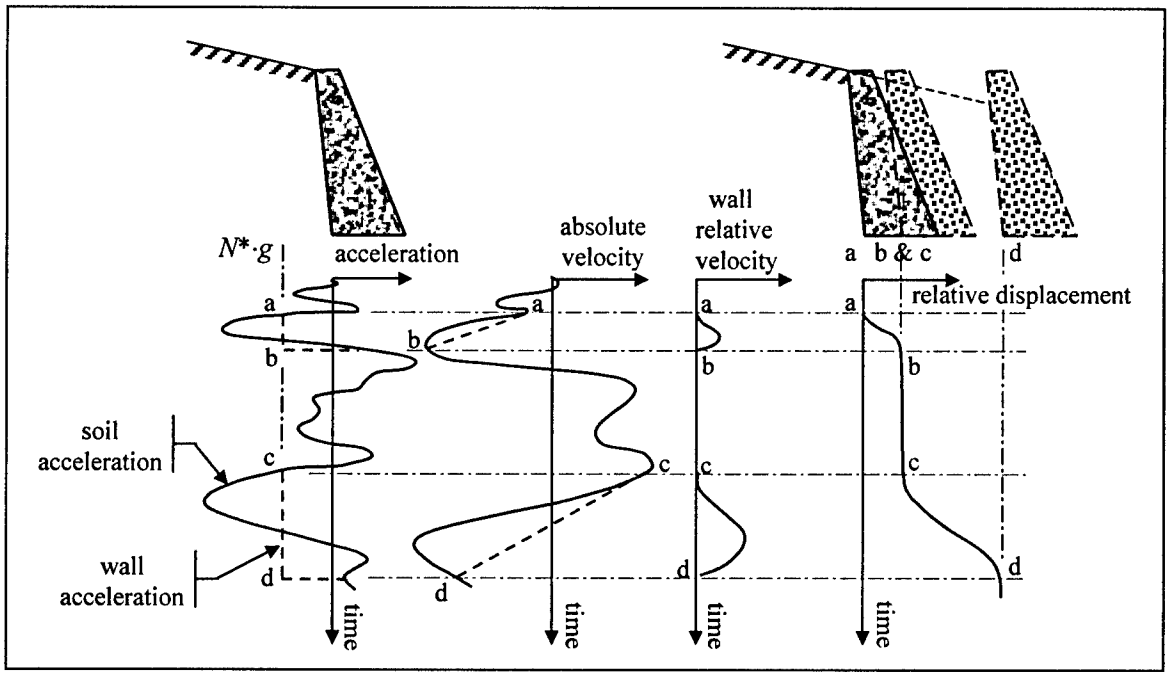

Figure C-1. Incremental failure by base sliding (adapted from Richards and Elms 1979)

soil continues until their velocities become equal, as occurs at time *b* in Figure C-1. The wall incrementally displaces away from the backfill each time horizontal acceleration $a_h \geq N^* \cdot g$.

The Newmark sliding block procedure is implemented in the computer program CWROTATE (Ebeling and White, in preparation), which was used to evaluate candidate ground motions for use in the FLAC analyses, the selection criterion being that enough permanent relative displacement occurs that active earth pressure conditions exist.

C.1 CWROTATE Analysis of Cantilever Retaining Wall

In order to perform a Newmark sliding block analysis, $N^* \cdot g$ is required. CWROTATE computes $N^* \cdot g$ by performing an equilibrium analysis of the structural wedge. The forces acting on the structural wedge are shown in Figure C-2.

Summing the forces in the horizontal direction results in:

$$T - P_{AE,\,heel} - k_h \cdot W_w = 0 \qquad \text{(C-1a)}$$

where

$$T = N' \cdot \tan(\phi_b') \qquad \text{(C-1b)}$$

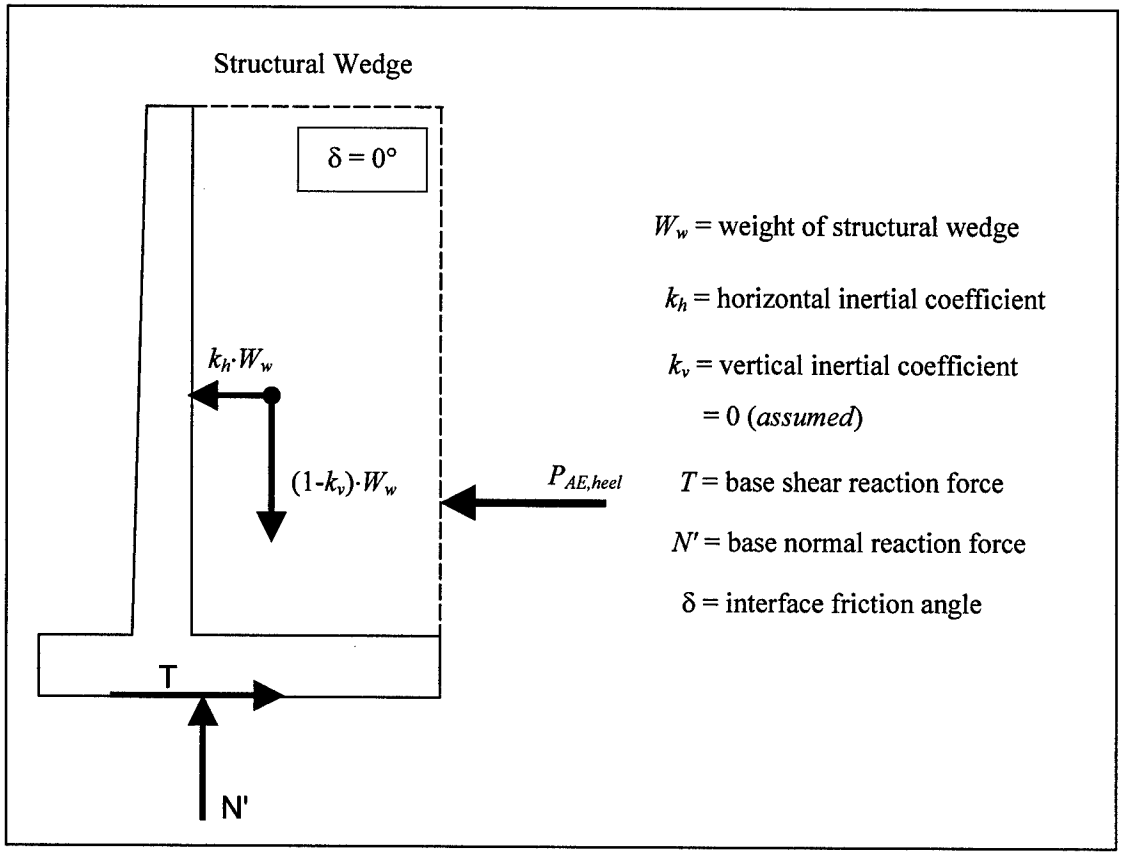

Figure C-2. Forces acting on the structural wedge

$$N' = W_w \quad \text{for} \quad k_v = 0 \tag{C-1c}$$

where $P_{AE,\,heel}$ is the resultant force of the static and dynamic stresses acting on the vertical section through the heel and ϕ'_b = effective internal friction angle of foundation soil (use of δ_b, i.e., interface friction angle between base and foundation soil, may be also appropriate).

Substituting Equations C-1b and C-1c into Equation C-1a and solving for k_h gives:

$$k_h = \tan(\phi'_b) - \frac{P_{AE,\,heel}}{W_w} \tag{C-2}$$

In order to solve Equation C-2 $P_{AE,heel}$ is needed. The formulation in CWROTATE uses the (active) wedge method of analysis and is based on the engineering formulation given in Appendix A of Ebeling and Morrison (1992) to determine the value for $P_{AE,heel}$. A sweep search algorithm was devised and implemented within CWROTATE to ensure that the thrust force computed for a

particular wedge geometry by the wedge method corresponds to the maximum force (i.e., the pseudo-static active earth pressure force, $P_{AE,heel}$). In this wedge method of analysis a planar slip surface is assumed. The sweep search investigates the potential slip planes for the trial wedges by CWROTATE in 1-degree increments. Bilinear backfill surfaces may be analyzed via CWROTATE (i.e., a sloping backfill surface up to an elevation at which the backfill surface is horizontal). For CWROTATE, Ebeling and Morrison (1992) Appendix A, formulation for the (active) wedge method of analysis was expanded to consider both effective stress (c', ϕ') and total stress S_u shear strength parameters for the soil. The current 2002 version of CWROTATE is capable of analyzing "dry" (i.e., moist) backfills with no water table within the backfill nor foundation. Based on the engineering formulations given in Chapter 4 and Appendix A of Ebeling and Morrison (1992), the computer program CWROTATE is being expanded by Ebeling to include consideration of "wet" sites; i.e., partially submerged backfills and submerged foundations.

For the cantilever wall retaining dry, level backfill that was designed using the procedures outlined in Appendix A, CWROTATE computed N^*g equal to $0.22g$. This value of maximum transmissible acceleration was also obtained using Equation C-2 in conjunction with the Mononobe-Okabe equation for $P_{AE,heel}$. Note that because the Mononobe-Okabe relationship (given in Appendix B of this report and in Chapter 4 of Ebeling and Morrison 1992) is a function of k_h, an iterative process is used to compute the k_h ($=N^*$) value for this wall by this alternative method of analysis. The value for $P_{AE,heel}$ computed by CWROTATE was also verified using the Mononobe-Okabe relationship. Recall that the Mononobe-Okabe formulation is valid for homogenous backfills with constant backfill surface slopes (including level backfills as in this problem). Thus, the wedge method of analysis as implemented in CWROTATE is applicable to more types of Corps retaining wall configurations than is the Mononobe-Okabe equation.

In order to evaluate the candidate motion, a site response analysis was performed on the profile shown in Figure 3-2 using a modified version of SHAKE91 (Idriss and Sun 1992). The acceleration time-history SG3351 was specified as an outcrop motion in a SHAKE analysis, and the interlayer ground motion was computed at a depth corresponding to approximately midheight of the cantilever retaining wall. This motion was used in conjunction with the N^*g in CWROTATE to perform a Newmark sliding block-type analysis of the cantilever retaining wall. The results of the analysis are shown in Figure C-3. As may be observed from this figure, a permanent relative displacement of 2.147 in. (54.5 mm) is predicted, which is sufficient to ensure active earth pressure conditions (minimum displacement for (seismic) active earth pressures behind the 20-ft- (6-m-) high retaining wall was determined using the Ebeling and Morrison (1992) Table 1 data).

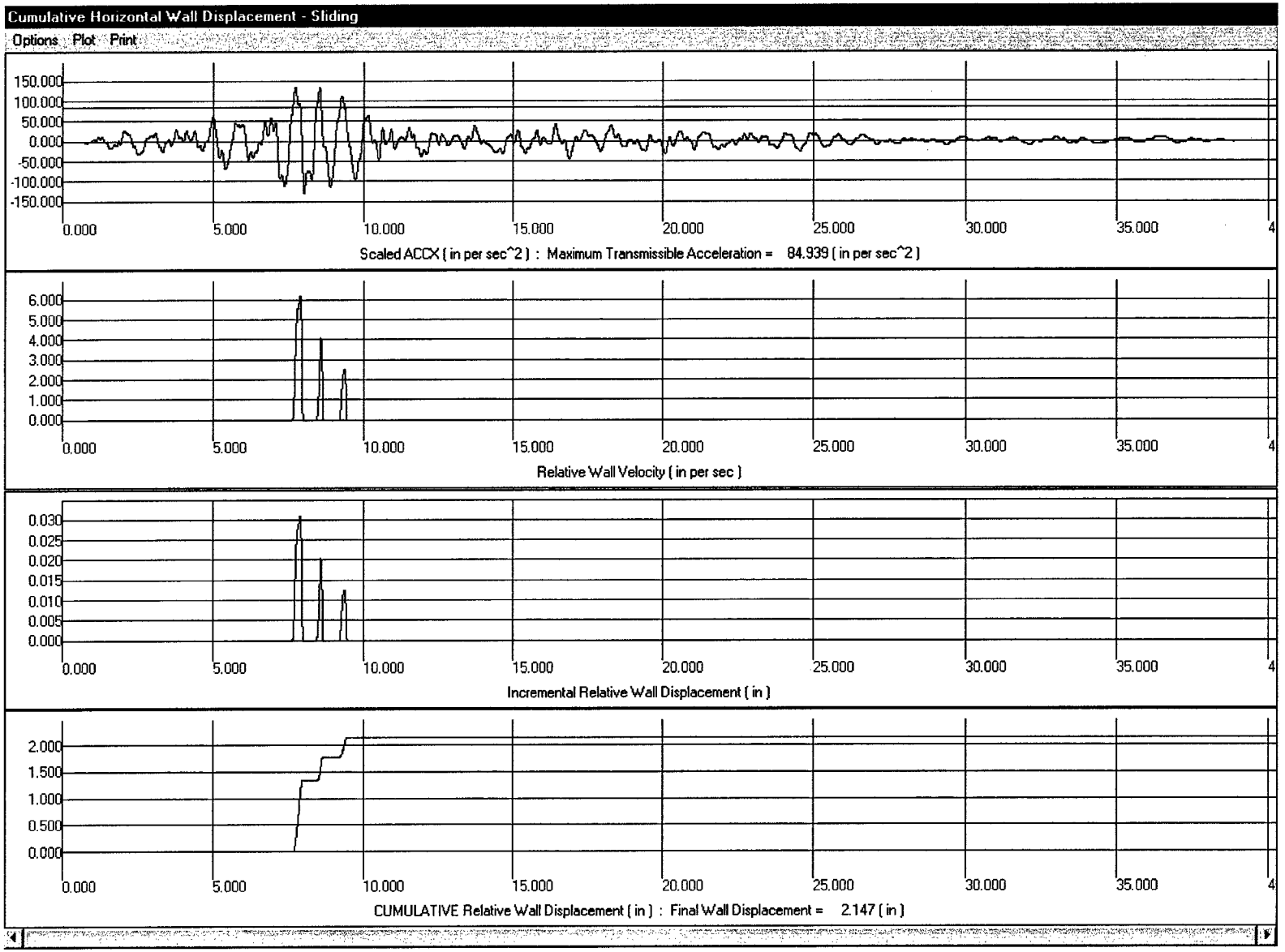

Figure C3. Results of Newmark sliding block-type analysis performed using CWROTATE

C.2 Displacement-Controlled Design Procedure

The following is a summary of the steps listed in Ebeling and Morrison (1992), Section 6.3.2, for the displacement-controlled design procedure for a wall retaining dry backfill, for which k_v is assumed equal to zero. The procedure pertains to the global stability of the wall and is repeated here for reference purposes only. It is applicable to walls whose geometry has already been established (e.g., an existing wall or established during a static design step). These steps are geared toward hand computations with the earthquake hazard defined in terms of peak acceleration and peak velocity values only and not for time-history analysis of permanent wall displacement (as is the case when using CWROTATE to analyze retaining walls). Interface friction between the driving wedge and the structural wedge is assumed to be zero for illustrative purposes only in the following equations. The reader is directed to Ebeling and Morrison (1992) for more detailed information on the simplified engineering procedure and for the case when interface friction between the structural wedge and the driving wedge is nonzero.

a. Determine the value for the average site-specific peak horizontal acceleration $A \cdot g$ and the value for the average peak horizontal velocity V at the site.

b. Calculate the maximum transmissible acceleration $N^* \cdot g$ coefficient N^*. An iterative method consisting of the following steps is required to compute the value for N^*.

(1) Using an assumed value for N^*, compute the value for the dynamic active earth pressure force $P_{AE,heel}$ using the Mononobe-Okabe relationship given in Appendix B (or in Chapter 4 of Ebeling and Morrison 1992).

(2) Calculate the values of the shear force required for equilibrium along the base of the wall, T:

$$T = P_{AE,heel} + W \cdot k_h \tag{C-3}$$

(3) Calculate the normal force, N:

$$N = W \tag{C-4}$$

(4) Calculate the value for the ultimate shear force along the base of the wall T_{ult} using the smaller of the following two values for T_{ult}:

$$T_{ult} = N \cdot \tan(\delta_b) \tag{C-5}$$

or

$$T_{ult} = N \cdot \tan(\phi'_b) \tag{C-6}$$

where

δ_b = interface friction angle between base of the wall and foundation soil

ϕ'_b = effective internal friction angle of foundation soil

(5) If the value for T is not equal to the value for T_{ult}, adjust the value used for N^* and repeat steps (1) through (4) until $T = T_{ult}$. The resulting value for N^* is equal to the maximum transmissible acceleration coefficient.

c. Calculate the permanent relative displacement d_r using Whitman and Liao (1985):

$$d_r = \left[\frac{495 \cdot V^2}{(A \cdot g)}\right] \cdot \exp^{\left(-9.4 \cdot \frac{N^*}{A}\right)} \qquad \text{(C-4)}$$

where

$A \cdot g$ = expressed in units of in./sec^2

V = expressed in units of in./sec

d_r = expressed in units of inches

g = 386 in/sec^2

d. The value for d_r must be consistent with those movements that are required to develop the dynamic active earth pressure used in Step b(1). Refer to Table 1 in Section 2.2.2 of Ebeling and Morrison (1992).

e. Dimension the wall so that the Corps' overturning criterion (Headquarters, U.S. Army Corps of Engineers, 1989) is satisfied.

Appendix D
Specifying Ground Motions in FLAC

As briefly outlined in Chapter 3, dynamic analyses can be performed with FLAC, wherein user-specified acceleration, velocity, stress, or force time-histories can be input as an exterior boundary condition or as an interior excitation. A parametric study was performed to determine the best way to specify the ground motions in FLAC for earthquake analyses. The parametric study involved performing a series of one-dimensional site response analyses using consistently generated acceleration, velocity, and stress time-histories. Generally, earthquake ground motions are not defined in terms of force time-histories and therefore were not considered in the parametric study.

Using the acceleration time-history SG3351, a SHAKE analysis was performed on a 5 percent damped, nondegrading profile, shown in Figure D-1, wherein the SG3351 was specified as an outcrop motion. Interlayer acceleration and stress time-histories were computed at bedrock and at depths of 50, 35, and 25 ft (15, 10, and 8 m), in addition to the surface acceleration time-history being computed. Interlayer velocity time-histories were computed by integrating the interlayer acceleration time-histories using the trapezoidal rule. The interlayer acceleration, velocity, and stress time-histories were used as base motions in a series of FLAC analyses, in which the acceleration time-histories at the surface of the FLAC profiles were computed. The profiles used in the FLAC analyses were comparable to the 225-ft (69-m) SHAKE profile down to the depths corresponding to the interlayer motions. This is illustrated in Figure D-1. An elastic constitutive relation, with 5 percent Rayleigh damping, was used to model the soil layers in the FLAC profiles. The central frequency of the damping was set to the fundamental frequency of the respective FLAC profiles.

Fourier amplitude spectra (FAS) and 5 percent damped, pseudo-acceleration spectra (PSA) were computed from the acceleration time-histories of the surface motions of the SHAKE and FLAC profiles. Error analyses were performed on the spectra corresponding to the different profiles and different types of specified input motions. In the error analyses, the spectra for the SHAKE motions were used as the "correct" motions. The word "correct" does not imply that SHAKE correctly models the behavior of an actual soil profile subjected to earthquake motions. Rather, SHAKE gives the analytically correct motion for a visco-elastic

profile with constant damping applied to all frequencies of motion. On the other hand, the FLAC models used in this study give only numerical approximations of the correct analytical solution. The percent error in the FLAC spectral values, as a function of frequency, was computed using Equation D-1:

$$Error\,(\%) = \frac{FLAC\ Spectral\ Value - SHAKE\ Spectral\ Value}{SHAKE\ Spectral\ Value} \times 100\% \qquad \text{(D-1)}$$

In Figures D-2a, D-3a, D-4a, and D-5a, the 5 percent damped PSA are shown for the surface motions of the respective profiles and types of input motions. The errors in the PSA computed using Equation D-1 are presented in Figures D-2b, D-3b, D-4b, and D-5b. Because the scales of these figures do not allow a clear presentation of the errors in the spectral values for the motions corresponding to acceleration and velocity input motions, Figures D-2c, D-3c, D-4c, and D-5c are provided. In these figures, only the errors in the spectral values for the motions corresponding to acceleration and velocity input motions are plotted.

As may be observed from these figures, the specification of the input motion in terms of stress time-histories gives the least accurate results. Although it appears that specification of input motions in terms of acceleration time-histories gives slightly more accurate results than using velocity time-histories, the apparent error may be related to how the interlayer velocity time-histories were computed from the interlayer acceleration time-histories. Regardless, the errors corresponding to specifying the motions in terms of acceleration and velocity time-histories are approximately equal. The input motions used in the FLAC analyses of the retaining walls were specified in terms of acceleration time-histories.

Similar error analyses were performed on the FAS of the surface motions, with similar conclusions being drawn. However, the explicit solution scheme used in FLAC introduces considerable high-frequency noise, which dominated the scales of the error plots of the FAS. Accordingly, these plots are not presented.

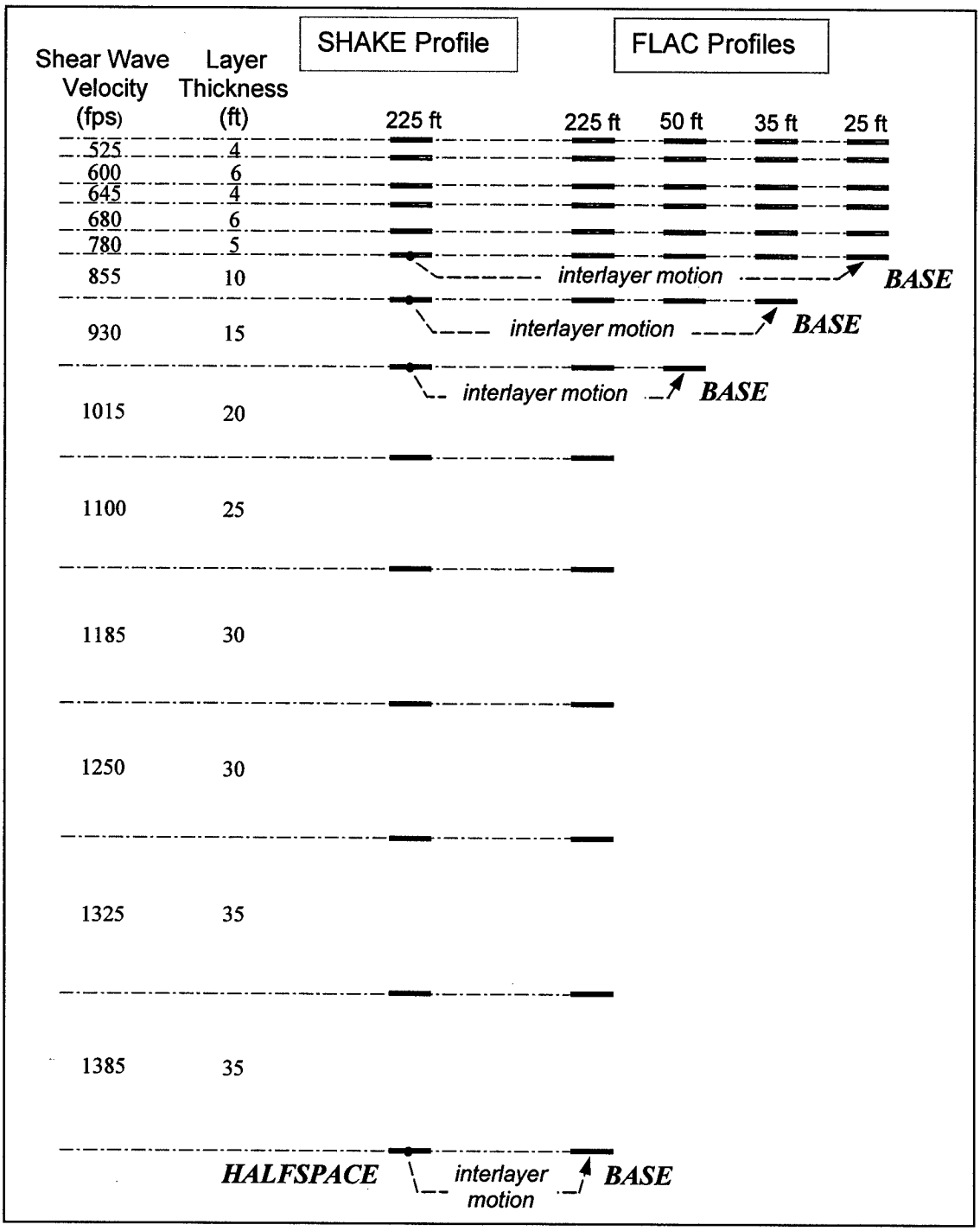

Figure D-1. Profiles used in the parametric study to determine the best way to specify earthquake ground motions in FLAC

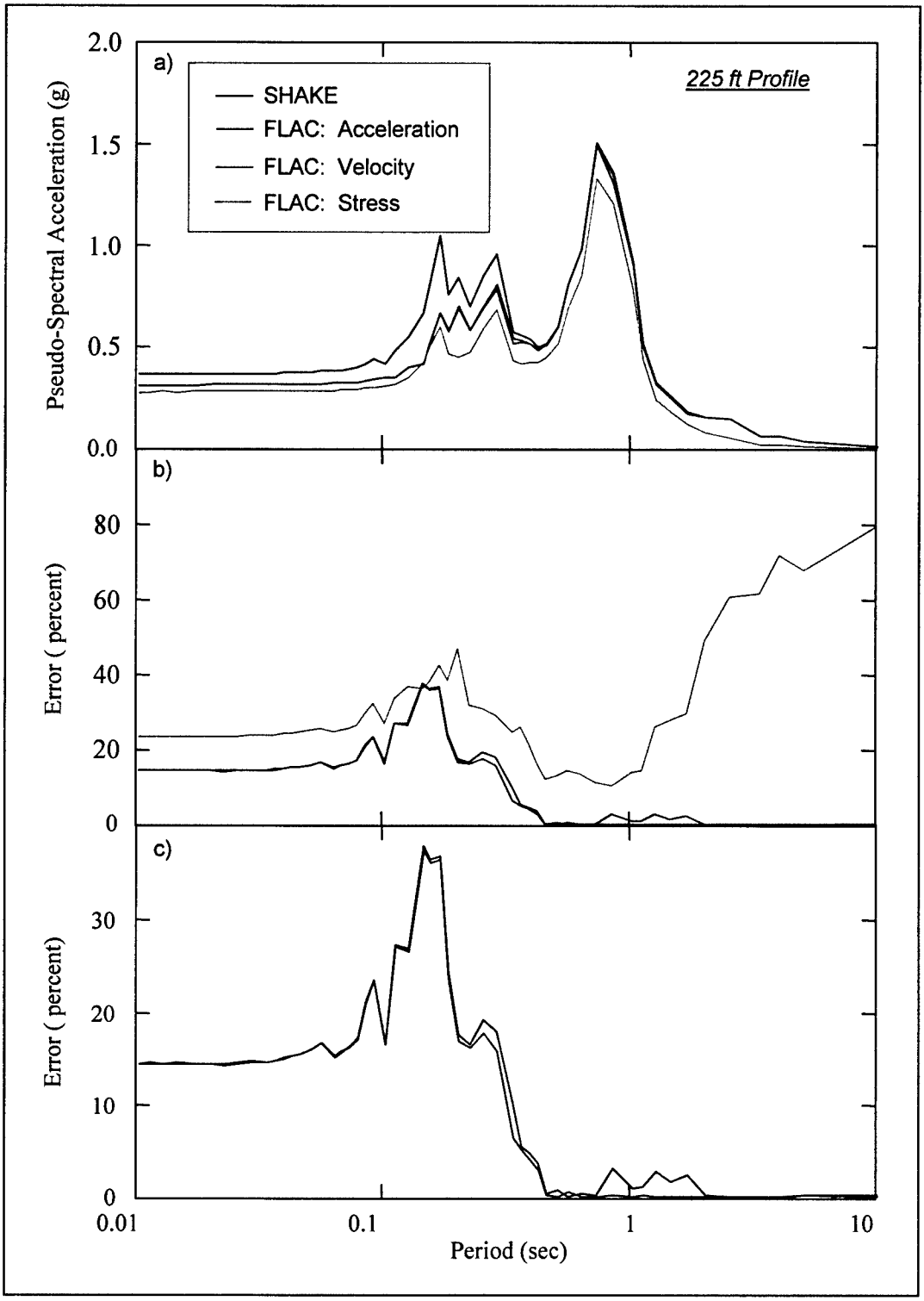

Figure D-2. Results of the error analysis for the 225-ft (69-m) profile: (a) Pseudo-acceleration spectra of surface motions, (b) percent error in pseudo-spectral values corresponding to input motions specified in terms of stress, acceleration, and velocity time-histories, (c) percent error in pseudo-spectral values corresponding to input motions specified in terms of acceleration and velocity time-histories (i.e., same as (b) except plotted using a different scale)

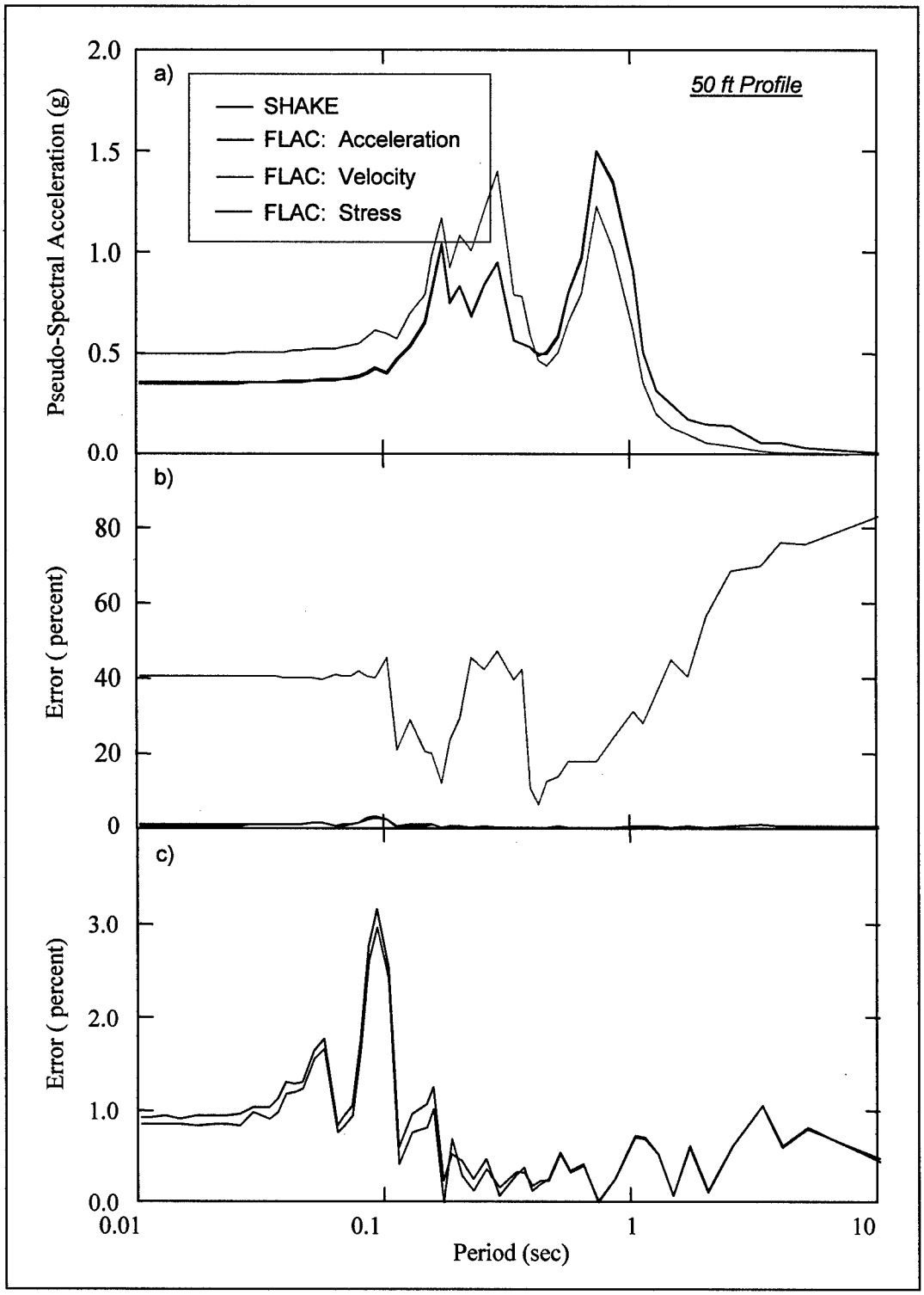

Figure D-3. Results of the error analysis for the 50-ft (15-m) profile: (a) Pseudo-acceleration spectra of surface motions, (b) percent error in pseudo-spectral values corresponding to input motions specified in terms of stress, acceleration, and velocity time-histories, (c) percent error in pseudo-spectral values corresponding to input motions specified in terms of acceleration and velocity time-histories (i.e., same as (b) except plotted using a different scale)

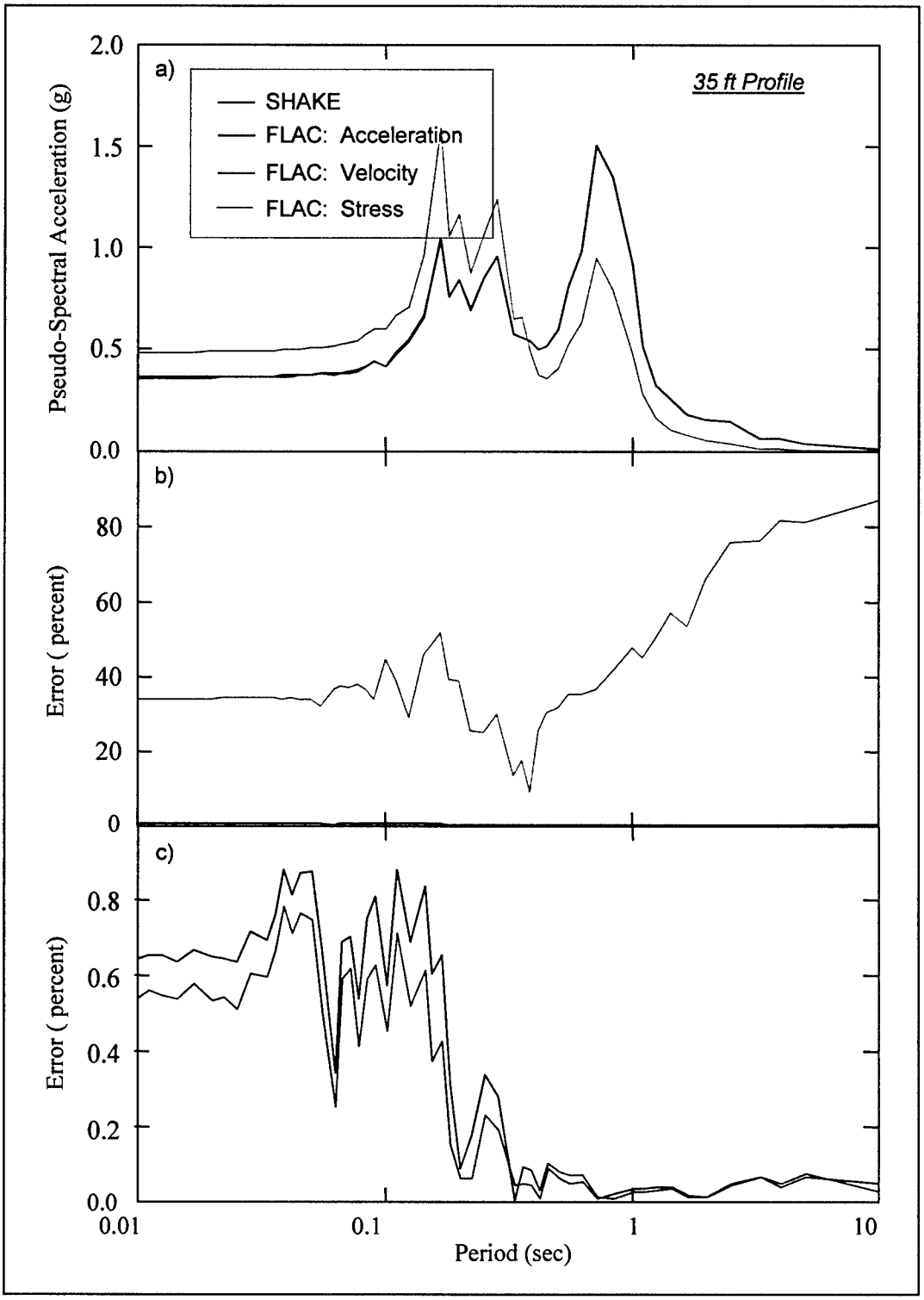

Figure D-4. Results of the error analysis for the 35-ft (11-m) profile: (a) Pseudo-acceleration spectra of surface motions, (b) percent error in pseudo-spectral values corresponding to input motions specified in terms of stress, acceleration, and velocity time-histories, (c) percent error in pseudo-spectral values corresponding to input motions specified in terms of acceleration and velocity time-histories (i.e., same as (b) except plotted using a different scale)

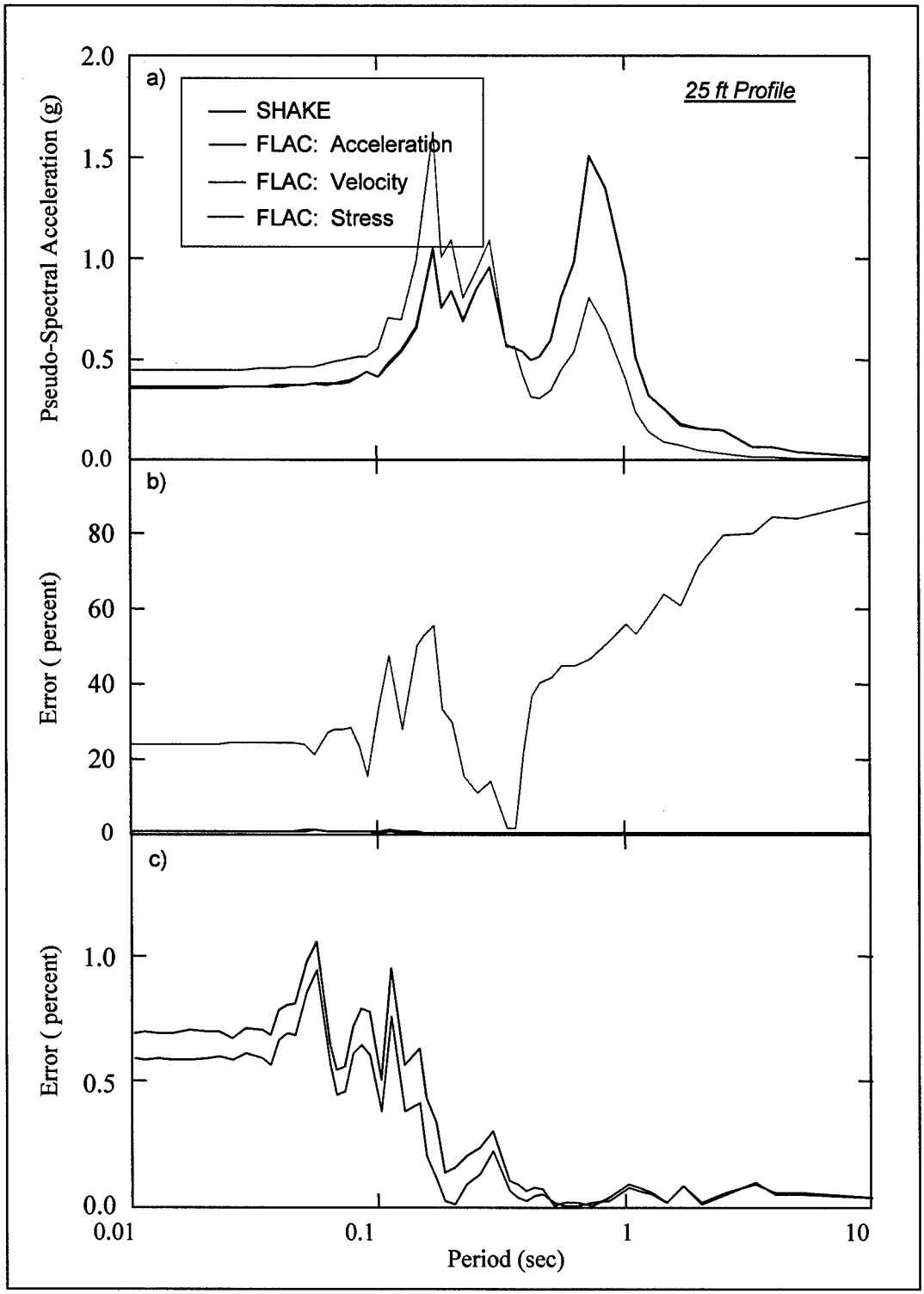

Figure D-5. Results of the error analysis for the 25-ft (8-m) profile: (a) Pseudo-acceleration spectra of surface motions, (b) percent error in pseudo-spectral values corresponding to input motions specified in terms of stress, acceleration, and velocity time-histories, (c) percent error in pseudo-spectral values corresponding to input motions specified in terms of acceleration and velocity time-histories (i.e., same as (b) except plotted using a different scale)

Appendix E
Notation

a_h	Horizontal acceleration
A_g	Cross-sectional area
C_k	Interface stiffness ratio
d_r	Relative displacement
E_c	Elastic modulus
f	Frequency
f_{max}	Highest frequency
f_c'	Compressive strength of concrete
F_{sr}	Lateral seismic force component
F_V	Vertical component of the resultant force acting on the heel section
$F_H^{'}$	Horizontal component of the resultant force acting on the heel section
$F_{i,j}^{top}$	Force acting on the top node of element *i* and at time increment *j*
$F_{i,j}^{bottom}$	Force acting on the bottom node of element *i* and at time increment *j*
FDM	Finite difference method
FEM	Finite element method
FLAC	Fast Lagrangian Analysis of Continua

g	Acceleration due to gravity
G	Shear modulus
h_i	Length of beam element i
H	Height of the wall
I	Second moment of area, or moment of inertia
k_h	Dimensionless horizontal inertial coefficient
k_n	Normal stiffness for interface element
k_s	Shear stiffness for interface element
k_{vj}	Vertical inertial coefficient at time increment j (assumed to be zero)
K	Lateral earth pressure coefficient
K'	Bulk modulus
K_A	Active earth pressure coefficient
K_{AE}	Active dynamic earth pressure coefficient
K_I	Dimensionless interface stiffness number for initial loading
K_{PE}	Passive dynamic earth pressure coefficient
K_o	At-rest earth pressure coefficient
K_{si}	Initial shear stiffness of the interface
K_{urj}	Unload-reload stiffness number for interfaces
m	Seismically induced bending moment on a section of the stem portion of a cantilever wall
M	Magnitude of the earthquake
$\overline{M}$	Mean magnitude of the earthquake
MDE	Maximum Design Earthquake
n_j	Dimensionless stiffness exponent
N'	Normal reaction force to forces acting on the structural wedge

$N^*{\cdot}g$	Maximum transmissible acceleration
OBE	Operational Basis Earthquake
pga	Peak ground acceleration
P_a	Atmospheric pressure
$P_{AE,heel}$	Resultant force of the static and dynamic stresses acting on the vertical section through the heel
$P_{E,stem}$	Resultant force of the static and dynamic stresses acting on the stem of the wall
P_{heel}	Resultant forces acting on the heel section
P_j	Total force acting on the stem or heel section at time increment j
P_{static}	Total resultant force prior to shaking
P_{stem}	Resultant forces acting on the stem section
PSHA	Probabilistic seismic hazard analyses
R	Site-to-source distance of the ground motion
$\overline{R}$	Mean site-to-source distance of the ground motion
R_{fj}	Failure ratio for interface
s	Seismically induced shear moment on a section of the stem portion of a cantilever wall
S	Slider; yield strength of interface element
SASW	Spectral analysis of surface waves
T	Base shear reaction force to the static and dynamic stresses acting on the vertical section through the heel
T′	Tensile strength of interface element
v_s	Shear wave velocity
WUS	Western United States
y_i	Vertical distance from the base of the retaining wall to the center of beam element i

Y	Vertical distance from the base of the retaining wall to the resultant force
Y_{heel}	Vertical distance from the base of the wall to the point of application of the resultant forces acting on the heel section
Y_j	Vertical distance from the base of the retaining wall to the point of application of the total resultant force acting on the stem or heel section at time increment j
Y_{static}	Vertical distance from the base of the retaining wall to the point of application of the total resultant force acting on the stem or heel section prior to the shaking (i.e., Y_j at $j = 0$)
Y_{stem}	Vertical distance from the base of the wall to the point of application of the resultant forces acting on the stem section
$(Y \cdot P)_{heel}$	Resultant forces multiplied by the corresponding vertical distance above the base at which they act for the heel section
$(Y \cdot P)_{stem}$	Resultant forces multiplied by the corresponding vertical distances above the base at which they act for the stem section
α	Mass-proportional damping constant
β	Stiffness-proportional damping constant
γ	Unit weight of the soil
γ_t	Total unit weight of the soil
γ_w	Unit weight of water
δ	Interface friction angle
Δl	Length of an element
ΔP_j	Incremental dynamic forces at time increment j
ΔY	Vertical distance from the base of the retaining wall to the point at which ΔP_j acts
Δz_{min}	Smallest width of a zone in the normal direction of the interfacing surface
λ	Wavelength
ξ	Critical damping ratio

ν	Poisson's ratio
ρ	Mass density
$\sigma_{i,j}$	Average lateral stress acting on element i and at time increment j
σ_n	Normal stress acting on the interface, and determined iteratively in FLAC by first assuming a small value for k_s and then constructing the wall
$\sigma_{i,j}^{bottom}$	Lateral stress acting on the bottom of element i and at time increment j
$\sigma_{i,j}^{top}$	Lateral stress acting on the top of element i and at time increment j
ϕ	Internal friction angle
ω	Angular frequency associated with ξ

REPORT DOCUMENTATION PAGE

Form Approved
OMB No. 0704-0188

1. REPORT DATE *(DD-MM-YYYY)*	2. REPORT TYPE	3. DATES COVERED *(From - To)*
September 2002	Final report	

4. TITLE AND SUBTITLE
Seismic Analysis of Cantilever Retaining Walls, Phase I

5a. CONTRACT NUMBER

5b. GRANT NUMBER

5c. PROGRAM ELEMENT NUMBER

5d. PROJECT NUMBER

5e. TASK NUMBER

5f. WORK UNIT NUMBER
387-9456h

6. AUTHOR(S)

Russell A. Green, Robert M. Ebeling

7. PERFORMING ORGANIZATION NAME(S) AND ADDRESS(ES)

Department of Civil and Environmental Engineering
University of Michigan
Ann Arbor, MI 48109-2125;

U.S. Army Engineer Research and Development Center
Information Technology Laboratory
3909 Halls Ferry Road
Vicksburg, MS 39180-6199

8. PERFORMING ORGANIZATION REPORT NUMBER

ERDC/ITL TR-02-3

9. SPONSORING / MONITORING AGENCY NAME(S) AND ADDRESS(ES)

U.S. Army Corps of Engineers
Washington, DC 20314-1000

10. SPONSOR/MONITOR'S ACRONYM(S)

11. SPONSOR/MONITOR'S REPORT NUMBER(S)

12. DISTRIBUTION / AVAILABILITY STATEMENT
Approved for public release; distribution is unlimited.

13. SUPPLEMENTARY NOTES

14. ABSTRACT

This report summarizes the results of the first phase of a research investigation examining the seismic loads induced on the stem of a cantilever retaining wall. In this investigation, the computer program FLAC (Fast Lagrangian Analysis of Continua) was used to perform nonlinear dynamic analyses on a cantilever retaining wall designed by the Corps static design criteria. The procedures used to determine the various numerical model parameters are outlined and the results of the FLAC analyses presented, in which preliminary trends are identified. Further analyses are required to confirm the identified trends and to formulate design recommendations for Corps earth retaining structures.

15. SUBJECT TERMS

Cantilever retaining walls
Displacement controlled approach
Earthquake
FLAC
Seismic analysis

16. SECURITY CLASSIFICATION OF:			17. LIMITATION OF ABSTRACT	18. NUMBER OF PAGES	19a. NAME OF RESPONSIBLE PERSON
a. REPORT	b. ABSTRACT	c. THIS PAGE			19b. TELEPHONE NUMBER *(include area code)*
UNCLASSIFIED	UNCLASSIFIED	UNCLASSIFIED		102	